Final Report

Submitted to

The Florida Department of Transportation

Title

Cracking and Shear Capacity of High Strength Concrete Bridge Girders Under Fatigue Loading (Phase II)

Contract No. B-7896
WPI 0510612
FSU #6120-509-39

Principal Investigator

Kamal Tawfiq, Ph.D., P.E.
Associate Professor
Department of Civil Engineering
FAMU-FSU College of Engineering
Florida State University
Tallahassee, Florida
(904) 487-6121

November 11, 1996

Technical Report Documentation Page

1. Report No. Final	2. Government Accession No.	3. Recipient's Catalog No.
4. Title and Subtitle *Cracking and Shear Capacity of High Strength Concrete Bridge Girders Under Fatigue Loading.*		5. Report Date 11-16-1996 6. Performing Organization Code
7. Author(s) *Kamal Tawfiq, Ph.D., P.E.*		8. Performing Organization Report No. FL-DOT RMC
9. Performing Organization Name and Address FAMU-FSU College of Engineering Department of Civil Engineering 2525 Pottsdamer Street Tallahassee, Fl 32310		10.Work Unit No. 11. Contract or Grant No. B-7896
12. Sponsored Agency Name and Address State of Florida Department of Transportation Research Center 605 Suzanne Street, M.S. 30 Tallahassee, Fl 32301		13. Type of Report and Period Covered Final Report Oct. 1993 -Nov. 1996 4. Sponsoring Agency Code
15. Supplementary Notes Prepared in cooperation with the Federal Highway Administration		

16. Abstract

Two full scale high performance prestressed concrete AASHTO type II girders of compressive strengths 8,000 psi and 12,000 psi were used in this study. The girders were subjected to both fatigue and static loading. Each girder was first subjected to a constant amplitude cyclic loading ranging from 12 kips to 44 kips and subsequently tested under static loading until failure. The static testing was performed to evaluate the effect of fatigue loading on the ultimate shear and flexural capacity of the girder. The 8000 psi girder and the 12000 psi girder were subjected to 2 x 10^6 cycles and 3 x 10^6 cycles, respectively. In addition to the full scale testing, a thorough non-linear *Finite Element Analysis* was also conducted on simulated numerical models aiming at investigating the distribution of internal and external stresses in both beams. The FEA results conformed with the full scale testing in terms the shear and flexural capacity of the beams. Also, the FEA beams indicated the effect of buildup stresses at the south end even before commencing the shear test at that end. This testing practice on full scale beams should further be investigated for possible reduction in the actual shear capacity as compared with various codes. The FEA results were compared with both the full scale test results and results obtained by using the pertained AASHTO-LRFD and the ACI codes for the shearing capacity of prestressed concrete beams. The ACI code was found to provide better prediction of the shear capacity of the two high strength concrete beams. Nevertheless, the ACI code still overestimated the shearing capacity after fatigue loading by about 18% to 10% for the 8,000 psi and 12,000 psi girders, respectively.

17. Key Words High Strength Concrete, Cracking, Shear Capacity, Fatigue. Cyclic Loading		18. Distribution Statement No restriction. This document is available to the public through the National Technical Information Service, Springfield Va. 22161	
19. Security Classif. (of this report) Unclassified	20. Security Classif. (of this page) Unclassified	21. No. of Pages 124 Pages	22. Price *NA*

Form DOT F 1700.7 (8-72)

DISCLAIMER

The opinions, findings and conclusions expressed in this publication are those of the authors and not necessarily those of the Florida Department of Transportation and the Federal Highway Administration.

Prepared in cooperation with the Florida Department of Transportation and the Federal Highway Administration.

ACKNOWLEDGMENTS

The author would like to express his gratitude and sincere regards are extended to Dr. Mohsen Shahawy and Dr. Moussa Issa from the Florida Department of Transportation for their invaluable suggestions and creative criticism to this undertaking. Special gratitude to Dr. Moussa Issa for his comprehensive and constructive review of the results and the manuscript. Also, thanks to Kiran Kumar a graduate student at the department of Civil Engineering for his outstanding efforts in laboratory testing and analysis. My appreciation is extended to the Civil Engineering Department at FAMU-FSU College of Engineering for providing us with the needed facilities. Lastly, I acknowledge the support provided to us by the Florida Department of Transportation. Without their support this task would not have been feasible.

SI* (MODERN METRIC) CONVERSION FACTORS

APPROXIMATE CONVERSIONS TO SI UNITS

Symbol	When You Know	Multiply By	To Find	Symbol
LENGTH				
in	inches	25.4	millimeters	mm
ft	feet	0.305	meters	m
yd	yards	0.914	meters	m
mi	miles	1.61	kilometers	km
AREA				
in^2	square inches	645.2	square millimeters	mm^2
ft^2	square feet	0.093	square meters	m^2
yd^2	square yards	0.836	square meters	m^2
ac	acres	0.405	hectares	ha
mi^2	square miles	2.59	square kilometers	km^2
VOLUME				
fl oz	fluid ounces	29.57	milliliters	ml
gal	gallons	3.785	liters	l
ft^3	cubic feet	0.028	cubic meters	m^3
yd^3	cubic yards	0.765	cubic meters	m^3

NOTE: Volumes greater than 1000 l shall be shown in m^3.

MASS				
oz	ounces	28.35	grams	g
lb	pounds	0.454	kilograms	kg
T	short tons (2000 lb)	0.907	megagrams	Mg
TEMPERATURE (exact)				
°F	Fahrenheit temperature	5(F-32)/9 or (F-32)/1.8	Celcius temperature	°C
ILLUMINATION				
fc	foot-candles	10.76	lux	l
fl	foot-Lamberts	3.426	candela/m^2	cd/m^2
FORCE and PRESSURE or STRESS				
lbf	poundforce	4.45	newtons	N
psi	poundforce per square inch	6.89	kilopascals	kPa

APPROXIMATE CONVERSIONS FROM SI UNITS

Symbol	When You Know	Multiply By	To Find	Symbol
LENGTH				
mm	millimeters	0.039	inches	in
m	meters	3.28	feet	ft
m	meters	1.09	yards	yd
km	kilometers	0.621	miles	mi
AREA				
mm^2	square millimeters	0.0016	square inches	in^2
m^2	square meters	10.764	square feet	ft^2
m^2	square meters	1.195	square yards	ac
ha	hectares	2.47	acres	mi^2
km^2	square kilometers	0.386	square miles	
VOLUME				
ml	milliliters	0.034	fluid ounces	fl oz
l	liters	0.264	gallons	gal
m^3	cubic meters	35.71	cubic feet	ft^3
m^3	cubic meters	1.307	cubic yards	yd^3
MASS				
g	grams	0.035	ounces	oz
kg	kilograms	2.202	pounds	lb
Mg	megagrams	1.103	short tons (2000 lb)	T
TEMPERATURE (exact)				
°C	Celcius temperature	1.8C + 32	Fahrenheit temperature	°F
ILLUMINATION				
lx	lux	0.0929	foot-candles	fc
cd/m^2	candela/m^2	0.2919	foot-Lamberts	fl
FORCE and PRESSURE or STRESS				
N	newtons	0.225	poundforce	lbf
kPa	kilopascals	0.145	poundforce per square inch	psi

(Revised August 1992)

* SI is the symbol for the International System of Units. Appropriate rounding should be made to comply with Section 4 of ASTM E380.

TABLE OF CONTENTS

LIST OF TABLES

LIST OF FIGURES

NOTATION

A_{cs} = cross-sectional area of a strut in strut-and-tie model (in^2)
A_{ps} = area of prestressing steel (in^2)
A_s = area of non-prestressed tension reinforcement (in^2)
A^*_s = area of prestressing steel
A_{st} = total area of longitudinal mild steel reinforcement (in^2)
A_v = area of a transverse reinforcement within a distance s (in^2)
b' = width of a web of a flanged member
b_v = effective web width (in)
b_w = web width (in)
d = distance from extreme compressive fiber to centroid of the prestressing force (in)
d_b = nominal diameter of a reinforcing bar, wire or prestressing strand (in)
d_s = nominal diameter of a prestressing strand (in)
d_v = effective shear depth (in)
E_c = modulus of elasticity of concrete (ksi)
E_p = modulus of elasticity of prestressing tendons (ksi)
E_s = modulus of elasticity of reinforcing bars (ksi)
F_ϵ = reduction factor
f'_c = specified compressive strength of concrete at 28 days (ksi)
f'_{ci} = specified compressive strength of concrete at time of initial loading or prestressing (Ksi)
f_{cu} = the limiting concrete compressive stress for design by strut-and-tie model (ksi)
f_d = stress due to unfactored dead load, at extreme fiber of section where tensile stress is caused by externally applied loads
f_{pc} = compressive stress in concrete (after allowance for all prestress losses) at centroid of cross section resisting externally applied loads or at junction of web and flange when the centroid lies within the flange (In a composite member, f_{pc} is resultant compressive stress at centroid of composite section or at junction of web and flange when the centroid lies within the flange, due to both prestress and moments resisted by precast member acting alone)
f_{pe} = compressive stress in concrete due to effective prestress force only (after allowance for all prestress losses) at extreme fiber of section where tensile stress is caused by externally applied loads applied loads (1989 AASHTO)
f_{pe} = effective stress in the prestressing steel after losses (ksi) (1994 LRFD AASHTO)
f_{po} = stress in the prestressing steel when the stress in the surrounding concrete is 0.0 (ksi)
f_{ps} = average stress in prestressing steel at the time for which the nominal resistance of member is required (ksi)
f_{se} = effective steel prestress after losses
f_{si} = initial steel prestress before losses
f_{sy} = yield stress of non-prestressed conventional reinforcement in tension (ksi)
f_v = stress in transverse web reinforcement (ksi)
f_y = specified minimum yield strength of reinforcing bars (ksi)
I = moment of inertia about the centroid of the cross section
l_d = development length (in)
l_e = embedded length (in)
l_t = transfer length (in)

M_{cr} = moment causing flexural cracking at a section due to externally applied loads
M_{max} = maximum factored moment at a section due to externally applied loads
M_u = factored moment at the section (kip-in)
N_u = applied factored axial force taken as positive if compressive (kip)
P = pullout force
P_1 = pullout force at adhesion bond failure
P_e = effective prestress force
P_n = nominal axial resistance of a strut or tie (kip)
P_t = pullout force at mechanical bond failure
S_b = lower section modulus
s = spacing of reinforcing bars (in)
U_1 = bond stress at adhesion bond failure
U'_1 = U_1 divided by the square root of f'_c
U_m = maximum bond stress
U_p = bond stress at free end movement
U_t = bond stress at mechanical bond failure
U'_t = U_t divided by the square root of f'_c
U_{tl} = average bond stress over transfer length
U_s = maximum bond stress
V_c = nominal shear strength provided by concrete
V_{ci} = nominal shear strength provided by concrete when diagonal cracking results from combined shear and moment
V_{cw} = nominal shear strength provided by concrete when diagonal cracking results from excessive principal tensile stress n web
V_d = shear force at section due to unfactored dead load
V_i = factored shear force at section due to externally applied loads occurring simultaneously with M_{max}
V_n = nominal shear resistance of the section considered (kip)
V_p = component in the direction of the applied shear of the effective prestressing force, positive if resisting the applied shear (kip)
V_s = nominal shear strength provided by shear reinforcement
V_u = factored shear force at section (kip)
v = factored shear stress (ksi)
Y_t = distance from centroidal axis of gross section, neglecting reinforcement, to extreme fiber in tension
α = angle of inclination of transverse reinforcement to longitudinal axis (deg.)
β = factor relating effect of longitudinal strain on the shear capacity of concrete, as indicated by the ability of diagonally cracked concrete to transmit tension
ϵ_1 = principal tensile strain in cracked concrete due to factored loads
ϵ_x = longitudinal strain in web reinforcement on the flexural tension side of the member.
θ = angle of inclination of diagonal compressive stresses (deg)
θ_s = angle between compression strut and longitudinal axis of the member in a shear truss model of a beam (deg)
σ_s = the smallest angle between the compressive strut and adjoining tension ties (deg)
ϕ = resistance factor

ABSTRACT

Two full scale high performance prestressed concrete AASHTO type II girders of compressive strengths 8,000 psi and 12,000 psi were used in this study. The girders were subjected to both fatigue and static loading. Each girder was first subjected to a constant amplitude cyclic loading ranging from 12 kips to 44 kips and subsequently tested under static loading until failure. The static testing was performed to evaluate the effect of fatigue loading on the ultimate shear and flexural capacity of the girder. The 8000 psi girder and the 12000 psi girder were subjected to 2 x 10^6 cycles and 3 x 10^6 cycles, respectively. In addition to the full scale testing, a thorough non-linear *Finite Element Analysis* was also conducted on simulated numerical models aiming at investigating the distribution of internal and external stresses in both beams. The FEA results conformed with the full scale testing in terms the shear and flexural capacity of the beams. Also, the FEA beams indicated the effect of buildup stresses at the south end even before commencing the shear test at that end. This testing practice on full scale beams should further be investigated for possible reduction in the actual shear capacity as compared with various codes. The FEA results were compared with both the full scale test results and results obtained by using the pertained AASHTO-LRFD and the ACI codes for the shearing capacity of prestressed concrete beams. The ACI code was found to provide better prediction of the shear capacity of the two high strength concrete beams. However, the ACI code still overestimated the shearing capacity after fatigue loading by about 18% to 10% for the 8,000 psi and 12,000 psi girders, respectively.

CHAPTER 1

INTRODUCTION

1.1 PROBLEM STATEMENT

Highway bridges and pavements are subjected to daily cycles of repetitive loading. After a large number of such cycles of loading the stiffness of the bridge deck or girders reduces significantly such that failure might occur at a considerably less load than the design load. This type of failure is what is known in mechanics of materials as fatigue failure.

In the State of Florida, there are a total 8,100 concrete bridges. About 250 of these bridges are structurally deficient and 1,500 are functionally obsolete (1). The major factors that affect the performance and durability of these concrete elements under cyclic loading are cracking (crack initiation and propagation) and premature distress. It is believed that improving the efficiency of such structures can be achieved by controlling the cracking tendency of concrete elements. This, in turn, may be possible by improving the quality of concrete materials and construction.

The use of prestressed concrete beams in bridge superstructure has increased dramatically in the past 30 years. At the same time, strength reduction factors and load limits have been increased, effectively reducing load margins for existing bridges. As a result, the limit state of fatigue failure is now a more important consideration in the analysis of existing bridges and the design of new bridges. There are several reasons given by the ACI committee 215 to indicate that fatigue strength of concrete is an important design consideration; these include:

1. Use of concrete members in different types of applications which undergo continuous repetition of load, such as prestressed concrete in railway and highway bridges, reinforced concrete pavements, marine structures.
2. Widespread use of ultimate strength design procedures and higher performance materials.
3. New recognition of the effects of repeated load on a member, which lead to increase in the crack widths and deflections in comparison to identical static load (2).

In addition, the continuously increasing traffic volume and magnitude of loads, especially on railway and highway bridges, requires a special attention towards fatigue characteristics of these structures.

1.2 HIGH PERFORMANCE CONCRETE

In the 1950's, 4000 to 5000 psi (27.5 to 34.5 MPa) strength was used for prestressed concrete in the United States (3). Prior to the 1970s concrete designers were content with the utilization of 5000 and 6000 psi (34.5 and 41 MPa) strength as easily attainable compressive strengths for structural members. Later in the early 1980s it was demonstrated that the application of 9000 to 11,000 psi (62 to 76 MPa) strength concrete was not only practical but also economically feasible. The maximum attainable strength of precast concrete bridge girders varies with the quality of aggregate and with plant production techniques. Now materials for prestressed concrete bridge girders are usually specified by the AASHTO *Standard Specifications for Highway Bridges (9).*

Apart from the increase in compression capacity, high performance concrete has additional advantages: a considerable increase in concrete durability and an increase in flexural capacity. The disadvantages of high performance concrete are that the stiffness of the concrete is reduced. Utilization of high performance concrete presumes lighter weight and possibly thinner component members. There is a practical limit on how much the thickness of walls, flanges and webs can be reduced. As the cross sectional area reduces and mass decreases, there is a possibility of increased vulnerability to vibration and global and local buckling problems. Recent studies by Ngab et al (1980), Carrasquillo et al (1981) and Smadi et al (1982) concluded that high-strength concrete possesses higher tensile strength, higher elastic modulus, higher sustained stress level and lower creep coefficient, but less ductility. This can result in a design which is safe in collapse but in which cracking and/or deflection become more critical particularly under long term sustained and fatigue loading.

1.3 BACKGROUND ON FATIGUE CRACKING OF CONCRETE

1.3.1 Fatigue of Concrete

Failure of concrete under cyclic fatigue loading results from progressive micro-cracking which leads to progressive damage in the concrete indicated by the increase in the level of strain at f_{min} and f_{max}. The fatigue failure of concrete when part of a flexural member is very unlikely to occur. The fatigue strength of concrete decreases almost linearly with increasing the number of cycles when plotted on a semi-log scale. Concrete has a very substantial ability to resist many cycles of repeated loading. Consequently, the fatigue resistance of

prestressed concrete structures will typically be governed by the fatigue of reinforcement rather than fatigue of concrete.

1.3.2 Fatigue of Reinforcement

The fatigue failure of a reinforcing bar usually starts with the formation of a small crack at the surface of the bar. As the load is cycled the initial crack will propagate until eventually the remaining area of the bar cannot carry the load and failure occurs. The deformations on the reinforcing bar act as stress raisers and so are usually the location where fatigue failure is initiated. The fatigue characteristics of reinforcement are usually defined in terms of the relationship between the stress range and the number of cycles of such loading required to cause such a failure (*S-N* curves or Wohler diagrams).

1.4 RESEARCH OBJECTIVE

The primary objective of this study is to look at the effect of fatigue by dynamically loading two AASHTO Type II girders, (of compressive strengths 8,000 and 12,000 psi) in the laboratory and to compare the results obtained from fatiguing followed by static loading with the results of direct static loading on the solid beams. A third girder of strength 10,000 psi was also cast and will be tested without the slab. This study includes formulating and running theoretical *finite element models* and comparing the results with the experimentally obtained results. A schematic diagram of the current investigation is presented in Fig 1.1.

A previous study on the shear and cracking performance of High Performance Prestressed Concrete AASHTO Type II girders was conducted by John Poulson (16). The current study is aimed at investigating the effect of fatigue loading on similar beams with respective strengths. This research undertakes to load the beams dynamically and then test them statically to see the effect of the fatigue on the strength and performance of the beam.

The parameters which were studied are the effect of fatiguing on the stiffness of the beam, and a comparison of the stress levels between, the theoretical model, the statically tested beam (solid beam) and the dynamically tested beam. Also the obtained shear values were compared with the predicted values of the ACI code, the AASHTO code and the AASHTO LRFD code.

1.5 REPORT ORGANIZATION

This report is organized into 5 main chapters. Chapter 1 is the introduction. The problem statement and the necessity for this experimentation program is presented along with the objective of the experiment. Also this deals with the background on the key terms used throughout this report. Chapter 2 presents an extensive survey of all the related literature which has been used to prepare this report.

Chapter 3 is divided into three parts. The first part deals with the presentation of a detailed description of the sample preparation. The instrumentation is covered in the second part and the testing program, the equipment used and problems faced are described in the third part.

The analysis and results are presented in Chapter 4. A discussion is also presented along with the results. Also the directions for further research are speculated upon in this chapter. The conclusion and recommendations are presented in Chapter 5.

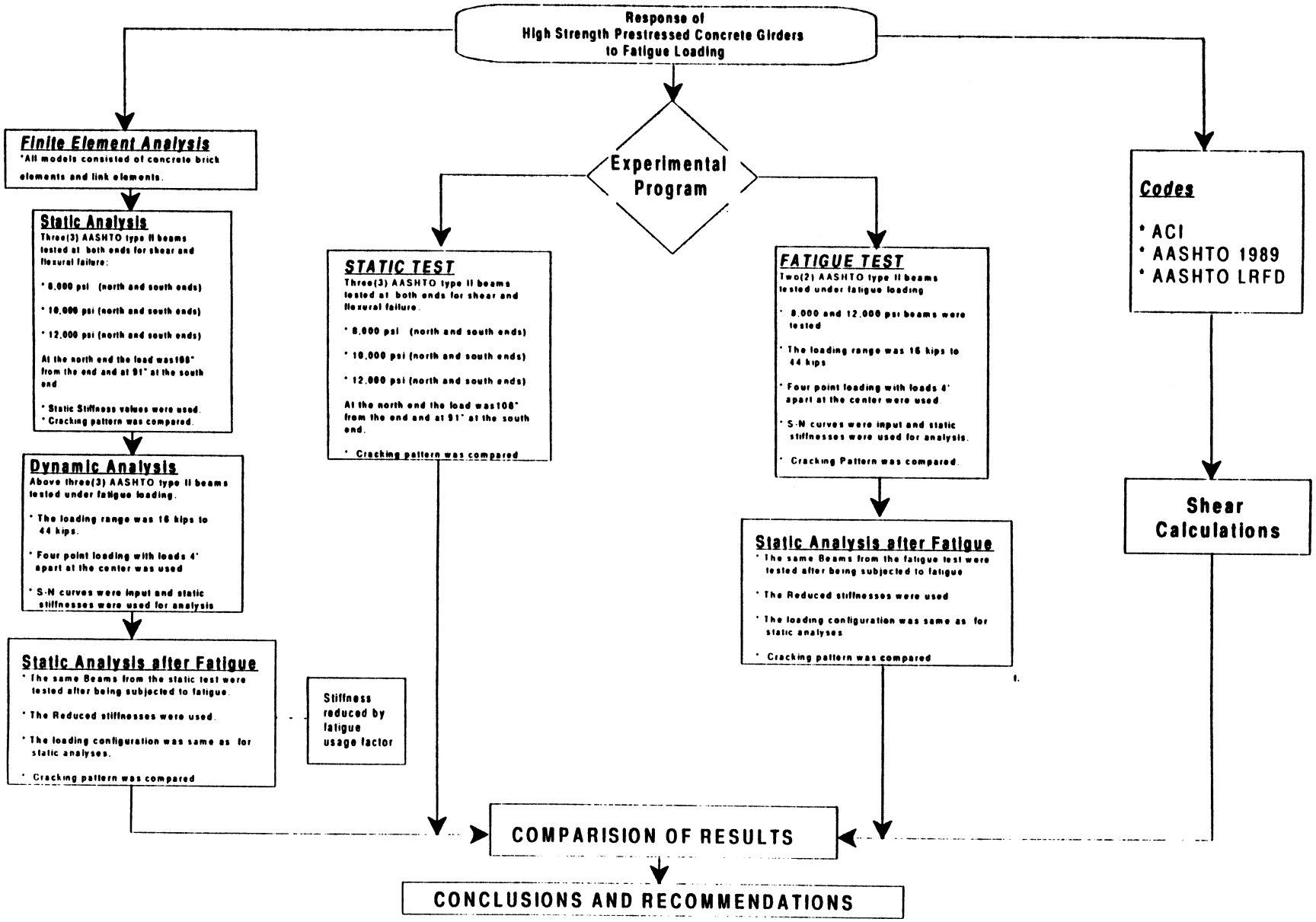

Fig 1.1 Schematic of Current Investigation

CHAPTER 2
LITERATURE REVIEW

2.1 FATIGUE OF PLAIN CONCRETE

Hilsdorf and Kesler (1966) extensively investigated the fatigue behavior of concrete under variable stress levels. their experiment was based on varying the maximum and minimum stress levels. During testing or when the applied loads are interrupted by rest periods, the performance of fatigue strength is enhanced. In the same manner, the influence of rest periods is remarkable at low stress levels. They also concluded that the sequence of applied repeated loading has considerable effect on the behavior such as, when low stress level is followed by high stress level, fatigue life is decreased and vice versa.

Shah and Chandra (1970) reported that for load ratios of 70% and below, a fairly stable and uniform small rate of crack growth developed, but for 80% and above, a rapid increase in cracking prior to failure was observed. They reported that increase in cracks in size and number was merely due to progressive micro cracking.

Nordby (1958) summarized that the slope of the loading curve changes from initially convex upward to essentially straight after a few cycles and finally becomes concave upward near failure. Alliche and Francois (1987) generalized that the strain in concrete increases rapidly at the beginning of the experiment and then increases slowly at each cycle leading to fracture by instability without visible cracking.

Holmen (1982) proposed that the decrease in concrete stiffness maybe considered as an indicator of the degree of damage experienced by the concrete. Aziz (1987), theorized that decrease in the material stiffness is high at the initial load application and changes to small and uniform and then starts to decrease significantly prior to failure. the rate of decrease is higher for lower strength concrete.

2.2 FATIGUE OF REINFORCED CONCRETE

J. M. Lovegrove and Salah El Din (7) tested reinforced concrete beams of different sizes and reinforcement arrangements. In their analysis curvature and deflection were presented as ratios of the initial values and a unique relation was obtained between each of these ratios and logarithm of the number of load repetitions. They found that the deflection, curvature and maximum crack width increased with increase in the

number of load cycles. They suggested equations for calculating the long-term-cyclic deflection and average curvature which are:

$$\Delta_n = 0.225\ \Delta_o .\ \log n \qquad (1)$$

$$k_n = 0.225\ k_o\ .\ \log n \qquad (2)$$

where Δ_n is the deflection and k_n is the curvature.

The values obtained by using these equations matched with experimental results and previous results.

2.3 FATIGUE OF PRESTRESSED CONCRETE

2.3.1 High Strength Concrete

Charles Dolan and Robert LaFraugh (8), report that a survey of producer members was conducted by the PCI Committee on High Strength Concrete, in 1990, to determine the use, benefits and liabilities of high strength concrete in the precast concrete industry. The survey requested producers to define their compressive strength value for high strength concrete and to identify the highest strength concrete which they felt they could produce. The average definition for high strength concrete was approximately 1000 to 2000 psi (6.9 to 14 MPa) greater than the average production strength which was about 5500 psi. The definition of high strength concrete was about 1000 psi (6.9 MPa) less than the local industrial capability. The maximum strength capability for prestressed concrete was reported to be 12,000 psi (83 MPa). The 12,000 psi testifies to the restraints imposed by initial transfer strength requirements. These restraints have two effects on the concrete mix and strength. First, the transfer strength requirement usually controls the mix design. Second, high transfer strengths require accelerated curing, which produces lower ultimate strength. Of the prestressed members requiring early transfer of prestress to the member, the highest release strengths are for bridge girders. Bridge girders have consistently have high design strengths. Bridge girders become significant because a large number of responses received for different members were for bridge girder members. This suggests that state and federal departments of transportation specifications may significantly impact all precast and prestressed concrete production.

Reduction in the size of the prestressed concrete members and increased durability are listed as the advantages of high strength concrete. Among the use of high strength concrete for construction, bridges girders

accounted for 40% and parking garages for 20% which was a result of increased durability. At the same time there was an expression of concern that increased cost and quality control were problems for high strength concrete.

Finally it is concluded by the authors that use of high strength concrete is unlikely to advance quickly without a clear economic incentive and a comfort level in the industry that the product can be confidently produced. Also, bridge girders represent the state-of-the-industry and may serve as the best product to showcase the industry's ability to advance the use of higher strength concrete.

Susan Lane and Walter Podolny, Jr. (3) suggest that some type of categorization or classification of concrete on the basis of compressive strength is needed as a standard in the United States. They say that specific design rules and production procedures could then be developed for each category. They cite examples from Finland and the classification given by the Strategic Highway Research Program (SHRP). They mention increase in compressive strength, in durability and flexural strength as advantages of high strength concrete. On the disadvantage side they cite the reduced stiffness and potential instabilities from the decreased stiffness. They recommend that more funding be given to experimental bridges constructed with high strength concrete.

2.3.2 Prestressed Concrete

Roller, Martin, Russell and Bruce Jr. (10) conducted an experimental evaluation of pretensioned prestressed bridge girders manufactured with high strength concrete. Three 70 ft long and 54 in. deep bulb-t girders were tested. The design compressive strength was 10,000 psi (69 MPa). One girder was tested in flexure with a slab deck and one was tested in flexure without the slab. The first girder was then tested for shear at both ends and the second girder was tested at one end. The third girder is under test for long term evaluation after which it will be tested for flexure. It was concluded that the full width of the slab deck was effective. This research primarily concentrates on the evaluation of the feasibility of utilizing high strength concrete in the design and construction of highway bridge structures.

In an exploratory study at The University of Texas at Austin by Kreger, Bachman and Breen (11), it was concluded that the ACI and AASHTO code specification provisions for prestressed concrete are inadequate for predicting shear fatigue strength of pretensioned concrete beams. Three beams were tested under an average loading range of 10-75 kips. From their study they suggest that shear fatigue can be minimized in fatigue critical regions by greatly reducing the assumed concrete contribution (V_c) to shear fatigue and load distribution factors. It was observed that flexural cracking occurred under fatigue loading conditions at a maximum bottom fiber tensile stress of slightly less than $6\sqrt{f'_c}$. The authors suggest that cracking might have

been induced by cyclic creep effects. They also concluded that following formation of inclined cracks, the apparent concrete contribution to resistance of shear under fatigue loading conditions decreased appreciably with increasing number of load cycles. It was also noticed that propagation of inclined web cracks into the bottom flange led to strand slip at beam end, resulting in accelerated flexural fatigue.

In another study on fatigue strength of prestressed concrete T-beams with welded wire fabric as shear reinforcement, Douglas W. Riedel of Rice University, Texas (12), it was concluded that a reduction in the amount of shear reinforcement had no visible effect on the fatigue strength of the section. They also concluded that fatigue failure of the beams was not caused due to fracture of the shear reinforcement but it was caused due to the fatigue fracture of the prestressing strands. They also found that the contribution of concrete in shear during static testing was found to be approximately 40% greater than the code predicted value.

Rabbat, Kaar, Russel and Bruce (13) conducted tests on full sized AASHTO Type II girders. They concentrated on the difference in the effects of having draped strands and blanketed strands. They tested three beams by having the tension of $6\sqrt{f'_c}$ in the bottom concrete fibers at mid span. The other three beams had zero tension in the bottom fibers at mid span. They found that the beams under the larger load failed at about 3 million cycles where as the other beams went on till 5 million cycles. They concluded that fatigue should be considered in the design of prestressed structures.

Russsel and Burns (14) tested three full sized Texas Type C pretensioned concrete with 10,000 psi concrete formed composite girders by the addition of deck slabs with 6,000 psi concrete. Two of the girders contained debonded strands and the third one contained draped strands. The span was 48 ft. They concluded that the elastic properties of pretensioned girders made with high strength concrete are similar to the elastic properties of normal strength concrete. Both flexural cracking and web shear cracking were predicted by assuming flexural cracking at $7.5\sqrt{f'_c}$ and web shear cracking at $4\sqrt{f'_c}$ if the effects of lab shrinkage are included. Also it was concluded that shrinkage of the slab was an important consideration affecting flexural load cracking and web shear cracking. Slab shrinkage may also significantly reduce the fatigue life of the pretensioned beams. They also suggest that debonded strands can be used safely by limiting the debonded length to regions where flexural cracking would not occur and by limiting propagation of web shear cracks with longitudinal and vertical shear reinforcement.

Price and Edwards (15) tested post-tensioned I-beams to investigate the fatigue strength of mild steel stirrups in shear. Each beam was precracked before the cyclic load was applied. The beams were tested using a minimum load of 25% of the ultimate shear strength and different maximum loads of 63%, 70%, and 77%. In all cases the beams failed due to the fatigue fracture of the stirrups. The beams under the smallest loading

range (25% to 63%) went to 3 million cycles. It was concluded that shear failures in prestressed beams with diagonal cracks may occur under fatigue loading due to the fracture of the web reinforcement. They also concluded that the beams may endure a large number of cycles after the initial fracture due to redistribution of stresses within the shear reinforcement.

2.5 SHEARING CAPACITY OF PRESTRESSED GIRDERS

The 1989 AASHTO code, ACI code and the 1994 LRFD code were reviewed and used as a comparison for the shear test results. Each code divides the ability of a prestressed member to resist shear into a concrete component and steel component. All of the codes use a truss analogy to predict the steel contribution. The current ACI and AASHTO codes are very similar. However, the ACI code offers an equation that may be used as a simplification to more detailed equations used to determine the concrete contribution. The shear section of the AASHTO LRFD code is based on a different theory than the shear sections of the ACI and 1989 AASHTO codes. The AASHTO LRFD code offers a significant departure from the current design codes in the determination of the concrete component. The theory used in the LRFD code also modifies the calculation of the steel component of the shear strength.

The truss analogy was initially developed by Ritter in 1899 to explain the interaction between concrete and reinforcing steel in resisting the shear forces (16). The truss model assumes that the web reinforcement acts as vertical tension members, diagonal compressive forces are resisted by the concrete and longitudinal reinforcement acts as tension members to balance the forces. Mörsch refined the truss model in the early 1900s. Mörsch assumed the diagonal compressive stresses, and thus the inclined cracks, to be inclined at 45°. Using this assumption and equilibrium, the shear force carried by vertical stirrups, V_s, is:

$$V_s = \frac{A_v F_y d}{s} \qquad (3)$$

Mörsch recognized the angle of the stresses was very significant in determining how the stresses would be carried by the member. Mörsch did not see a way to accurately predict the angle of inclination and thus he made the conservative assumption of 45°. If the angle of inclination, θ, was not assumed to be constant, the shear force carried by the stirrups would be:

$$V_s = \frac{A_v \cdot f_v \cdot d \cdot \cot\theta}{s} \qquad (4)$$

2.4.1 1989 AASHTO Code

Section 9.20 of the current AASHTO code (1989) gives the shear specifications for prestressed concrete girders. According to the code, the shear is carried by both concrete (V_c) and steel ie; the web reinforcement (V_s). The code specifies that

$$V_u \leq \phi (V_c + V_s) \qquad (5)$$

where V_u is the shear caused by the factored loads and ϕ is the factor of safety.

Concrete could either fail due to flexure -shear failure or due to web-shear failure. The difference between the two is that flexure-shear failure is caused by an initial flexural crack that extends and produces a shear crack. Web-shear failure is caused by a shear crack in the web of the girder. Following the AASHTO code, both the flexure-shear strength (V_{ci}), and the web-shear strength are calculated at some sections. The lower strength at any section is the value that controls the design. Thus, V_c is taken as the lower of V_{ci} and V_{cw}.

The code gives the following equations to compute flexural-shear strength V_{ci}:

$$V_{ci} = 0.6 b' d \sqrt{f'_c} + V_d + \frac{V_i M_{cr}}{M_{max}} \qquad (6)$$

$$M_{cr} = \frac{I}{Y_t} (6\sqrt{f'_c} + f_{pe} - f_d) \qquad (7)$$

$$V_{ci} > 1.7 b' d \sqrt{f'_c} \qquad (8)$$

In the above equations f_{pc} and f_d are calculated from the non-composite section and the remaining terms are calculated from the composite section.

The code gives the following equation to determine the web-shear strength V_{cw}:

$$V_{cw} = b' d (3.5\sqrt{f'_c} + 0.3 f_{pc}) + V_p \qquad (9)$$

The code uses the 45 degree truss analogy and an upper limit for the steel contribution to determine the shear strength provided by the reinforcement at any location:

$$V_s = \frac{A_v F_y d}{s} \qquad (10)$$

$$V_s < 8 b' d \sqrt{f'_c} \qquad (11)$$

The calculations were made using a factor of safety of unity. A factor of safety of one is appropriate for the laboratory testing where the results will be used to verify the analytical model.

2.4.2 ACI Code

The ACI code also specifies that the total shearing forces are carried in part by the concrete and in part by the steel. The force carried by the concrete, V_c and the force carried by the steel, V_s combine to give the total resistance of the prestressed member.

The ACI code gives a simplified method to calculate V_c. The equations used are:

$$V_c = (0.6\sqrt{f'_c} + 700 \frac{V_u d}{M_u}) b_w d \qquad (12)$$

where:

$$2\sqrt{f'_c} b_w d < V_c < 5\sqrt{f'_c} b_w d \qquad (13)$$

The ACI code also uses the 45 degree truss analogy model with an upper limit to compute the steel contribution to resisting the shear forces:

$$V_s = \frac{A_v f_y d}{s} \qquad (10)$$

$$V_s < 8 b_w d \sqrt{f'_c} \qquad (11)$$

As in the AASHTO Code calculations, the factor of safety is taken as unity.

2.4.3 1994 AASHTO LRFD Code

The AASHTO LRFD code offers a different methodology to design prestressed girders for shear. The LRFD code provisions for shear have been developed from the modified compression field theory, further called the MCFT theory. This theory was based on Wagner's tension field theory that explained the angle of inclination of the principal stresses in steel members. The MCFT also considers the concrete's ability to resist tensile forces between cracks. For low and high values of θ, the web reinforcement and the longitudinal reinforcement will be highly strained, respectively. Knowing θ, more detailed calculations of the shear forces can be performed. Ultimately, the theory should result in more accurate predictions of V_c and V_s. the shearing capacity of prestressed girders is given by the LRFD code as:

$$V_n = V_c + V_s + V_p \qquad (14)$$

$$V_n = 0.25 f'_c \cdot b_v \cdot d_v + V_p \qquad (15)$$

$$V_c = 0.0316 \beta \sqrt{f'_c} \cdot b_v \cdot d_v \qquad (16)$$

$$V_s = \frac{A_v f_y d_v (\cot\theta + \cot\alpha) \sin\alpha}{s} \qquad (17)$$

The LRFD AASHTO code gives additional equations to compute two factors, v and ϵ_x, which are used to determine θ and β beta using charts or tables provided in the code.

$$v = \frac{V_u - \phi V_p}{\phi \cdot b_v \cdot d_v} \qquad (18)$$

$$\epsilon_x = \frac{\frac{M_u}{d_v} + 0.5N_u + 0.5V_u \cdot \cot\theta - A_{ps} \cdot f_{po}}{E_s \cdot A_s + E_p \cdot A_{ps}} \qquad (19)$$

where:

$$f_{po} = f_{pe} + \frac{f_{pc} E_p}{E_c} \qquad (20)$$

if ϵ_x is negative then ϵ_x is multiplied by a factor F_ϵ

$$F_\epsilon = \frac{E_s \cdot A_s + E_p \cdot A_{ps}}{E_c \cdot A_c + E_s \cdot A_s + E_p \cdot A_{ps}} \qquad (21)$$

2.5 BONDING IN PRESTRESSED CONCRETE GIRDERS.

Hognestad and Janey (1954) studied the bond between a smooth single wire strand and concrete. They concluded that there are three factors that contribute to the bonding between the prestressing strands and the concrete. They are:

1) Chemical adhesion between the two media,

2) Frictional forces, and

3) Mechanical forces.

The chemical adhesion is lost as soon as there is a slip between the two media. So in the transfer of the prestressing force from the strands to the beam, only the frictional and mechanical forces are present.

Hanson and Kaar's (1959) noted that mechanical resistance is probably of little importance in a single smooth wire, but it may be a significant factor when considering a seven wire strand. They found that the mechanical interlock between the two media can support additional loads in a prestressed beams after a general

bond slip, when adhesion and friction have been lost. They concluded that mechanical bond resistance is an extremely important characteristic of bond performance.

CHAPTER 3

EXPERIMENTAL PROGRAM

Three (3) full scale AASHTO Type II high performance concrete girders were prepared for the purpose of this study. The concrete strength used for these beams were; 8,000 psi, 10,000 psi and 12,000 psi. The reinforcement provided was in accordance with the current AASHTO provisions. All the shear reinforcing (C) bars and the confinement (D) bars were prepared and instrumented at the FAMU-FSU College of Engineering and then transferred to the yard at DURASTRESS in Leesburg, Florida. These instrumented bars were installed and then the girders were cast in the DURASTRESS yard and then transported to the Florida Department of Transportation (FDOT) Structures Research Laboratory for testing.

3.1 INSTRUMENTATION

3.1.1 Instrumentation of the Rebars

Some of the C-bars and D-bars were instrumented before placing them in the bed for casting the beam. A flat smooth surface was needed to place the strain gages on the bars. To achieve this, each bar was ground using a rotary grinder to create a surface that was about 3 inches long and 3/8 inches wide. The surface was then cleaned first with an acid solution and then neutralized with a basic solution. This was necessary to eliminate any rust or dust which might have settled on the surface. The gage was then taken out of the packing and laid on a glass plate, and adhesive applied to the surface (sticking surface) of the gage. The adhesive used was supplied by Micromeasurements and called M-bond AE 200. The gages used were of Micromeasurements with Gage Factor of 2.055 . Each gage was fixed on the cleaned surface of the reinforcing bar. After attaching the gage on to the rebar it was secured by placing a rubber pad on it and tightening it using a clamp. The bar was then left undisturbed for 24 hours during which time it adhered securely to the bar. Lead wires were then connected to the strain gage which were later used to connect the gages to the data acquisition system. Splicing

tape was used to wrap around the instrumented portion of the bar for protection. To protect the gage from moisture and dust the taped portion of the bar was the sprayed with an enamel coat, M-coat, also supplied by Micromeasurements. The location of the instrumented bars in the beam is shown in Fig 3.2. These instrumented bars were then transported to the DURA STRESS yard in Leesburg, Florida, where they were arranged in the bed for casting the beam.

3.1.2 Instrumentation of the Prestressing Strands

The prestressing strands used were seven wire strands with nominal diameters of 1/2 inch. They had a minimum tensile strength of 270 ksi. The strands were placed in the casting bed and tensioned to approximately 31,000 lb per strand (202.5 ksi) with a hydraulic jack. The applied load was monitored by a pressure gage attached to the hydraulic jack. A total of 16 strands in the lower flange and 2 strands in the top flange were used. Embedded gages were installed on the center strand of the 16 strands in the lower flange to measure strain in the concrete. The gages used were TML gages of type PMS-60. The gage length was 60 mm and the gage factor was 2.06. A total of 8 embedded gages were used for each end of the beam, for each beam. The first gage at each end was located at 6 inches from the end and the rest of the gages were placed at 12 inch spacing. The gages were secured to the strand using plastic cable ties. The lead for each gage was then led to the top of the girder.

3.2 SAMPLE PREPARATION

After the embedded gauges were secured, the shear reinforcement was tied to the strands, carefully, avoiding the gages. Forms were then placed around the strands and concrete was poured. The concrete used was made on site by DURA STRESS, Inc.. Several cylinder samples were made out of this concrete. These were used to determine the average strength of the concrete for each beam. The results obtained from these compression tests are shown in table 3.1.

The strands were ready to be released when the concrete had reached 70 % of its design compressive strength. This generally took two to three days. The strands were released by flame cutting. The strands were cut at the ends of each girder. The releasing process was divided into four stages of four strands per stage.

The girders were then transported to the FDOT Structures Laboratory at Tallahassee, Florida. 8" x 42"

concrete slabs were poured on these girders. These slabs had the minimum reinforcing steel specified in the AASHTO code. The concrete used for the slabs had a design strength of 6000 psi and was provided by Florida Mining and Materials in Tallahassee, Florida.

The girder was then moved on to two concrete blocks with rubber pads to be used as supports for the beam. The beam was simply supported on these pads which were placed at 6 inches from each end of the beam. This made the effective span of the beam equal to 40 ft. The beam was then instrumented.

3.2.1 Instrumentation of the Girder

In addition to the internal gages inside the beam other surface gages were also installed on the beam to measure the strain in the concrete at different sections. The critical section along the center of the beam was completely instrumented with gages. The gages used for surface instrumentation were PL-60-11 with gage length 60 mm and with gage factor 2.10. Gages were also placed along the bottom flange where the beam was expected to crack in flexure.

A total of 5 deflection gages were placed under the beam to note the deflection. Two of these were placed at each support, one was placed under the center section of the beam and two gages were placed under the section where the actuators were loading the beam.

In addition slip gages were also placed at one end of the beam with the four strands from the top being monitored for slip. No slip was expected in the other strands during fatiguing of the beam. The other end was not instrumented for slip as the beam was being loaded symmetrically. Figure 3.9 shows the external gauge layout for the whole beam for the fatigue test.

3.3 TESTING PROGRAM

The leads from all the gages were then connected to the data acquisition system. the system used was the MEGADEC, manufactured by OPTIM Electronics Corporation. The data acquisition system allowed the instantaneous reading of up to 64 gages. The system was calibrated and gage reading was first taken without any load on the beam to get the zero reading.

The testing program proceeded in two stages. Since the objective of the experiment was to find the effect of fatigue on the beam, the first stage consisted of dynamically loading the beam. This involved constant

monitoring of the beam to spot any cracks. The second stage consisted of testing the fatigued beam at both ends with the same configuration as was used in a previous study of cracking and shear capacity of high performance prestressed concrete girders under static loading, by John Poulson (16). The girders of strength 8,000 psi and 12,000 psi were tested in fatigue and then for static strength. The 10,000 psi girder is going to be tested statically without the slab.

3.3.1 Fatigue Testing

Before loading the beam the maximum moment capacity in flexure for the beams was determined. This was done from the results of the previous static study of similar beams (16). The beams were loaded to 90 % of their maximum flexural capacity.

This moment could not be applied with only the dynamic actuators. So the beam was first uniformly loaded at the rate of 1 kip/ft. This was done using 20 concrete blocks each weighing 2 kips. The blocks were 4' x 2' x 2'.

The hydraulic loading system consisted of two loading actuators. The actuators, attached to the loading frame were used to load the beam dynamically. The actuators were 4 ft apart from each other and were each 2 ft away on either side of the center of the girder. The frequency used was 1 Hz and the loading range was between 16 kips and 44 kips for each actuator. The frequency used to fatigue the 12,000 psi girder was 2 Hz. The data was transferred by a Megadec Data Acquisition System to an IBM PC.

The 8,000 psi girder was loaded to 2 million cycles and the 12,000 psi girder was run for 3 million cycles with this setup. So each fatigue test took about two weeks of continuous cycling. The data acquisition was set to take 128 scans/sec. Readings were taken at an interval of every one hour for the first three days. This was to see if the beam lost any stiffness due to sudden fatiguing. When not much change was observed, the reading frequency was decreased to 64 scans/sec and readings were taken twice a day. All this while, the beam was continuously monitored for any cracks or any change in the deflection or strain gage readings.

3.3.2 Static Testing

After the fatigue test reached 2 million cycles and no further change in the strain values or the stiffness seemed to be apparent, the test was stopped and the beam was prepared for a static test. Some additional

gauges were connected to the data acquisition system to match the gauge configuration with that of previous statically tested beams. The gauge configuration is as shown in Figures 3.10 and 3.11.

The testing procedure was suggested and performed in other experimental studies by FDOT. Two different loading configurations were used and were designated as North and South end tests. The north end test was done first. The major features of the north end test were the span length of 40 ft and the distance of the load from the support of 8.5 ft. The major features of the south end test were the span length of 27.5 ft and the distance between the load and support of 7.08 ft.

End - slip LVDTs were placed on all the 16 prestressed strands for both static tests. Deflection gages were also placed on the respective support, one at the load, and one at the center section of the girder. The schemes of these gages and other surface strain gages are shown in **Figures 3.10 and 3.11.**

Before starting the test all the gages were set to zero readings and checked for reading accuracy. The concentrated load was then applied by a hydraulic jack which was controlled by an electric pump. As the load was increased, readings were taken approximately every 10 kips of applied load. The load at the first crack was noted and the crack was marked on the girder surface. The load was then further increased and additional cracks were marked and the load recorded. The load was increased till it reached the ultimate failure load . This was noted by the inability of the girder to take any more load. The load was then taken off and periodic readings were recorded.

3.4 COMPUTER MODELING

3.4.1 About ANSYS FEA PROGRAM

The finite element software ANSYS was used to model the three beams. The ANSYS program works with a large database that stores all the input data and results in separate data files. The ANSYS program has two levels:

a) Begin Level

b) Processor level

The program is entered into from the begin level and goes to the processor level. At the processor level several routines are available each serving a specific function. The processor is a set of commands which are required to communicate with the program.

The building of a model in the ANSYS 5.1 program involves selecting geometric shapes to represent the model. Once the geometry is created it can be defined as a material and meshed into appropriate finite elements using elements form the element library of the ANSYS program. Loads can then be applied, type of analysis can be defined and the program can be run. The ANSYS program has a post processor form which the results can either be listed or plotted.

Element Description

Two types of elements were used for this analysis. The concrete, with the shear reinforcement included, was divided into finite elements using the ***SOLID65 3-D Reinforced Concrete solid element***. The prestressing strands were modeled using the ***LINK8 3-D Spar (or Truss)*** element.

3.4.2 Static Test Modeling

Features of SOLID65

SOLID65 is used for three-dimensional modeling of solids with or without reinforcing bars (rebars). The solid is capable of cracking in tension and crushing in compression. The element is defined by eight nodes having three degrees of freedom at each node; translations in the nodal x, y, and z directions. Up to three different rebar specifications can be used (each for a rebar in each direction). The concrete material is assumed to be isotropic. It is also assumed that whenever the reinforcement capability is used it is assumed to be smeared throughout the element. The stress-strain matrix [D] used for this element is modeled as:

$$[D] = [1 - \sum_{i=1}^{N_r} V_i^r]\ [D^c] + \sum_{i=1}^{N_r} V_i^R\ [D^r]_i \qquad (22)$$

where:

N_r = number of reinforcing materials (maximum of three, all reinforcement is ignored if MAT1 equals zero. Also if MAT1, MAT2, OR MAT3 equals the concrete material number, the reinforcement with that material number is ignored).

V_i^R = ratio of the volume of reinforcing material to the total volume of the element.

$[D^c]$ = stress-strain matrix for concrete.

$[D^r]_i$ = stress-strain matrix for reinforcement.

(The stress-strain matrices are functions of The stiffness and poisson's ratio).

Features of the Link Element

The three-dimensional spar element is a uniaxial tension-compression element with three degrees of freedom at each node: translations in the nodal x, y, and z directions. As in a pin-jointed structure no bending of the element is considered. The cross-sectional area and initial strain in the element are required to be input. The length of the element must not be zero and the area must not be negative. The stress is assumed to be uniform throughout the bar. The element stiffness matrix and the mass matrix are calculated.

Since both the elements are defined for non-linear analysis the ANSYS program used the Newton-Raphson method to solve the problem. The Newton-Raphson method iterates using the equation:

$$[K^T]\{\Delta u\} = \{F^{app}\} - \{F^{nr}\} \qquad (23)$$

where:

$[K^T]$ = the tangent stiffness matrix

$\{\Delta u\}$ = the displacement increment

$\{F^{app}\}$= the applied load vector

$\{F^{nr}\}$ = the Newton-Raphson restoring force (the loads generated by the current element stresses).

$\{F^{app}\} - \{F^{nr}\}$ is called the *residual*.

3.4.3 Fatigue Modeling

The ANSYS program can postprocess existing stress results to determine the fatigue usage factors for any solid or shell element model. For the program to calculate the fatigue usage factors an S-N curve must be input for the material. The ANSYS program use the ASME Boiler and pressure Vessel Code, Section III for guidelines on range counting, and cumulative fatigue summations by Miner's rule. The following steps are

followed in the fatigue calculations:

1. Each loading is compared to each other loading to compute a maximum alternating shear stress:

   A. First a vector of stress differences is computed:

$$\{\sigma\}_{ij} = \{\sigma\}_i - \{\sigma\}_j \qquad (24)$$

where: $\{\sigma\}_I$ = stress for loading ℓ_I

$\{\sigma\}_j$ = stress for loading ℓ_j

   B. Second, a stress intensity ($\sigma(i,j)$)is computed based on $\{\sigma_1\}_{ij}$.

   C. Then, the interim maximum alternating shear stress is:

$$(\sigma)^d_{ij} = \sigma_1(i,j)/2. \qquad (25)$$

   D. The maximum alternating shear stress is calculated by ANSYS:

$$\sigma^c_{i,j} = K_e\,(\sigma)^d_{ij} \qquad (26)$$

   where K_e is determined by the program based on the analysis type.

2. There are a total of (L-1) loading case combinations, where L is the number of loadings. These loadings are then sorted, with the highest value of $\sigma^c_{i,j}$ first.

3. Designate the highest value of $\sigma^c_{i,j}$ as occurring with loading ℓ_I, event k_i together with loading ℓ_j, event k_j. Let M_T be the minimum number of times that either event k_i or event k_j is expected to occur. Compute a usage factor following Miner's rule as:

$$f_u = \frac{M_T}{M_A} \qquad (27)$$

where: f_u = usage factor (output quantity PARTIAL USAGE)

M_A = number of allowable cycles at this stress amplitude level (obtained by entering the allowable alternating stress amplitude (S_a) versus cycles (N) table from the S_a axis and reading the allowable number of cycles M_A.

Next cumulatively add f_u to f_u^c, where f_u^c = output quantity cumulative fatigue factor usage. Then decrease the number of possible occurrences of both events k_i and k_j by M_T (so that one of them becomes zero).

4. Repeat step 3, using the next highest value of $\sigma^c_{i,j}$ until all of the $\sigma^c_{i,j}$ values have been exhausted. It may be seen that the number of times this cycle is performed is equal to the number of events (or less).

Table 3.1 28 Day Strength of the Girders

Design Strength (psi)	Beam Strength (psi)	Average Strength (psi)	Compression Modulus (psi)	Poisson's Ratio (μ)	Uniaxial Tensile Strength (psi)
8000	7994 8348 8490	***8277***	5,420,000*	0.2	630
10000	10134 10099 10011	***10081***	6,060,000*	0.19	700
12000	12230 11980 12008	***12073***	6,640,000*	0.18	770

* Large variations have been obtained in the compression modulus of high strength concrete. The values in the table represent the best average of the laboratory test results and some empirical relationships. These values were kept constant throughout the application of the FEA. For further information, compression modulus values obtained from testing as well as analytical formulas are shown below:

A. Laboratory Testing

I. From Axial Compression Testing (ASTM C-469)

$E_{(8,000)}$ = *5100 ksi*
$E_{(10,000)}$ = *5350 ksi*
$E_{(12,000)}$ = *5800 ksi*

II From ULTRASOUND Test

f'c (psi)	8000 psi	10,000 psi	12,000 psi
E (ksi)	*7040*	*7300*	*7450*

B. Comparable Empirical Relationships

III. From Compressive Strength

Using ACI 318 $Ec = 57{,}000(f'_c)^{½}$

f'_c	8000 psi	10,000 psi	12,000 psi
E	*5098 ksi*	*5700 ksi*	*6244 ksi*

Using ACI 363 $E_c = 40{,}000\,(f'_c)^{½} + 1.0x10^6$

f'_c	8000 psi	10,000 psi	12,000 psi
E	*4378 ksi*	*5000 ksi*	*5382 ksi*

Using CEB-90 (European Model) $E_c = 10\,(f'_c + 8)^{1/3}$

f'_c	8000 psi =55.158MPa	10,000 psi = 68.947 MPa	12,000 psi = 82.7364 MPa
E	5776 ksi = 39.8238 GPa	6169 ksi = 42.533 GPa	6516 ksi = 44.935 GPa

Using NS-3473 (Norwegian Model) $E_c = 9.5\,(f'_c)^{0.3}$

f'_c	8000 psi = 55.158 MPa	10,000 psi =68.947 MPa	12,000 psi = 82.7364 Mpa
E	4587.5 ksi = 31.63 Gpa	4906.4 ksi = 33.828 Gpa	5182.26 ksi = 35.73 GPa

1 psi = 6.89476x10^{-3} MPa

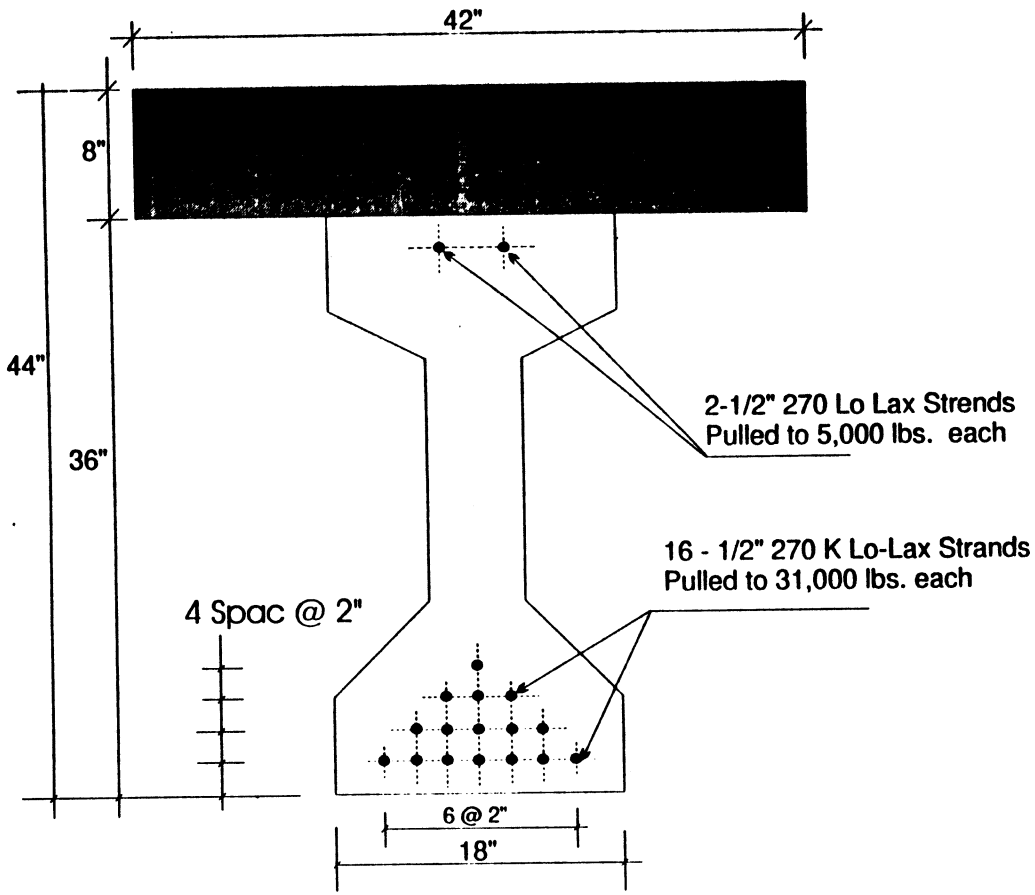

Figure 3.1 Cross-Section of Test Girders

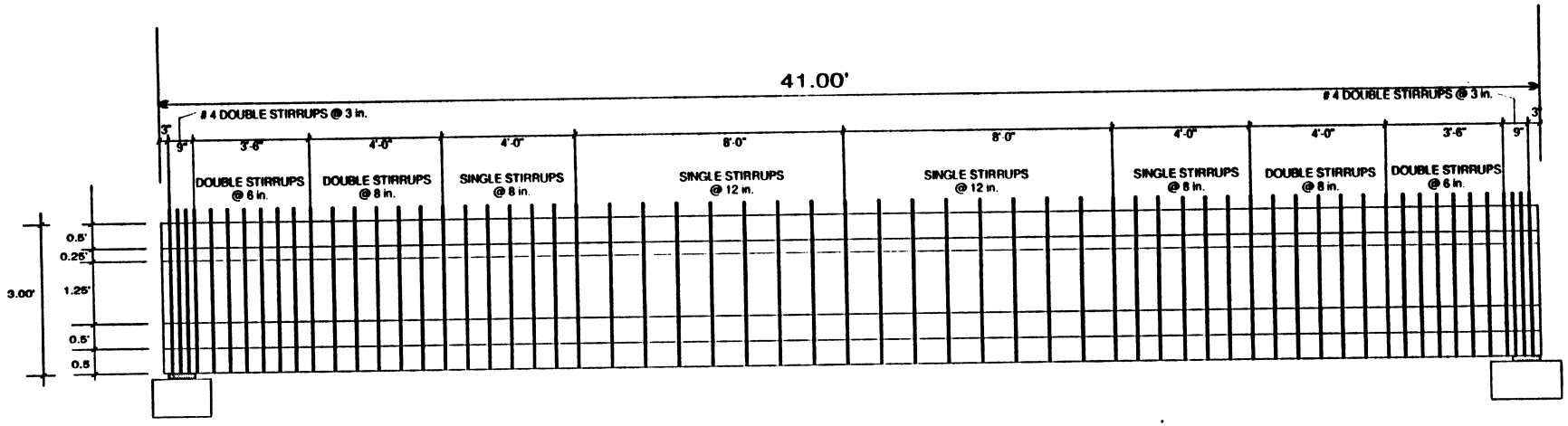

Figure 3.2 Web Reinforcement in R Girders

Fig 3.3 Prestressing Strand Layout in the Bed.

Fig 3.4 Layout of C-bars.

Fig 3.5 Layout of D-bars.

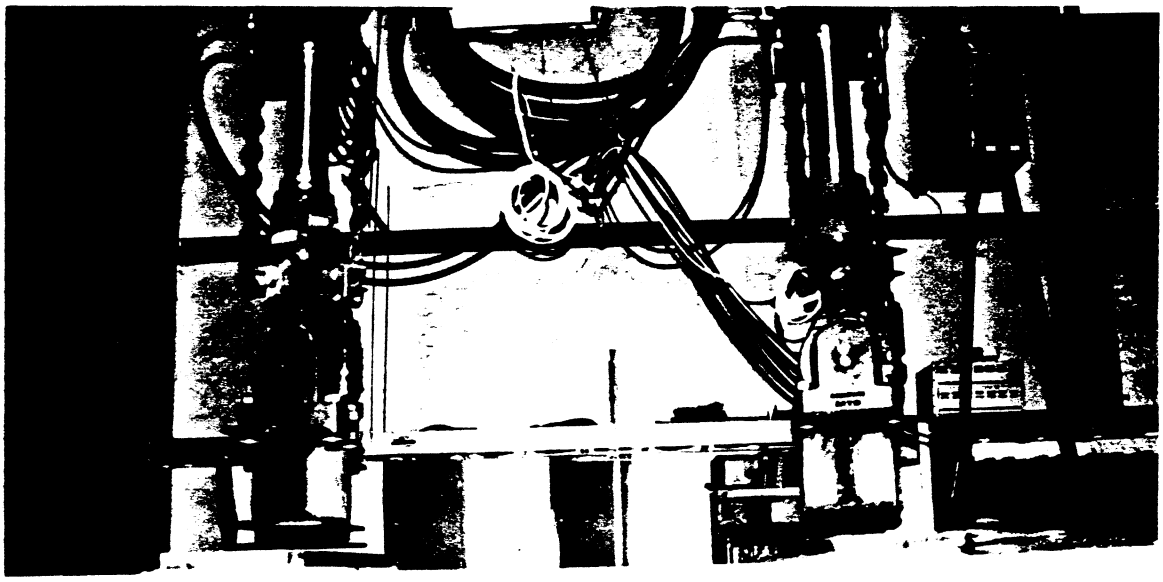

Fig 3.6 Laboratory Fatigue Test Setup.

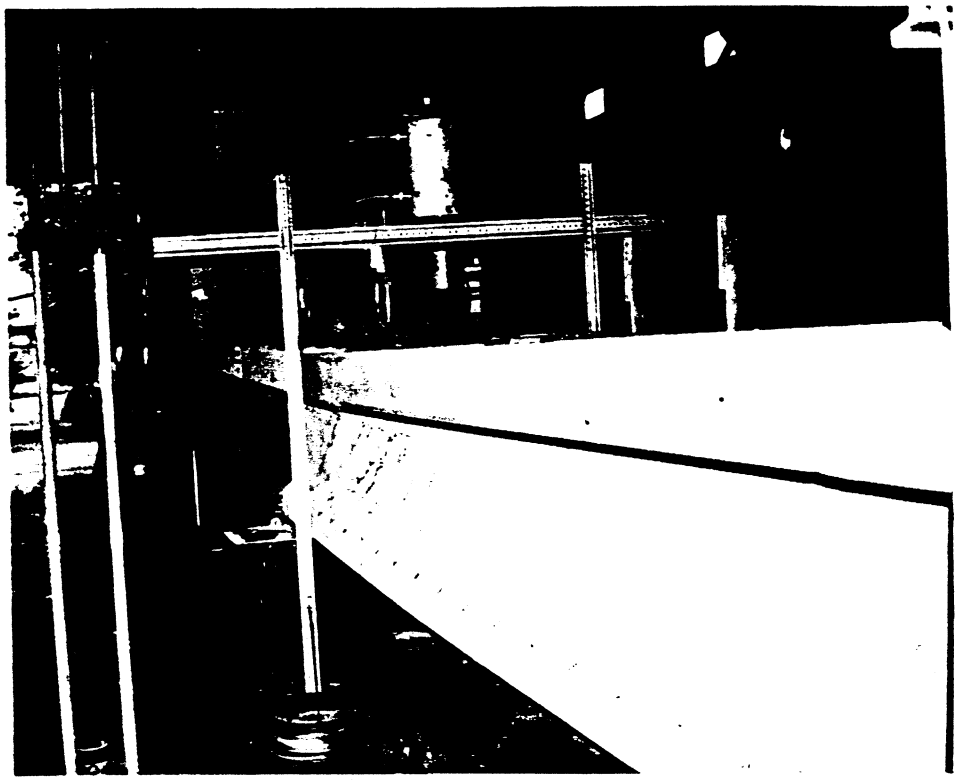

Fig 3.7 Laboratory Static Test Setup.

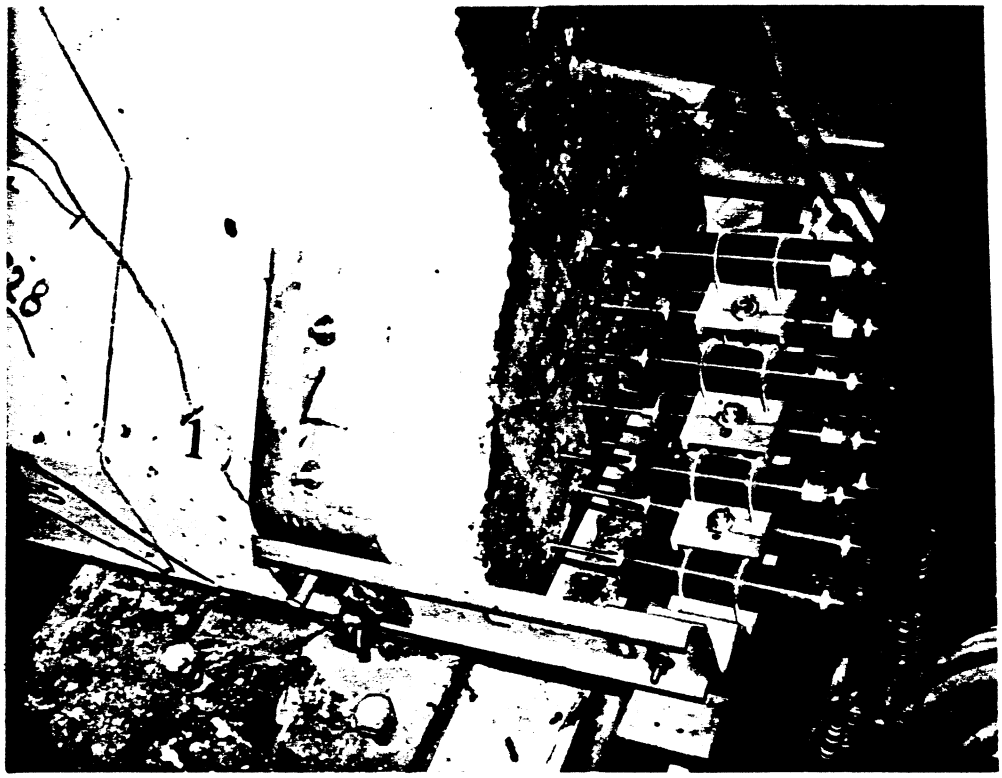

Fig 3.8 Slip Gauge Setup.

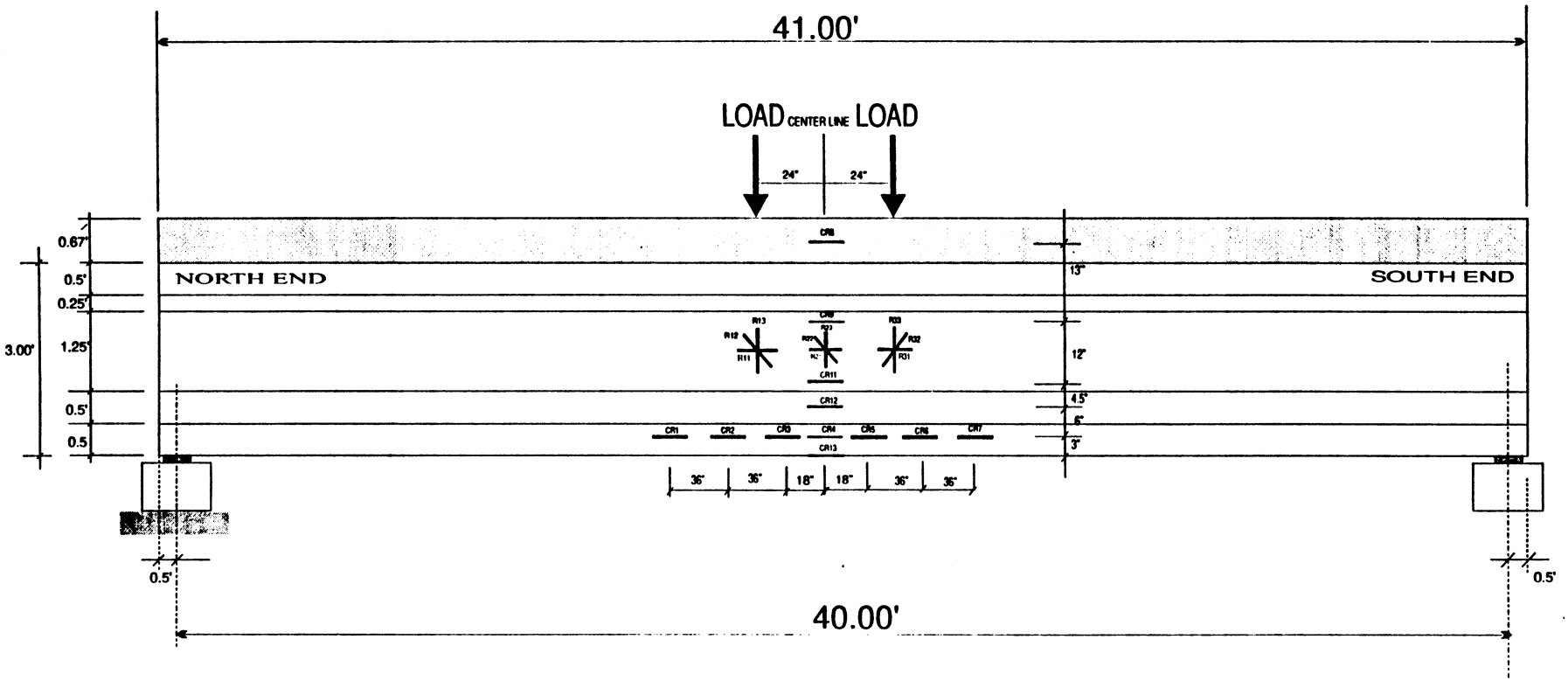

Figure 3.9 Fatigue Test External Gauge Configuration

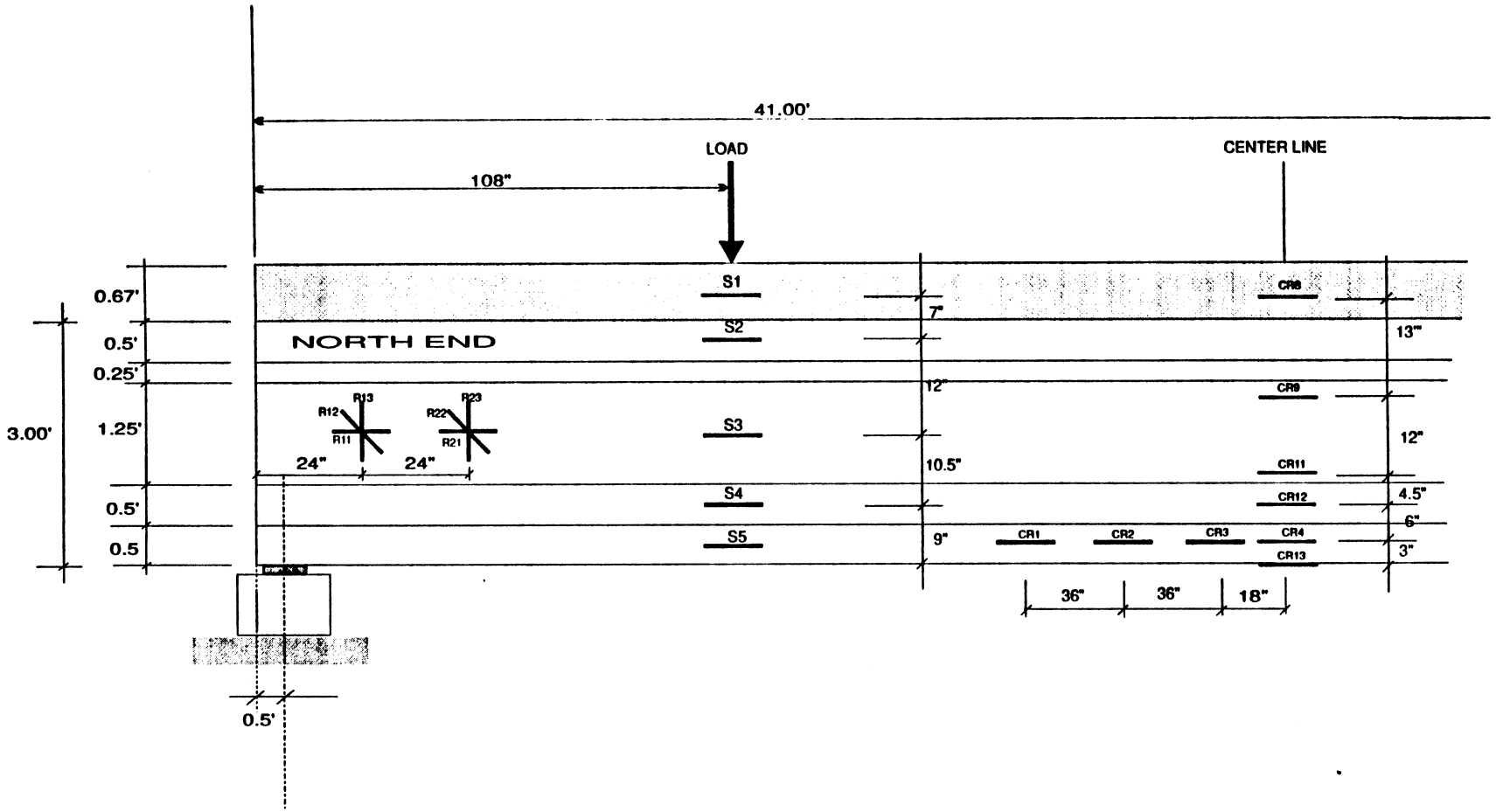

Figure 3.10 Location of External Gages for North End Tests

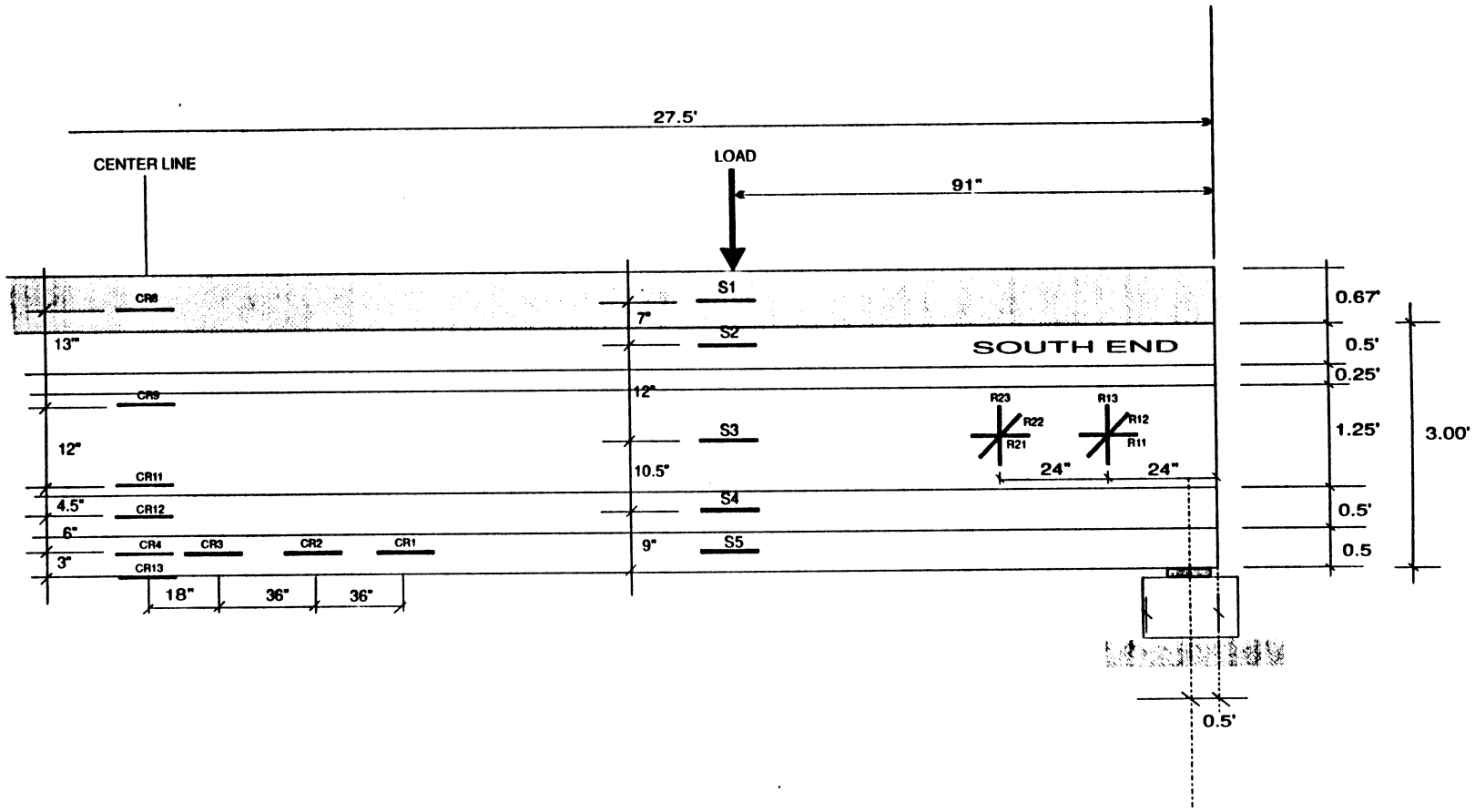

Figure 3.11 Location of External Gages for South End Tests

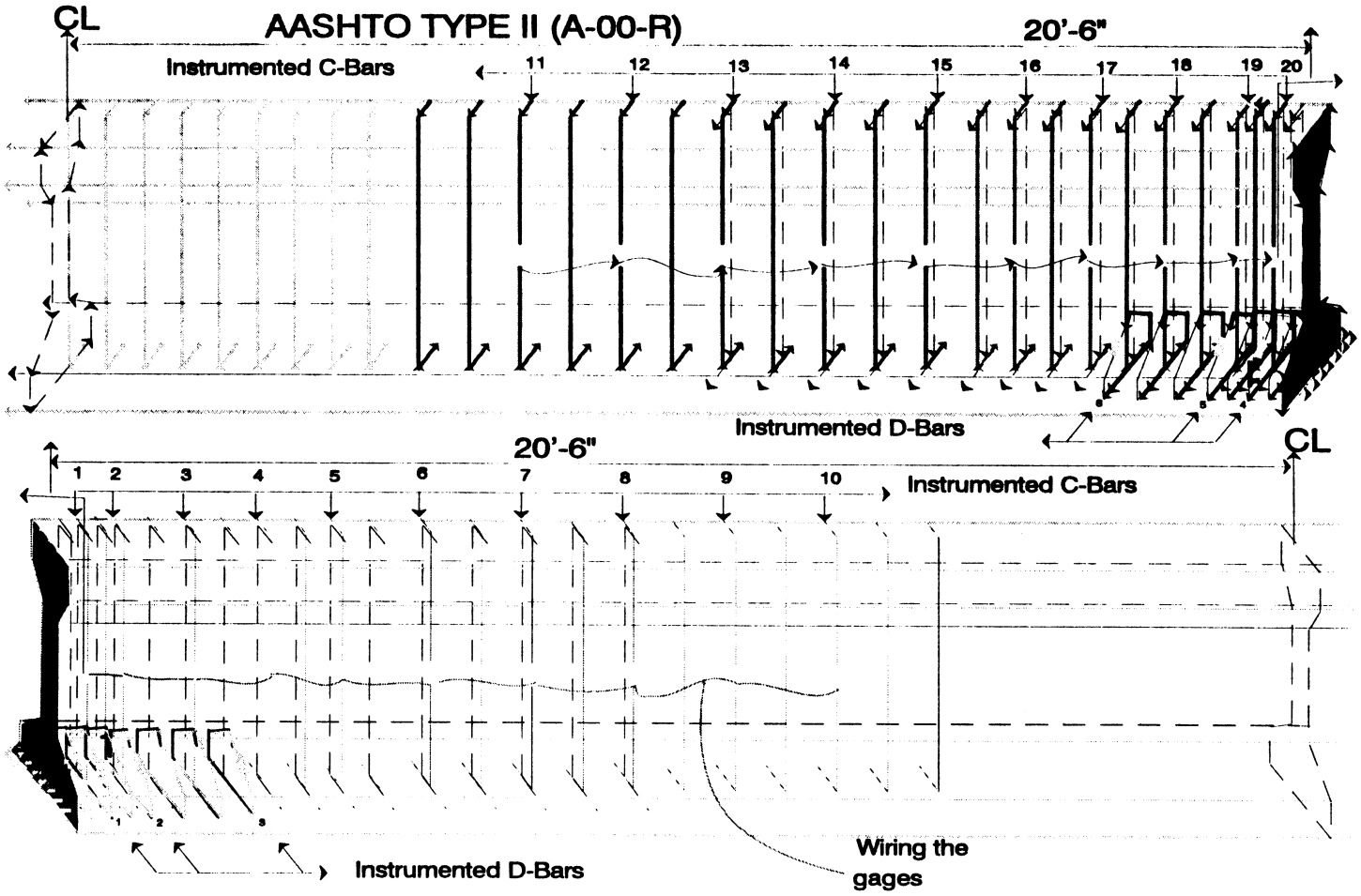

Fig 3.12 Internal Gauge Location

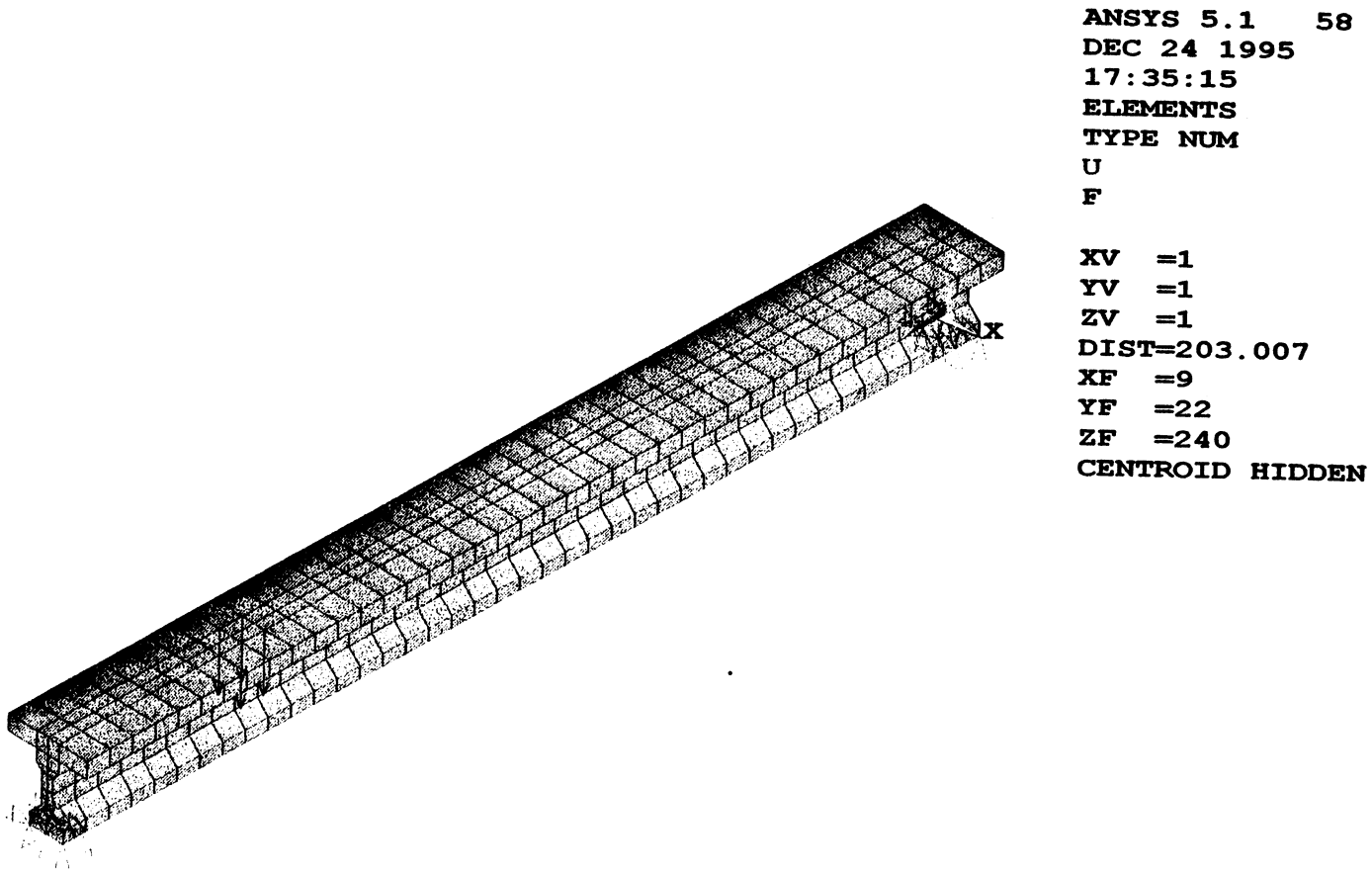

Fig 3.13 Finite Element Model of the Girder Showing North End Configuration.

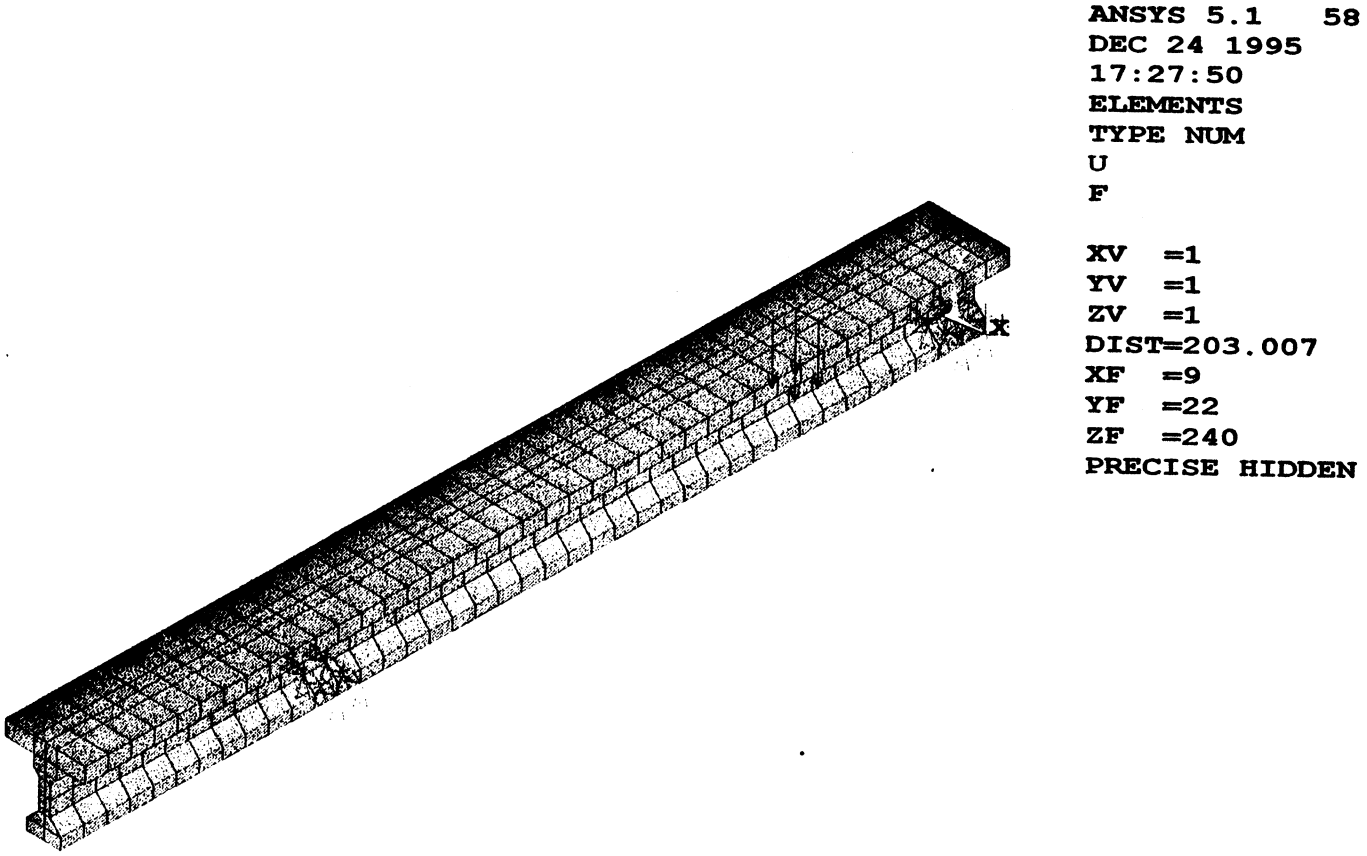

Fig 3.14 Finite Element Model of the Girder Showing South End Configuration.

CHAPTER 4

EXPERIMENTAL and ANALYTICAL RESULTS

4.1 FATIGUE TEST

The 8,000 psi girder was first run to a million cycles without any static load on it. No reduction in the stiffness was observed. The girder was then uniformly loaded at 1 kip/ft and fatigued to 2 million cycles. The loading range was 16 kips to 44 kips. The cycling frequency was 1 Hertz. Figure 4.1 to 4.5 show plots of the stress-strain loops (hysteresis loops) for some surface gages at various stages of cycling for the girder. The chord modulus, which is the slope joining the high and low point of the loop, was found to have decreased by an average of 15% at the end of fatiguing. The chord modulus is a measure of the stiffness of the beam. The plots of the chord modulus against the number of cycles was plotted and a geometric fit was made to the data to obtain the degradation trend of stiffness in the beam at various gages. The plots are shown in Figures 4.8 to 4.11. There were two small cracks at the center section of the girder in the bottom flange. This occurred at about 400,000 cycles. Crack gauges were installed on the cracks. Initially the cracks seemed to be increasing in width but after a while (at around 1.2 million cycles) there was no change in the crack width. The cracks did not show any propagation either upward or sideways nor did they increase in the width afterwards. The beam was cycled to the full 2 million cycles with out any more cracks or any further change in the crack gauge readings. The maximum deflection at the center for any cycle was 0.48 inches. There was no slip during the fatigue loading. A lot of the surface gages and embedded gages were spoiled during the fatigue test.

The 12,000 psi girder was loaded from the beginning with the live load of 1kip/ft and was fatigued to 3 million cycles. The hysteresis loops are shown in Figures 4.6 and 4.7. The stiffness degradation plots are shown in Figures 4.12 and 4.13. Surface gauge CR4 showed a reduction in stiffness of nearly 29%. There was a small crack in the bottom flange at the center section of the girder. This occurred around 300,000 cycles. There was no further propagation of the crack . There appeared to be some slip in strands 2 and 3 around 1

million cycles. But there was no further increase in the slip in the strands. Surface gauge CR13 showed some sudden increase in the strain at the same time.

4.2 STATIC TESTS

The shear tests were conducted after the girder had been fatigued. These were then compared with the results of static tests on similar girders but without being subjected to any cyclic loading. The results are shown in **Table 4.1**. The maximum test shear was plotted along with predicted shear strength form the three codes as discussed in the literature review. Plots of moment and slip vs deflection were plotted. **Figures 4.15 to 4.18** show these graphs.

4.2.1 North End Test

The cracking pattern of the north end test for the 8,000 psi girder is shown in Figure 4.40. Slip started occurring when the moment reached 1500 kip-ft. All the strands started slipping at almost the same time. Plots of moment vs slip of all the strands for the north end test is shown in Figures 4.19 to 4.21. This phenomenon did not occur in beams subjected to static loading. For those beams subjected to static loads, the first slip occurred at a moment of 2250 kip-ft. Also, the first slip occurred in the first four strands and not in all the strands. There was a complete loss of bonding for the fatigued beam at its slipping moment. The slip for the statically-loaded beam was in the range of 0.01 inches to 0.05 inches.

The maximum moment achieved was 1600 kip-ft. This is shown in **Figure 4.15a and 4.15b**. The maximum moment for the statically-loaded beam was 2350 kip-ft. So the fatigue caused a reduction in the flexural moment capacity by 31.9%. The maximum load taken by the girder was 220 kips and the first shear crack appeared at a load of 120 kips. In the statically-loaded beam the maximum load taken by the beam was 333 kips. The first crack appeared at a load of 220 kips. The decrease in the load carrying capacity for the fatigued beam was 33% for flexure.

For the 12,000 psi beam plots of moment vs slip are shown in 4.25 to 4.27. The first slip occurred at a moment of 1400 kip-ft. The first two strands slipped first. The rest of the strands slipped at a moment of 1800

kip-ft. For the previously static testing girder the first slip had occurred at a moment of 1700 kip-ft. The maximum moment was 2300 kip-ft at which all the strands slipped. Strand 1 and strand 2 slipped to almost 0.5 inches. In the static tested girder the maximum slip was 0.2 inches.

The maximum moment for the fatigued beam was 1800 kip-ft. The maximum moment for the statically-loaded girder was 2300 kip-ft. This was a reduction of 22% in the maximum moment capacity. The maximum load taken by the fatigued beam was 255 kips. The maximum load for the statically-loaded girder was 335 kips. The decrease in the load capacity was 22.9 %.

4.2.2 South End Test

The cracking pattern of the south end test of the 8,000 psi girder is shown in Figure 4.41. Web-shear cracks caused the concrete web failure after the general bond slip had occurred. The slip for the south end test started at a moment of 1080 kip-ft. The slip for the statically-loaded beam started at 1640 kip-ft. The strands did not all slip at the same time but slipped in phases. There were already major shear cracks in the web. The deflection under the load at the time the strands started slipping was almost 0.3 inches. The deflection at failure was almost 0.7 inches. The slip of the strands was in the range of 0.1 inches to 0.15 inches. The maximum moment for the shear test was achieved at 1320 kip-ft. The maximum moment in shear for the statically-loaded beam was 2120 kip-ft. Deflection under the load at the time the strands started slipping was almost 0.4 inch. The deflection at failure was 1.2 inches. The slip for the statically-loaded girder was in the range of 0.125 inches to 0.2 inches. At failure both girder had massive cracking in the web. The cracks extended all along the web and into the flange.

For the 12,000 psi south end test the slip started at 1440 kip-ft. The slip for the statically-loaded girder started at 1500 kip-ft. The maximum moment achieved in the statically-loaded girder test was 1800 kip-ft which was the same for the statically-loaded girder south end. Deflection at the time the first strand slipped was 0.4 inches as compared to 0.3 inches for the statically-loaded girder. The maximum load taken by the fatigued beam in shear was 356 kips. The maximum load for the statically-loaded girder was 361 kips. The slip was in the range of 0.25 inches for both the beams.

4.2.3 Shear Strength Results

as for the shear predicted by the codes. **Figures 4.34a to 4.39b** show the plots. The shear from the finite element model are also included in the the plots. Since the self weight of the girder is small as compared to the load taken by the girder, the shear is nearly constant between the support and the load. A summary of the shear strength results and slip for the girders is tabulated in **Table 4..**

4.2.4 Cracking Results

The cracking pattern for the tested beams is shown in Fig 4.40- Fig 4.41. The cracking pattern for the fatigued girders was compared to the pattern obtained from the statically-loaded girders. The number of cracks in a unit area was checked to see which girder had more cracks. The sections 3, 4 and 5 were used to fix the area as this area had most cracking in all the tests. The fatigued 8,000 psi girder had 13 cracks for the north-end test and 12 cracks for the south-end test. In comparison, the statically-loaded 8,000 psi girder had 19 cracks at the north-end and 18 cracks at the south end.

For the 12,000 psi fatigued girder, the number of cracks at the north-end were 11 and for the south-end the number was 8. From the statically-loaded girder the number of cracks were 15 and 16 for
The crack lengths were also compared for the fatigued and statically-loaded girders. It was found that the maximum crack length in the fatigued 8,000 psi girder north end test was 7 feet in length. In comparison the maximum crack length in the statically-loaded for the same test was 4.6 feet. For the south end test the maximum crack length for the fatigued girder was 7.5 feet and for the statically-loaded girder was 4 feet. On an average, for the same sections the cracks on the statically-loaded girder were smaller than the cracks on the fatigued girders.

For the 12,000 psi girder the maximum crack length in the fatigued girder was 7 feet and 5.5 feet for the statically-loaded girder for the north end test. For the south end test, the maximum crack length was 7 feet for the fatigued girder and 4.4 feet for the statically-loaded girder. the north and south ends respectively.

4.3 FINITE ELEMENT MODELING

4.3.2 Static test modeling

The results of the failure loads from ANSYS for the three girders is shown in Table 4.1. The results from the static test of the statically-loaded beams are also listed in the Table. It can be seen that from the model

that for the north end 8,000 psi test, the maximum load was 319 kips. The maximum moment achieved is about 2000 kip-ft as shown in Figure 4.57b. The moment vs deflection plots for all the statically-loaded girders from the model are plotted in Figures from 4.57b to 4.62b. The results for all the beams are listed in Table 4.1.

4.3.3 Fatigue Modeling

For modeling the fatigue a fatigue analysis was done on the same model for each of the girders. A ***fatigue usage factor*** was obtained from this analysis. The fatigue usage factors were then used to reduce the stiffness or Young's modulus by that factor for the model. The model was then run with this reduced stiffness. The fatigue usage factors and the resulting stiffness are listed in Table 4.5. The load capacities obtained from this run with the reduced stiffness are also listed in Table 4.1. The loads obtained from the fatigue experimentation are also listed in the same Table.

From the finite element analysis model, the reinforcing bar strains were also obtained. These are compared to the results obtained from the static and fatigue tests in Figures 4.63a to 4.74b. Most of the confining bars from the experiment were spoiled during the test. The strain at some of the gauge locations from the actual test are also plotted in Figures 4.75a to 4.80b.

4.4 DISCUSSION OF RESULTS

4.4.1 Effect of Fatigue

From the results it can be seen that fatigue definitely has an effect on the load carrying capacity and flexural moment capacity of the girders. In the static tests for the fatigued beams from the experiment, all the beams tested experienced a significant decrease in the load and moment capacities for the north end tests. The 8,000 psi girder capacity was reduced by 31.9% and that of the 12,000 psi girder by 22%. In the north end test both the girders failed first in flexure ie; by the failure of bond-flexure. For the south end tests the reduction in the load carrying capacity was much less than that for the north end tests. For the 8,000 psi girder the reduction was 27% and for the 12,000 psi girder the decrease in the capacity was about 1%.

From the finite element model however, we have got similar results that indicate that the reduction in the capacity of the girder for the south end ie; in shear is very low as compared to the effect on flexure. The

north end tests for the model yielded an average reduction of 17% in the load capacity of the girders. The maximum decrease was for the 8,000 psi girder which ws 29.4%, followed by the 10,000 psi girder which was 15.38% and the least effect was on the 12,000 psi girder which was 5.9%. For the south end tests, the maximum reduction in capacity was again for the 8,000 psi girder followed by the 10,000 psi girder and least for the 12,000 psi girder (Table 4.6). From these results we can say that :

1) The effect of fatigue is more on the flexural strength of the girder.

2) The effect is more on the girder of lower compressive strength.

4.4.2 Moment - Deflection Plots

From Figures 4.15a to 4.18b it can be seen that the initial slope of the moment vs deflection curve decreases for the fatigued girders as compared to the statically-loaded girders. This means that the deflection resistance is decreased for the fatigued beam. If we look and compare just the statically-loaded girder plots, there is a certain trend which shows that the resistance to deflection is more for higher strength concrete girders. This is because of the higher elastic modulus of the higher strength concrete girders. Since the slope of the moment-deflection curve is lower for the fatigued beam, the elastic modulus of the concrete has also decreased. So it may be inferred that the girder, after fatigue, behaves more like a girder of lower strength concrete.

It can also be noticed that the second slope of the moment-deflection curve does not extend as much for the fatigued girders as it does for the statically-loaded girders. This may be because of the reduced strength and lower moment and load capacity. Because of the decrease in the capacity, the girder is not able to take as much load as before after the initial crack has occurred. This tells us that the mechanical bond stress capacity is also reduced by fatigue.

From the moment-deflection plots from the FEA model, it can be seen that there is no second slope of the curve. This is so because the slip could not be modeled. As a result there is no bond transfer when there is a crack.

4.4.3 Moment and Slip vs Deflection Plots

It can be seen from Figures 4.31a to 4.33b that the strands more often slip at the same time in the fatigued girders as compared to the statically-loaded girders. It can also be seen that the slip usually starts

when the first slope of the moment -deflection curve ends. In the area of the second slope of the moment-deflection curve the slip increases linearly and rapidly. For the fatigued girders the strands start slipping a little earlier and at a lower deflection as compared to the statically-loaded girders. This is more prominent in the north end tests which once again suggests that the flexural strength of the girder is affected more by fatigue than the shear capacity (Table 4.2).

4.4.4 Shear Strength Plots

From Figure 4.34a to 4.39b it can be seen that none of the codes are equipped to predict the shear strength after fatigue. The closest prediction among the codes is from the ACI code. But the closest prediction is by the FEA model. Also the ACI code seems to be predicting the shear strength of the 12,000 psi girder more accurately then for the 8,000 psi girder. This could be because the ACI code limits the amount of shear carried by the steel.

Table 4.1 Summary of Slip Results of Fatigued Girders

Girder Designation	Shear at First Strand Slip (kips)	Shear at Strands Slip (kips)	Shear at Beam Failure (kips)
F8N	*180*	*180*	*180*
R8N	*199*	*265*	*277*
F8S	*165*	*222*	*222*
R8S	*235*	*282*	*302*
F12N	*209*	*215*	*216*
R12N	*215*	*251*	*279*
F12S	*264*	*271*	*217*
R12S	*227*	*227*	*276*

F = Beam Tested in Fatigue
S = South End of the Beam
N = North End of the Beam
12 = 12,000 psi (Compressive Strength)
8 = 8,000 psi (Compressive Strength)

Table 4.2 Summary of Static Test Results

Girder Designation	Distance From Support to Load (ft)	Span (ft)	Max. Loading FEA (Kips)	Max. Load Test (kips)
R8N	8.5	40	319	333
R10N	8.5	40	325	341
R12N	8.5	40	351	335
R8S	7.08	27	353	395
R10S	7.08	27	359	391
R12S	7.08	27	356	361
F8N	8.5	40	225	220
F10N	8.5	40	275	
F12N	8.5	40	330	258
F8S	7.08	27	325	285
F10S	7.08	27	335	
F12S	7.08	27	350	356

R = Statically Loaded Girder

F = Beam Tested in Fatigue

S = South End of the Beam

N = North End of the Beam

12 = 12,000 psi (Compressive Strength)

8 = 8,000 psi (Compressive Strength)

Table 4.3 Crack Angle Comparison from Experiment and FEA For Fatigue Testing

Girder	Distance From Support (ft)	Crack Angle FEA (deg)	Crack Angle Test (deg)
F8S	4.00	27	30
F8N	8.00	30	30
F10S	4.00	31	
F10N	8.00	32	
F12S	4.00	30	35
F12N	8.00	35	35

Table 4.4 Crack Angle Comparison from Experiment and FEA For Static Testing

Girder	Distance From Support (ft)	Crack Angle FEA (deg)	Crack Angle Test (deg)
F8S	4.00	30	30
F8N	8.00	32	33
F10S	4.00	29	30
F10N	8.00	32	40
F12S	4.00	30	29
F12N	8.00	33	30

Table 4.5 Reduced Girder Stiffness Due to Fatigue Loading

Girder (Compressive Strength)	Initial Stiffness (psi)	Fatigue Usage Factor = 1- Damage Fatigue Factor	Final Stiffness (psi)
8000 (psi)	*5,4200,000*	*0.18*	*4,450,000*
10000 (psi)	*6,060,000*	*0.2*	*4,850,00*
12000 (psi)	*6,6400,000*	*0.2*	*5,310,00*

Table 4.6 Percentage Reduction in the load capacity of the Girders due to fatigue.

Girder	FEA			TEST		
	Static-Test	Fatigue	*% Reduction*	Static-Test	Fatigue	*% Reduction*
8N	319	225	*29.47*	333	220	*33.93*
10N	325	275	*15.38*	341		
12N	351	330	*5.98*	335	258	*22.99*
8S	353	325	*7.93*	395	280	*29.11*
10S	356	335	*5.90*	391		
12S	366	350	*4.37*	361	356	*1.39*

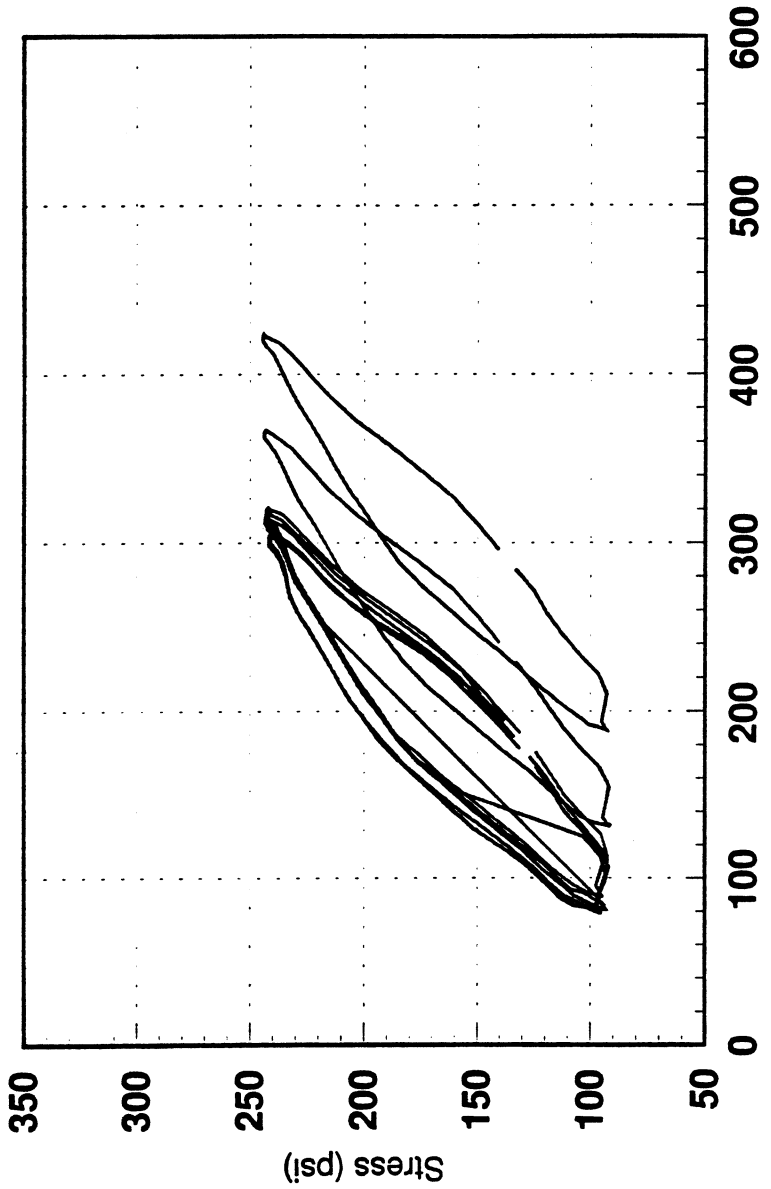

Fig 4.1 Hysteresis Loops of Surface Gage CR4 for 8000 psi

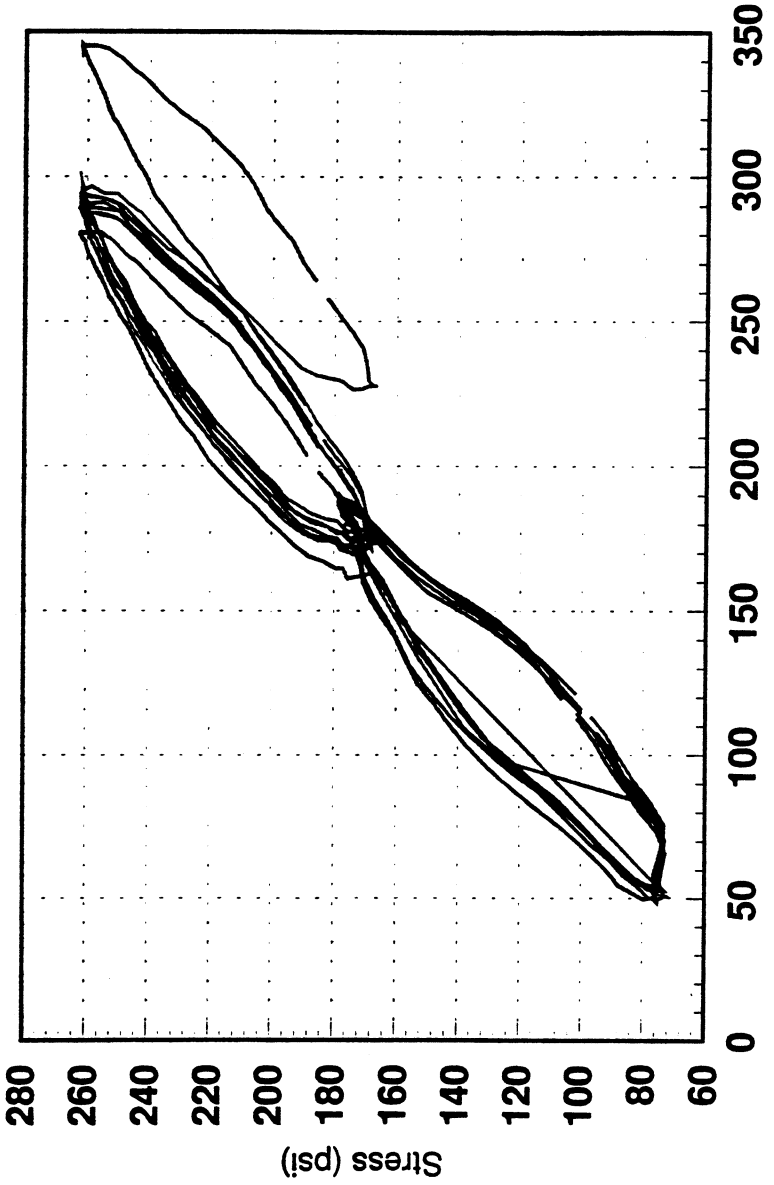

Fig 4.2 Hysteresis Loops of Surface Gage CR7 for 8000 psi

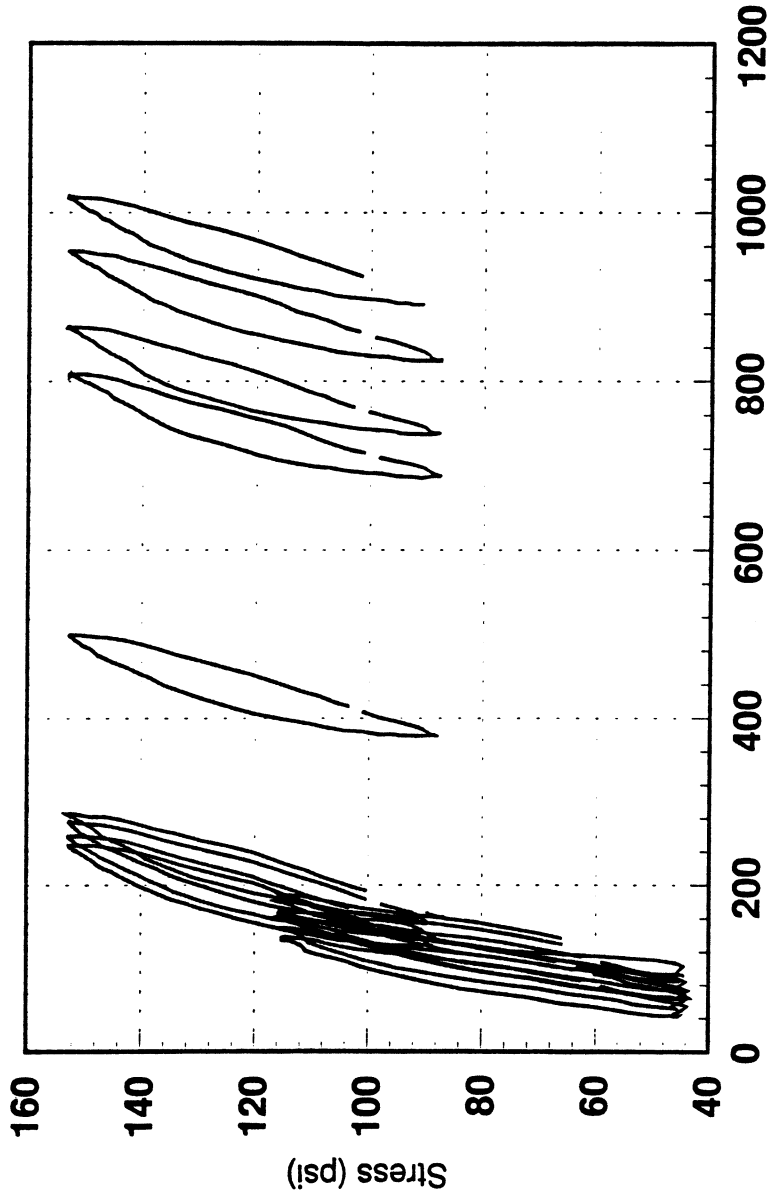

Fig 4.3 Hysteresis Loops of Surface Gage CR11 for 8000 psi

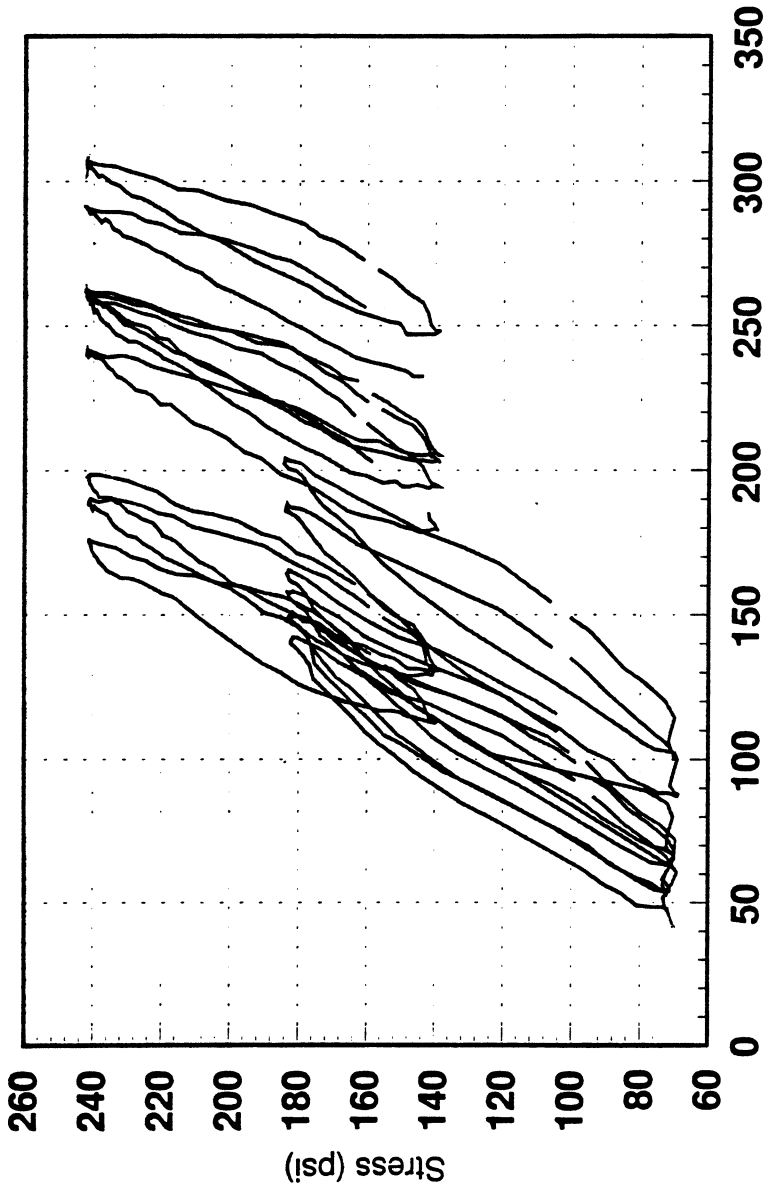

Fig 4.4 Hysteresis Loops of Surface Gage CR12 for 8000 psi

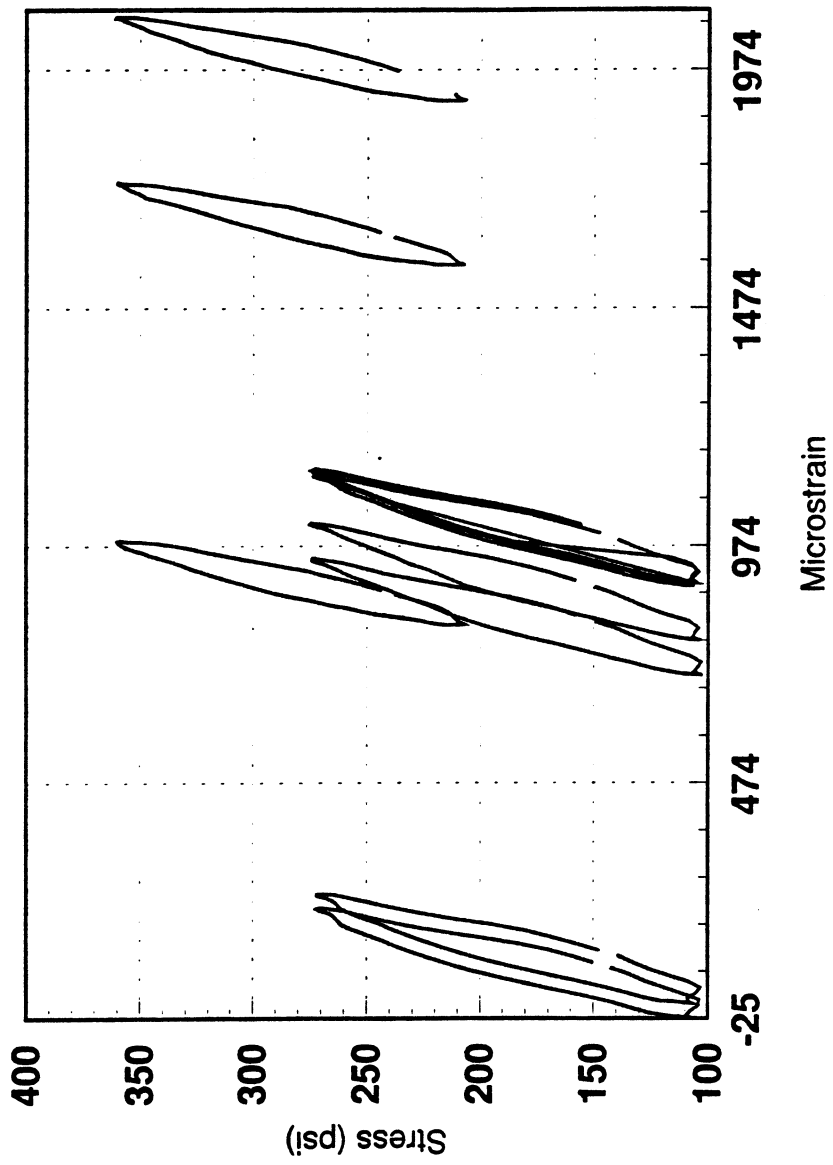

Fig 4.5 Hysteresis Loops of Surface Gage CR13 for 8000 psi

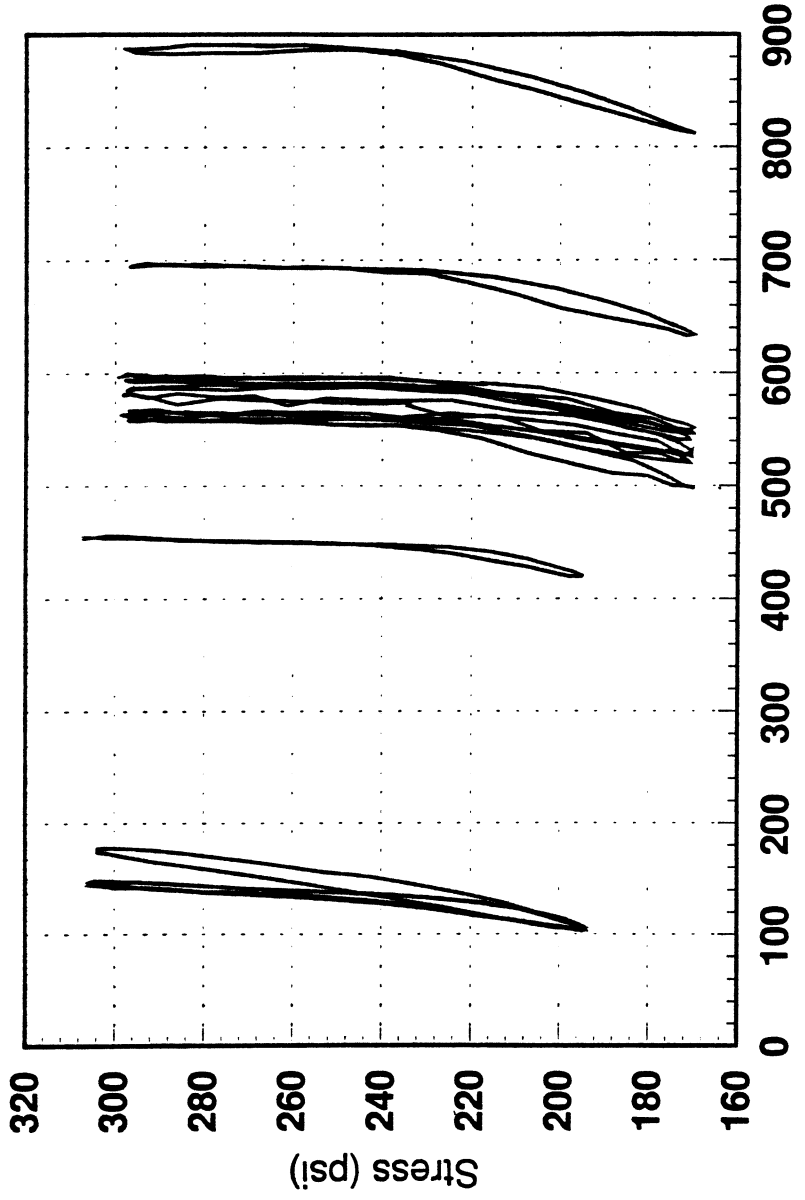

Fig 4.6 Hysteresis Loops of Surface Gage CR4 for 12000 psi

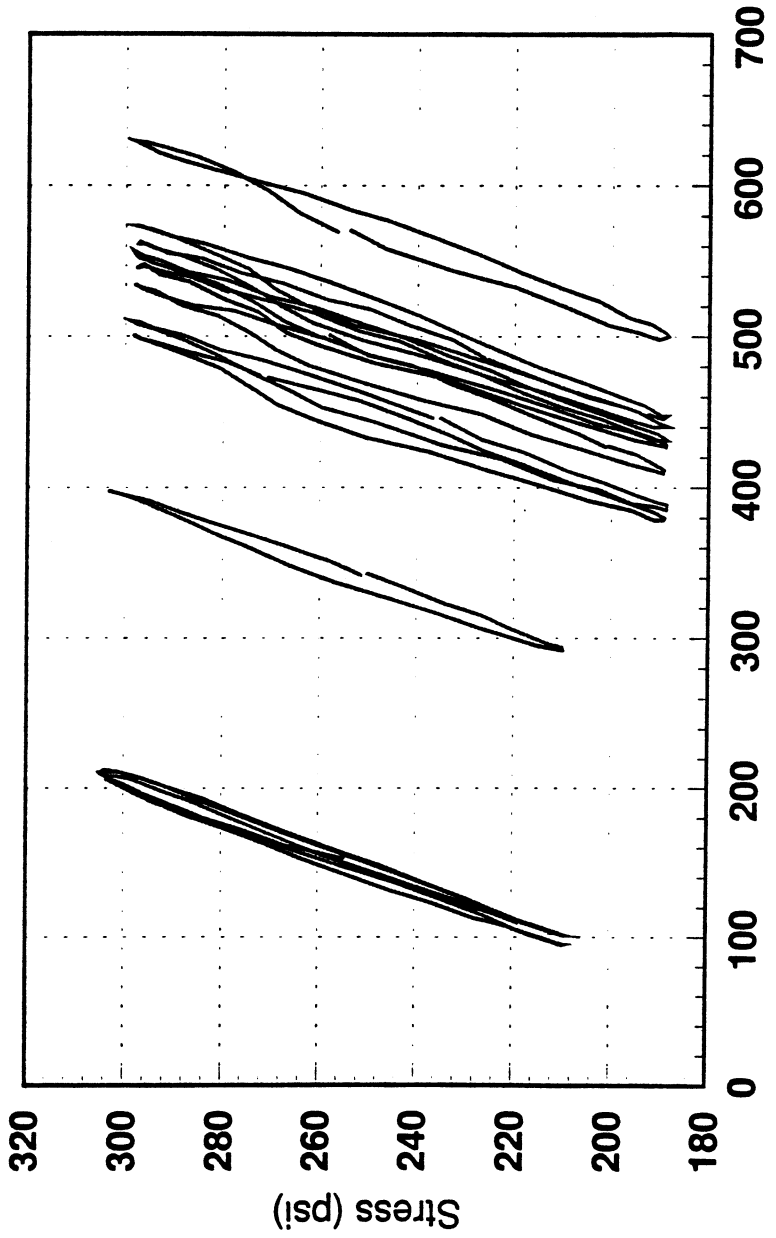

Fig 4.7 Hysteresis Loops of Surface Gage EMB4 for 12000 psi

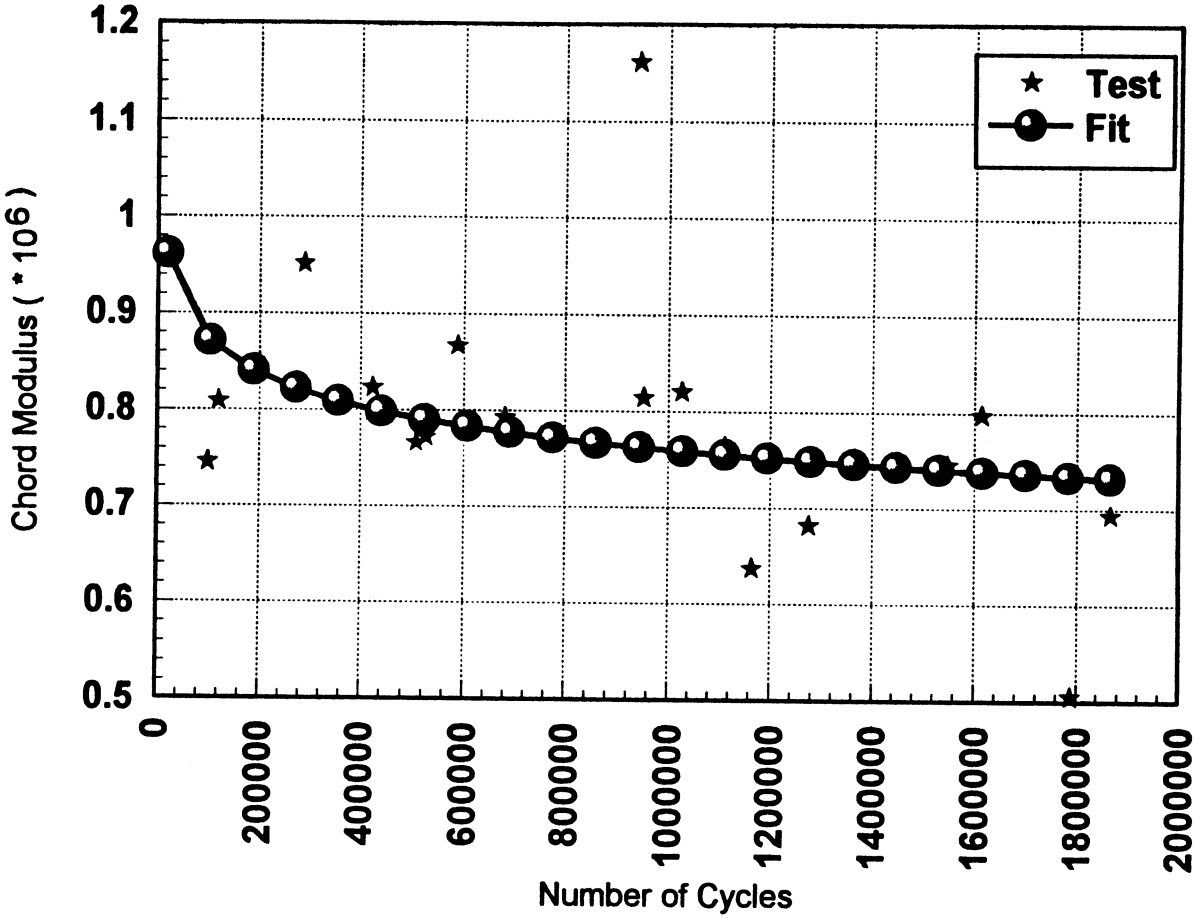

Fig 4.8 Stiffness Degradation Plot for Gage CR7 for 8000 psi

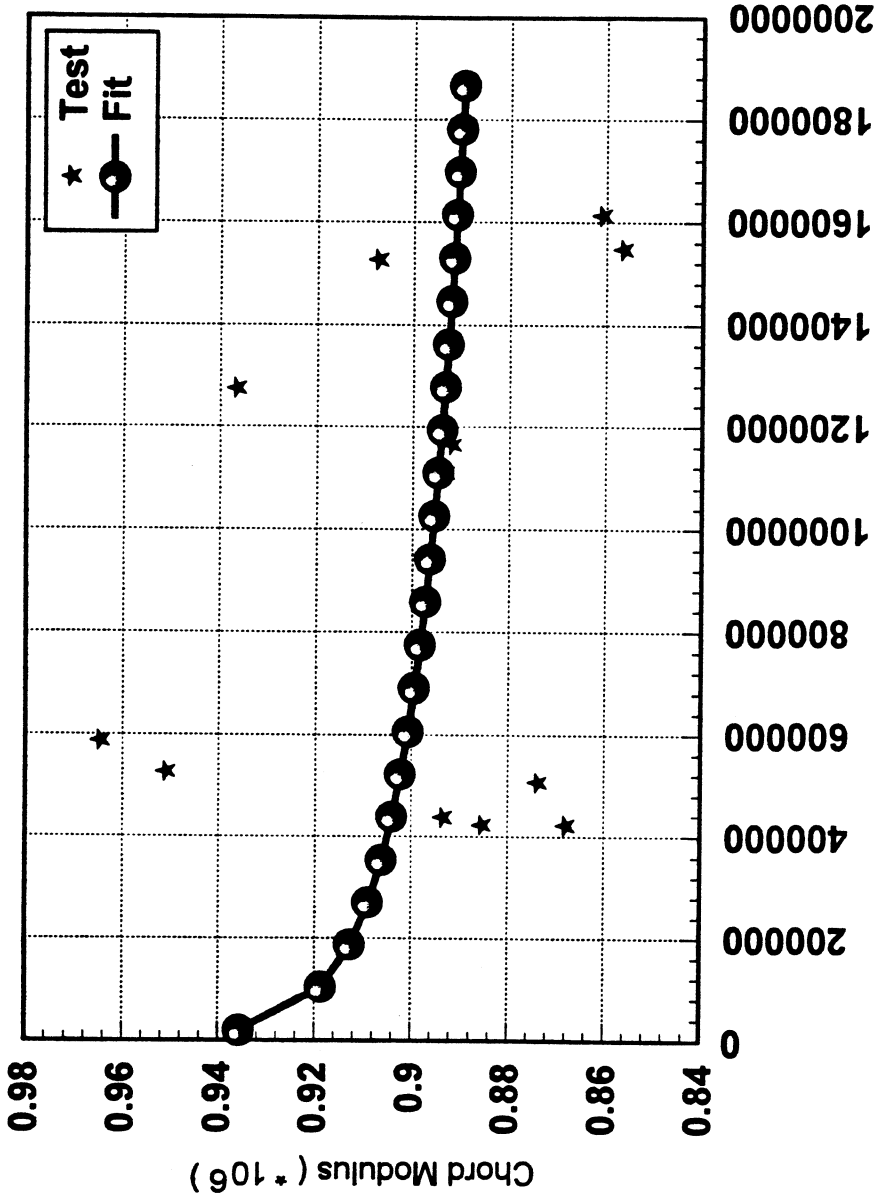

Fig 4.9 Stiffness Degradation Plot for Gage CR13 for 8000 psi

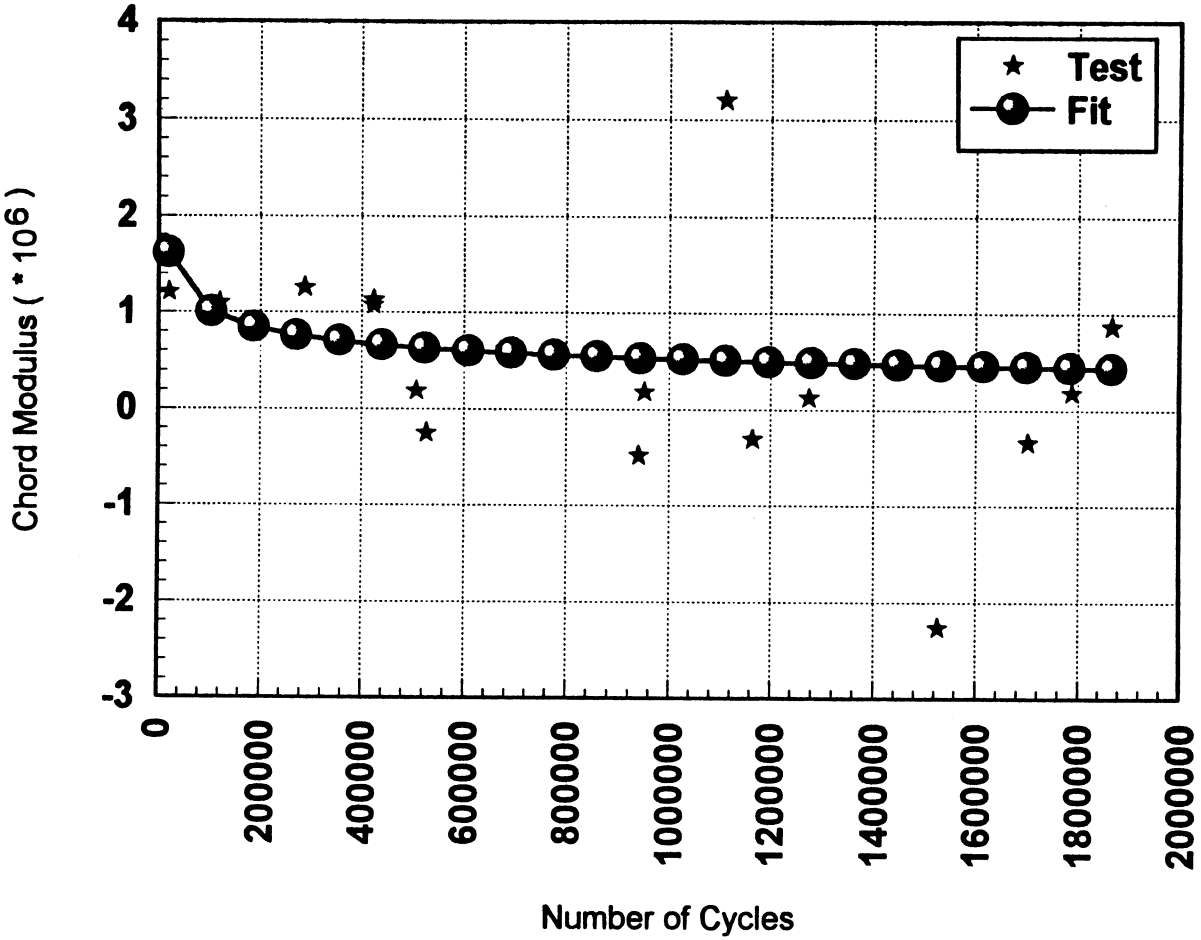

Fig 4.10 Stiffness Degradation Plot for Gage EMB4 for 8000 psi

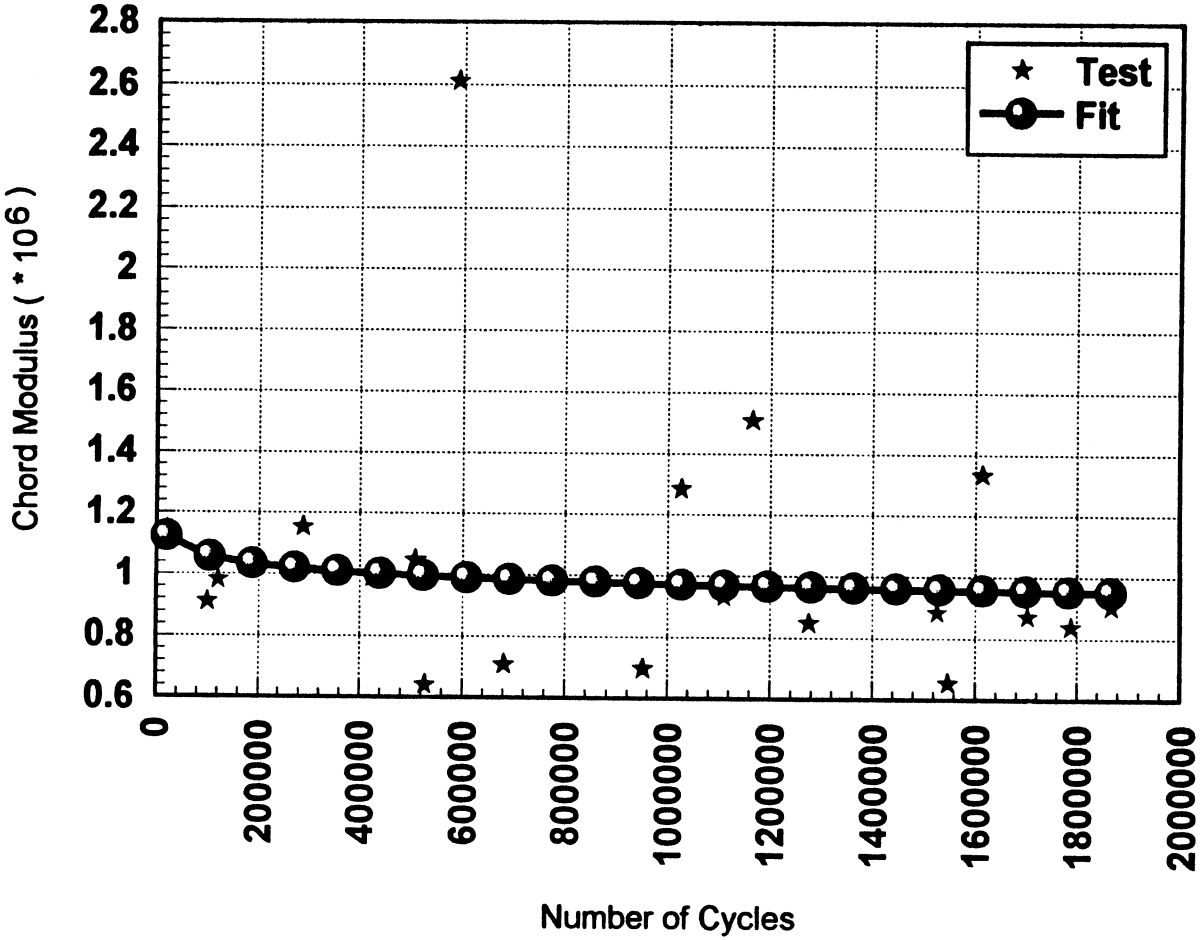

Fig 4.11 Stiffness Degradation Plot for Gage EMB8 for 8000 psi

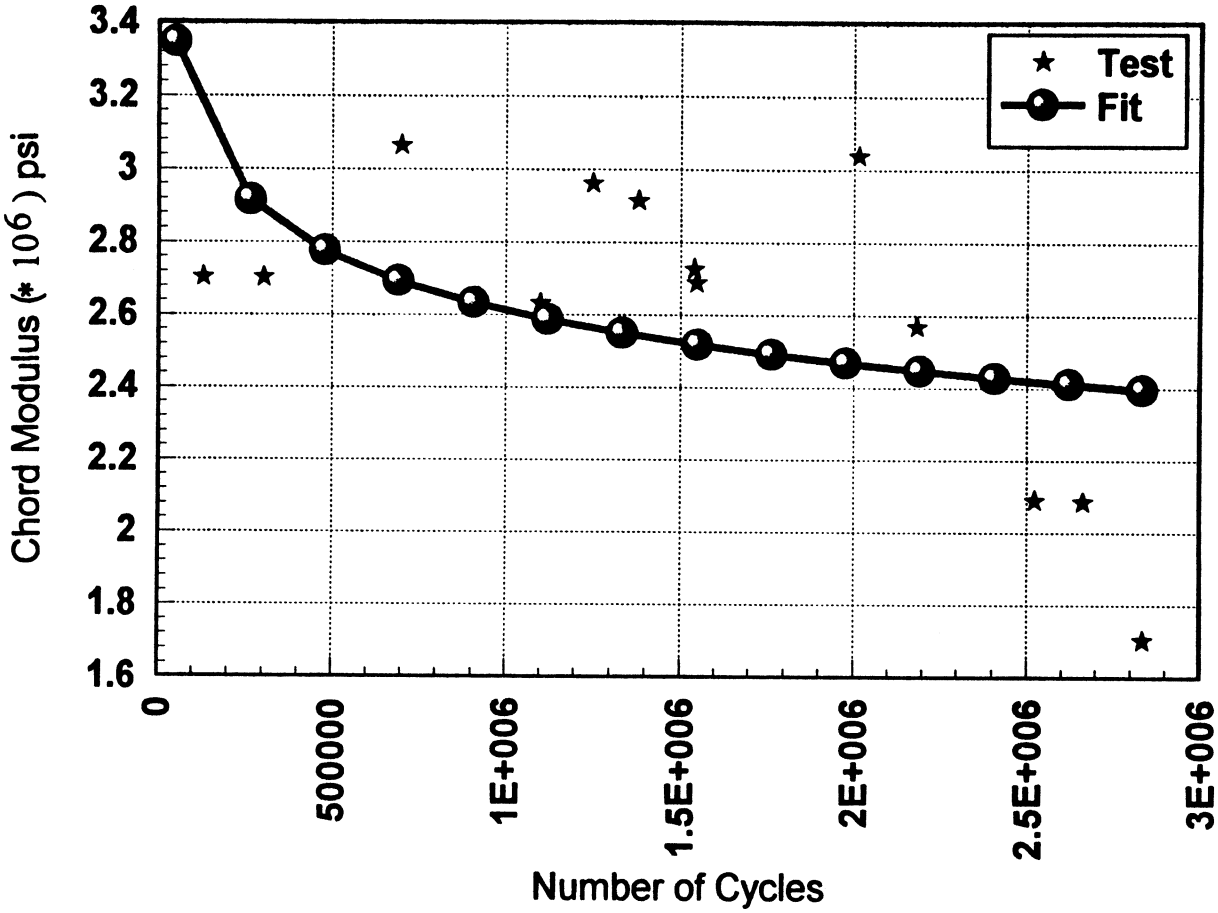

Fig 4.12 Stiffness Degradation Plot for Gage CR4 for 12000 psi

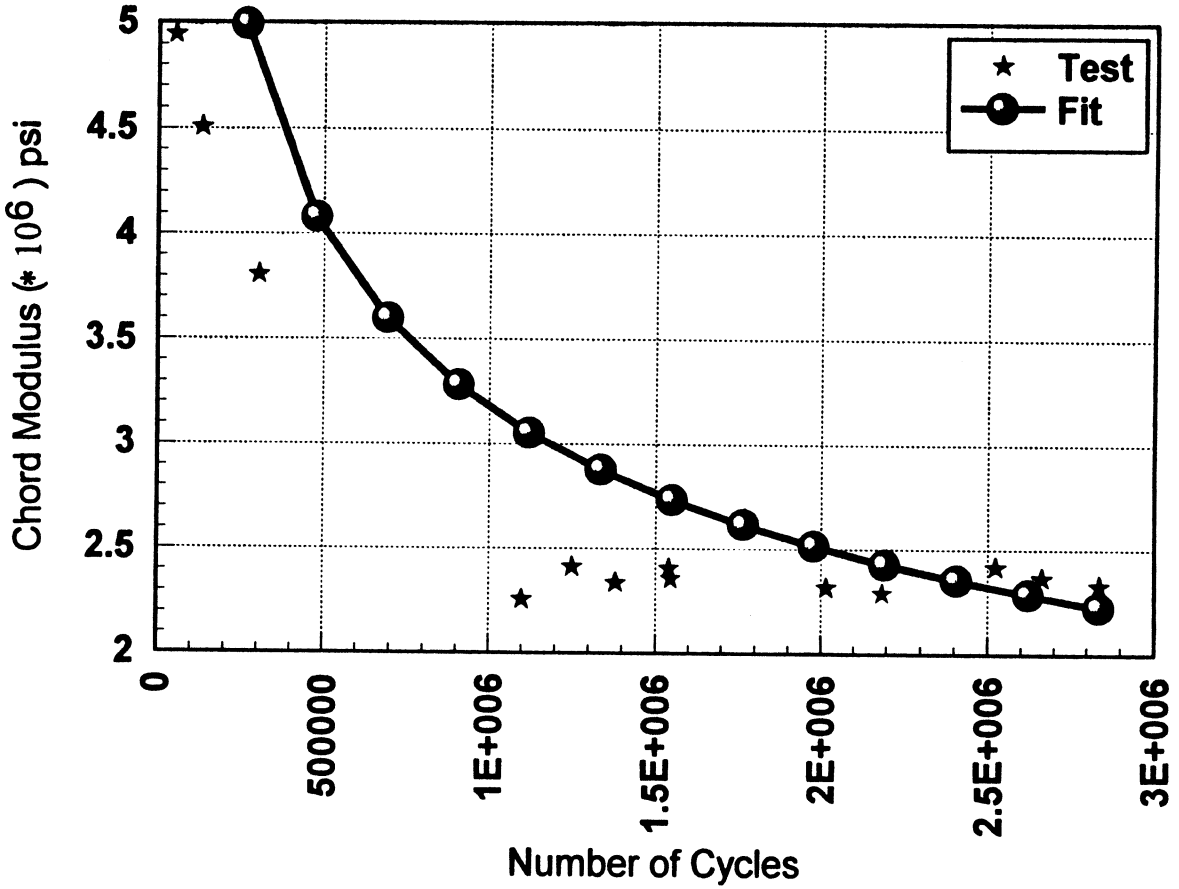

Fig 4.13 Stiffness Degradation Plot for Gage CR13 for 12000 psi

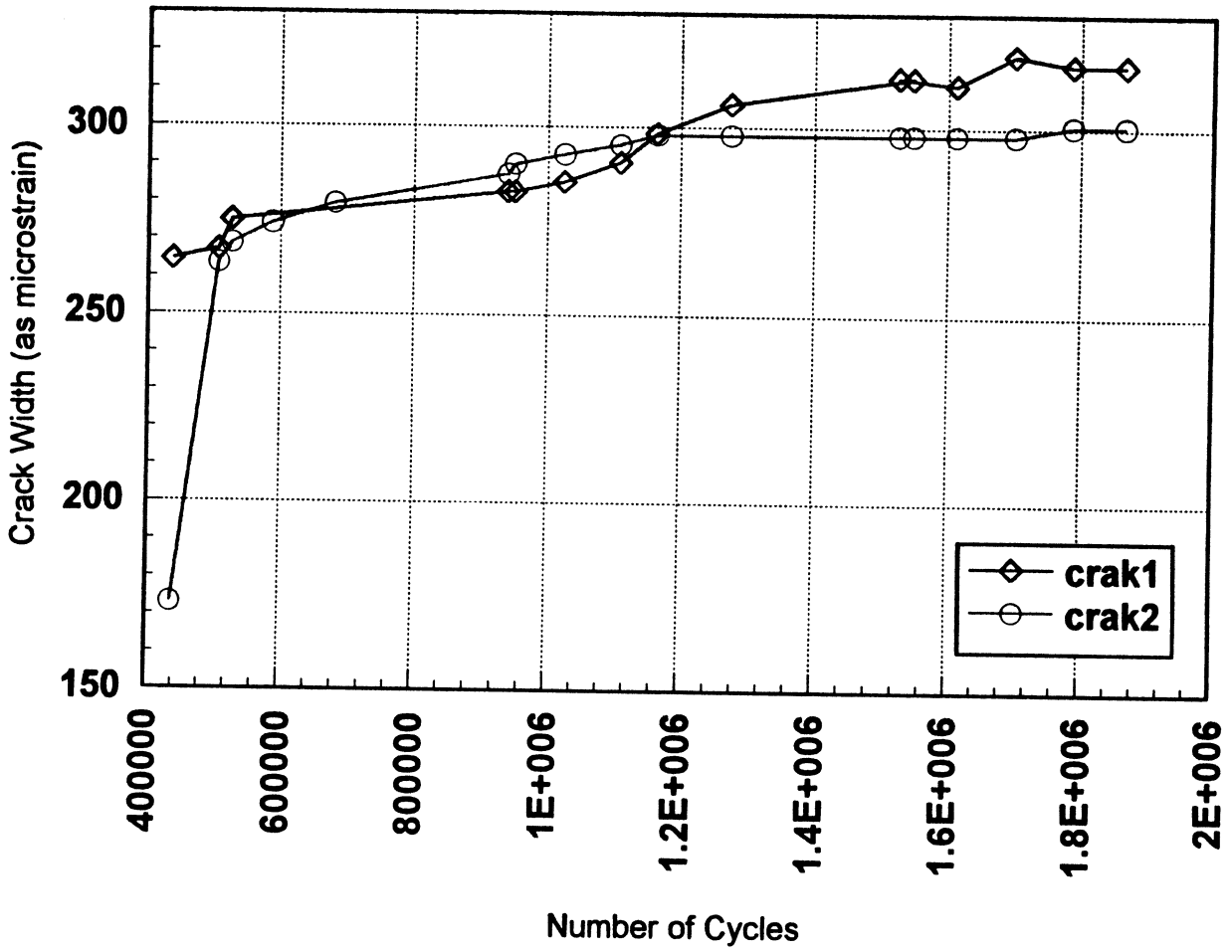

Fig 4.14 Growth of Crack Width for 8000 psi

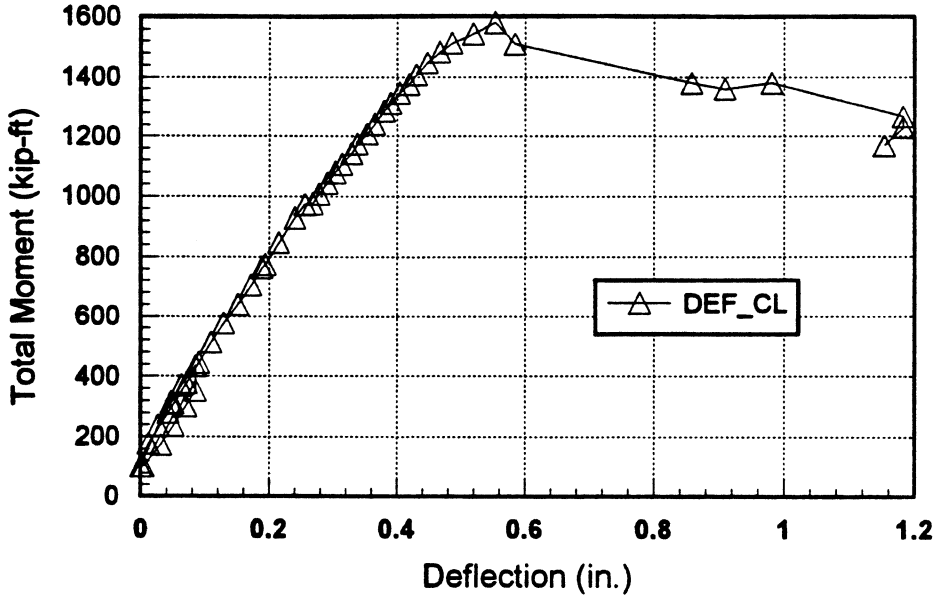

Fig 4.15a Moment vs Deflection for F-8-N

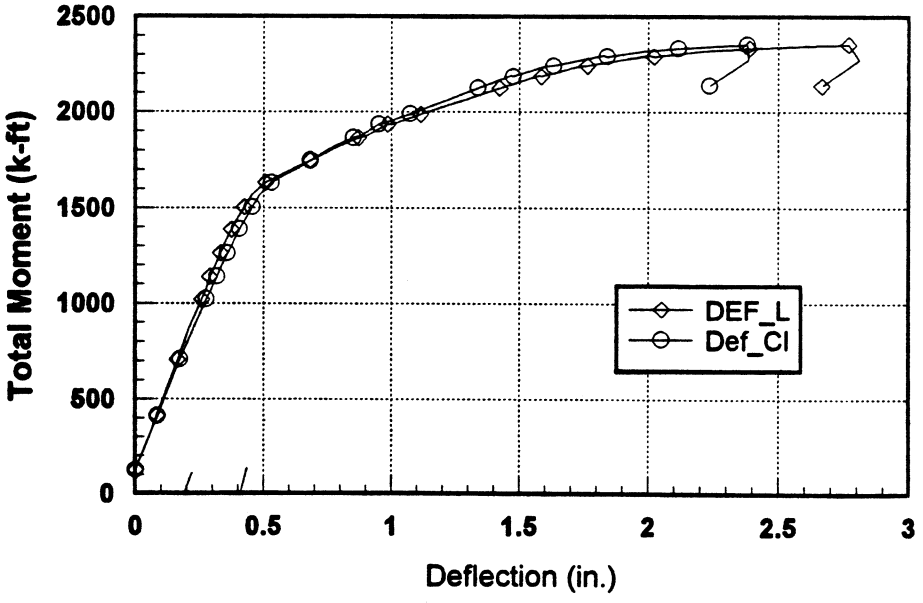

Fig 4.15b Moment vs Deflection for R-8-N

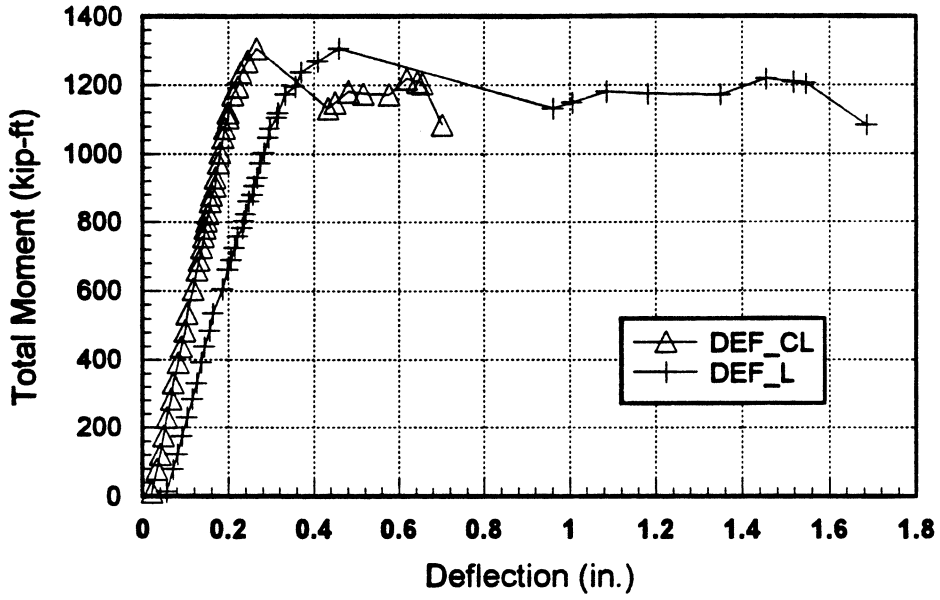

Fig 4.16a Moment vs Deflection for F-8-S

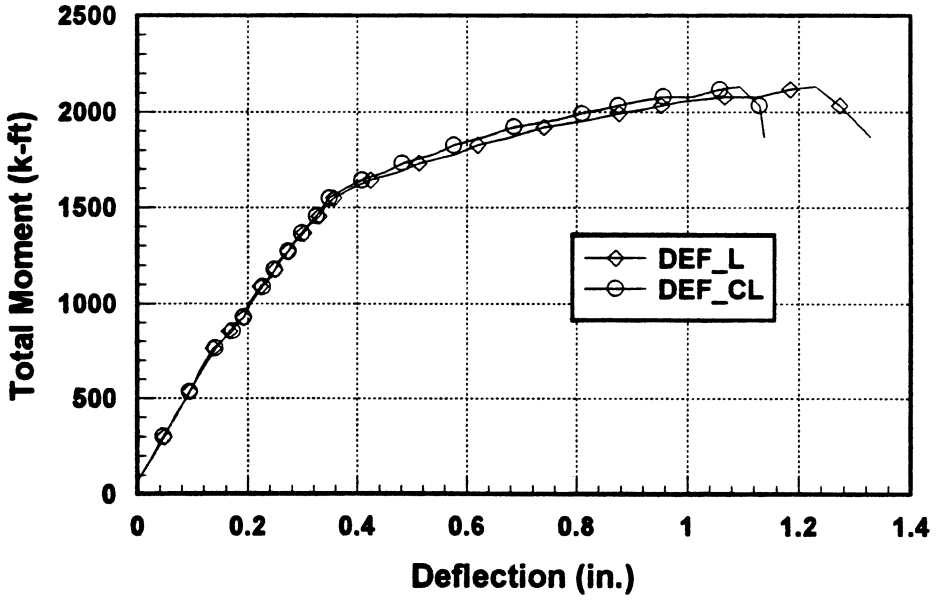

Fig 4.16b Moment vs Deflection for R-8-S

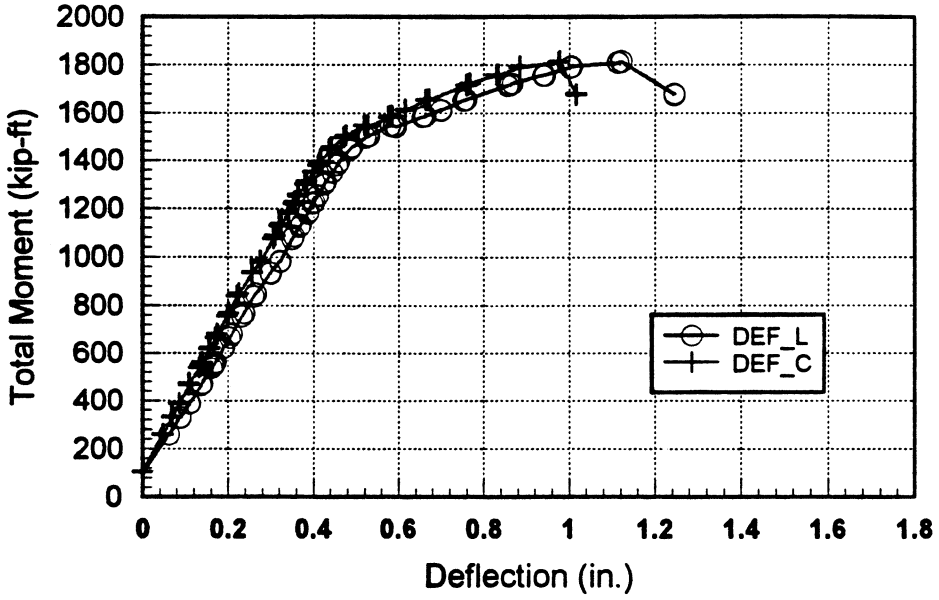

Fig 4.17a Moment vs Deflection for F-12-N

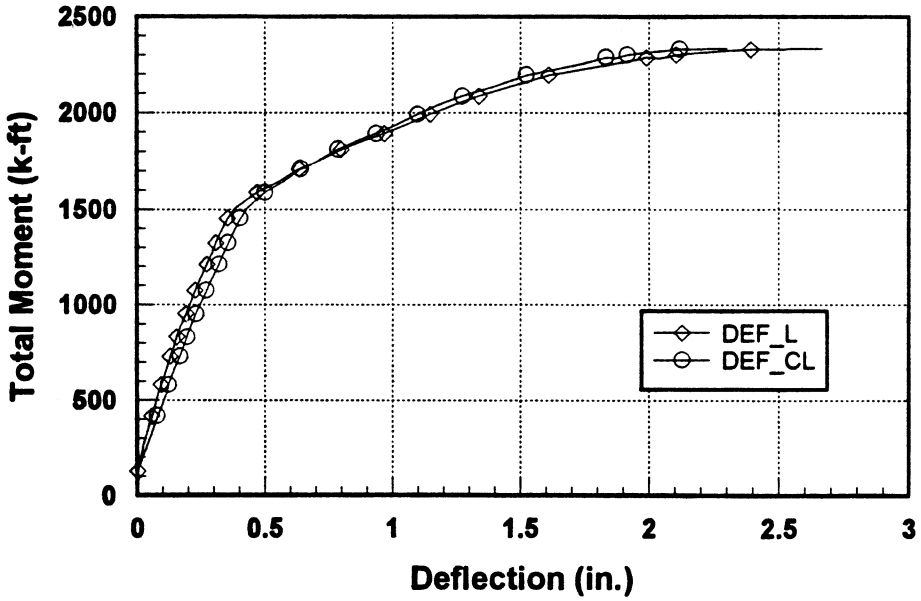

Fig 4.17b Moment vs Deflection for R-12-N

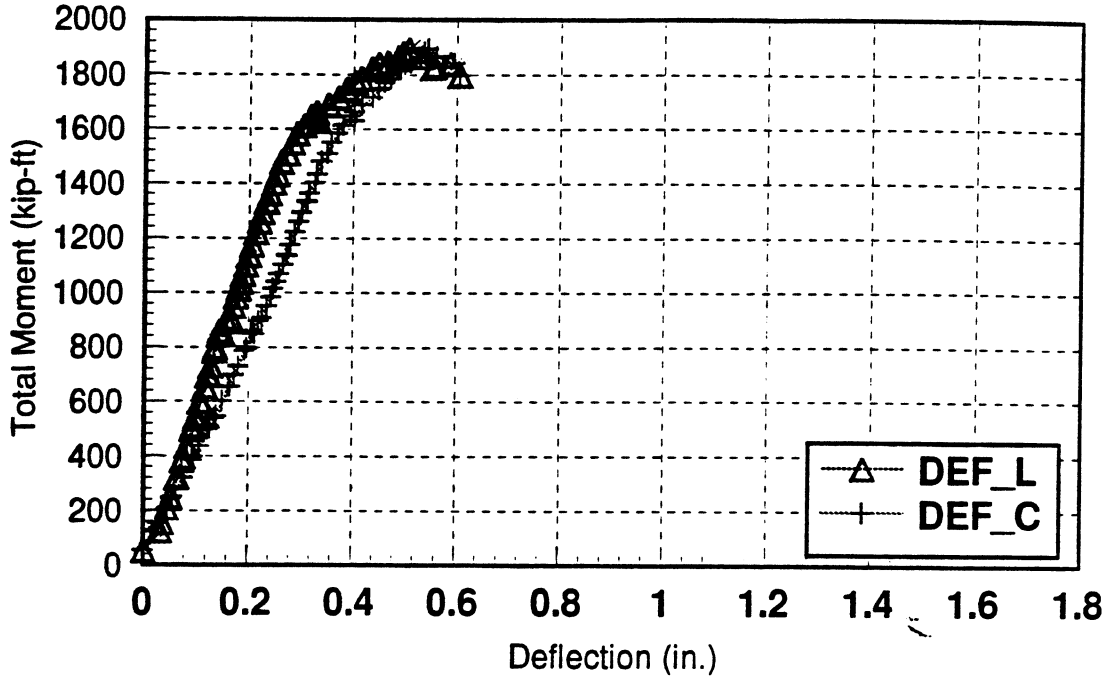

Fig 4.18a Moment vs Deflection for F-12-S

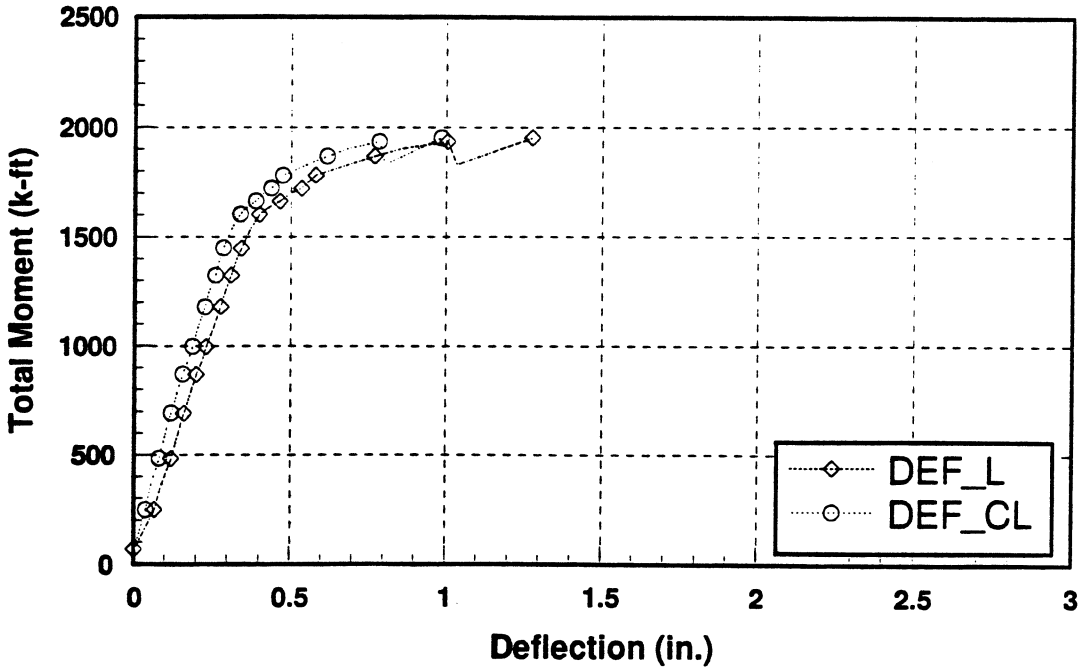

Fig 4.18b Moment vs Deflection for R-12-S

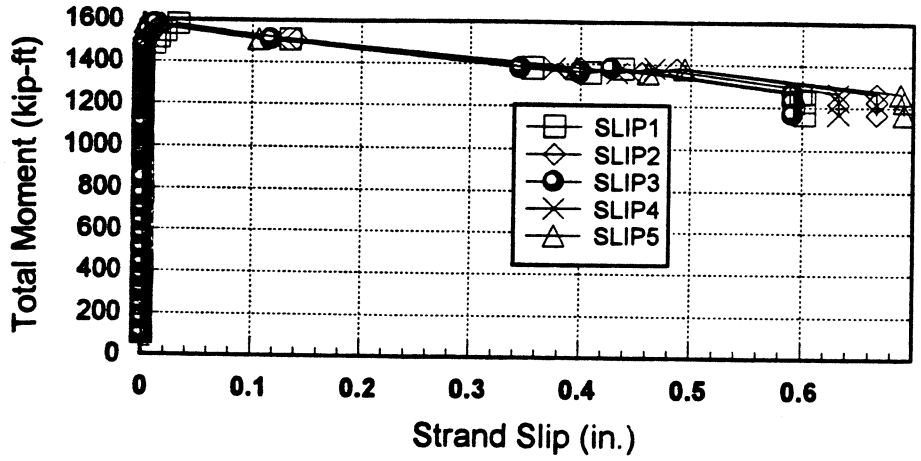

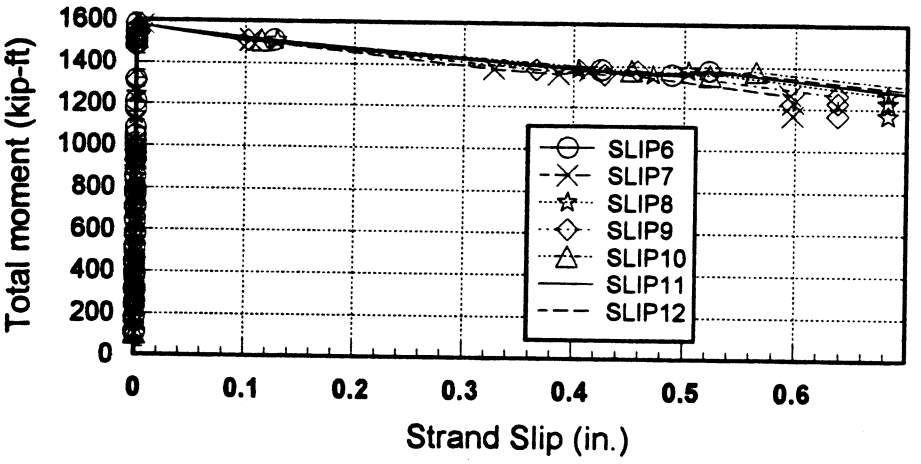

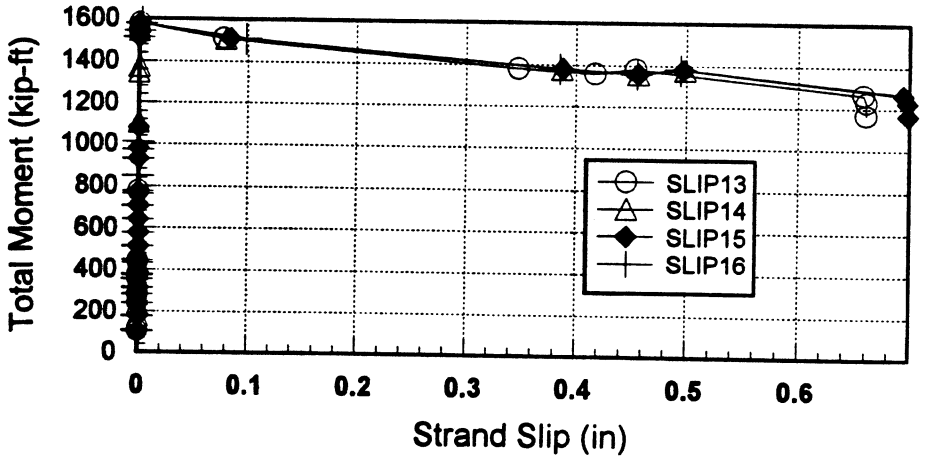

Fig 4.19 to 4.21 Total Moment vs Strand Slip for F-8-N

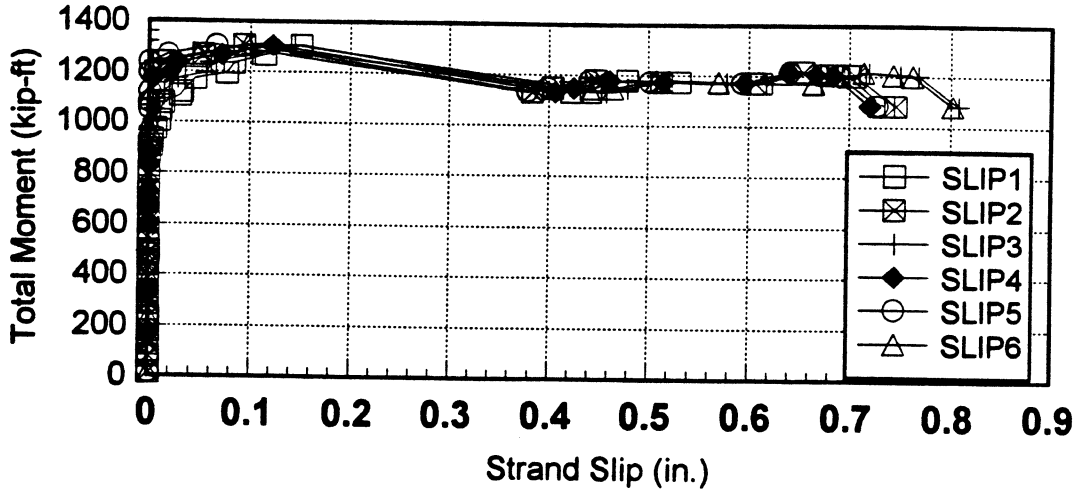

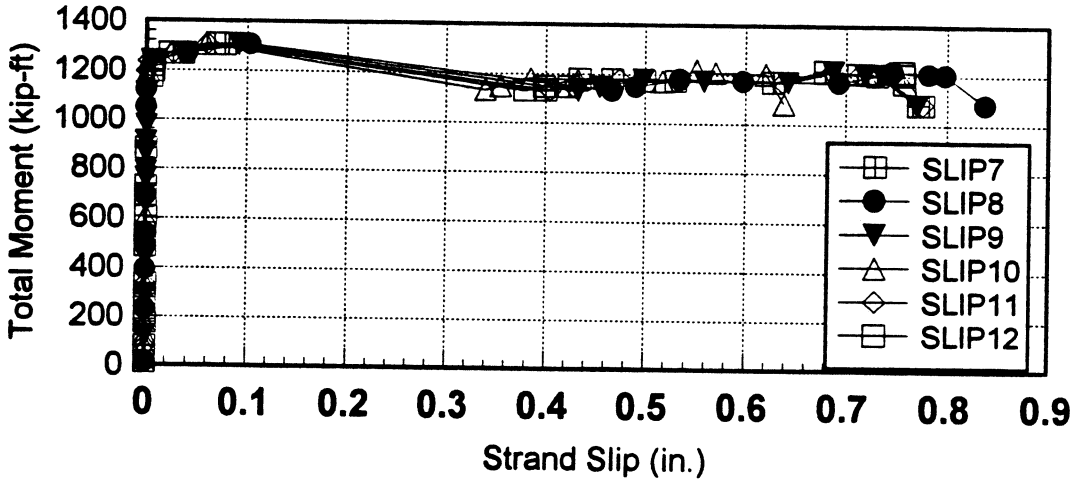

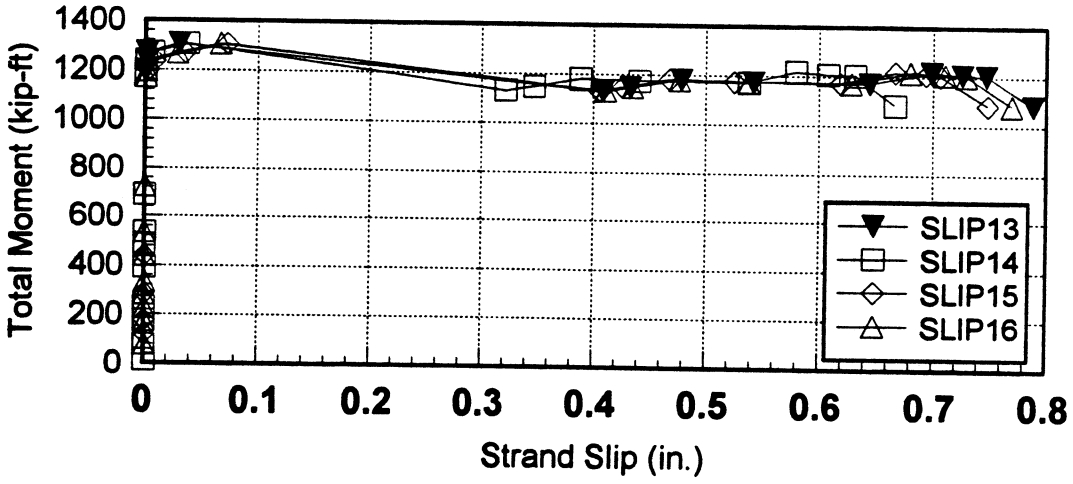

Fig 4.22 to 4.24 Total Moment vs Strand Slip for F-8-S

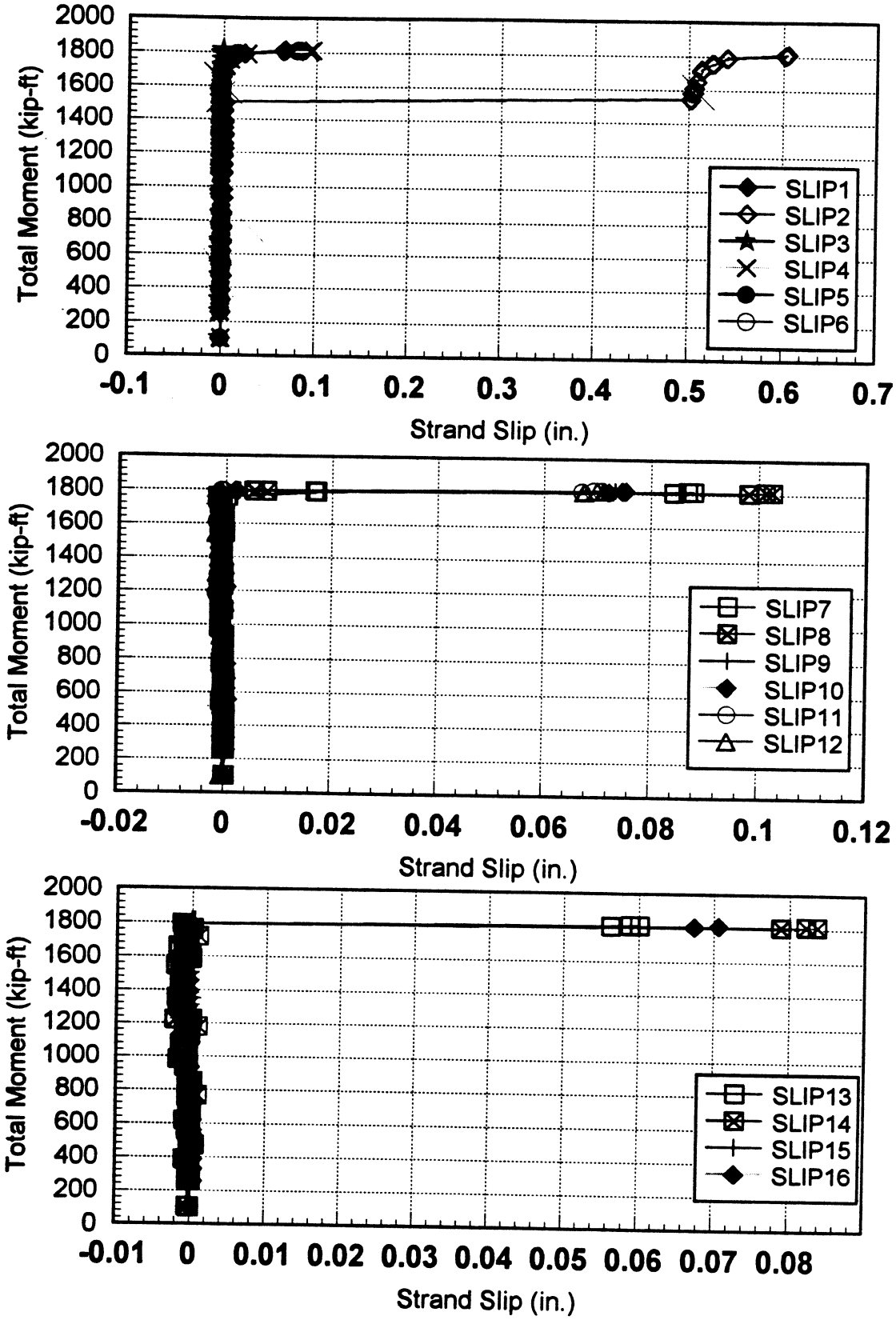

Fig 4.25 to 4.27 Total Moment vs Strand Slip for F-12-N

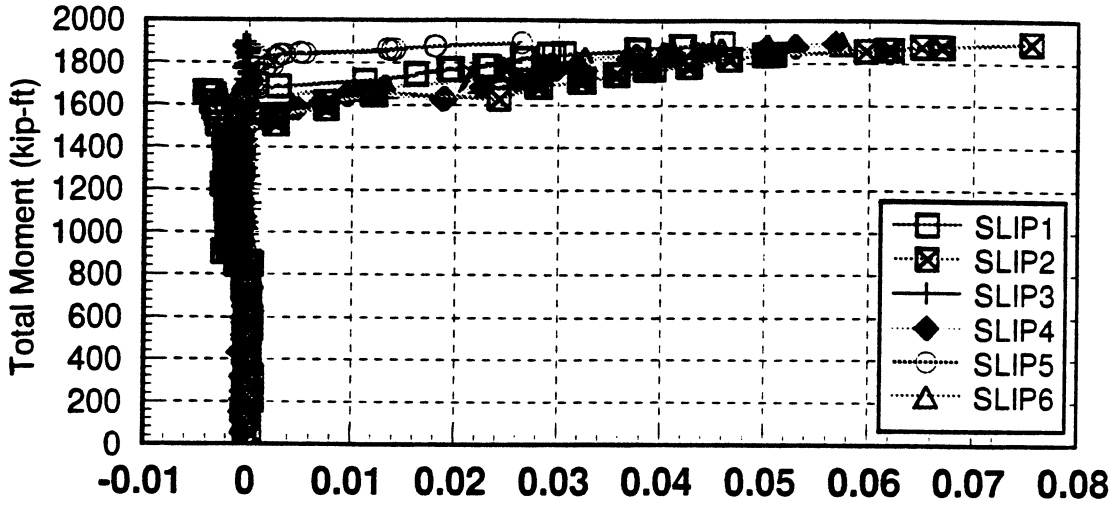

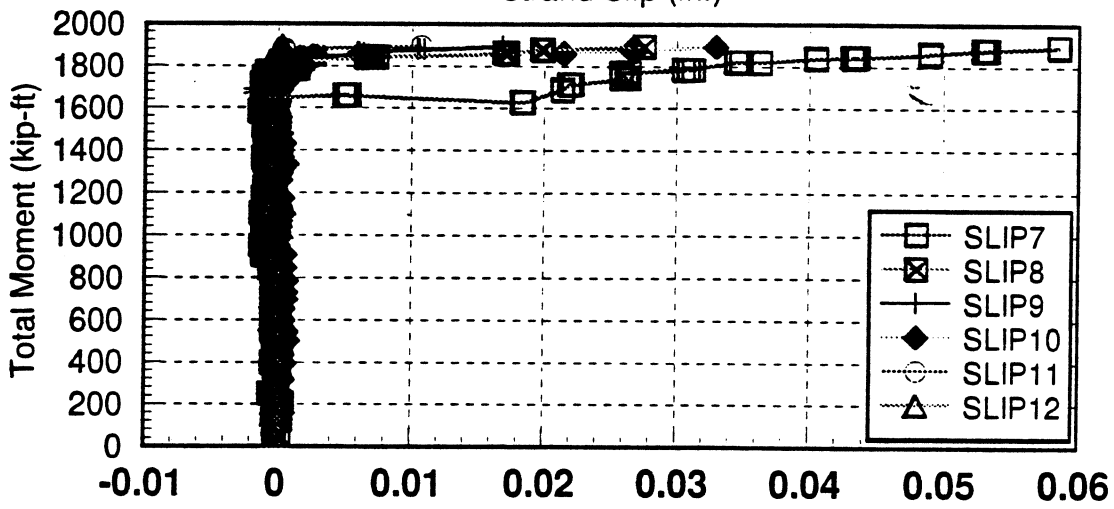

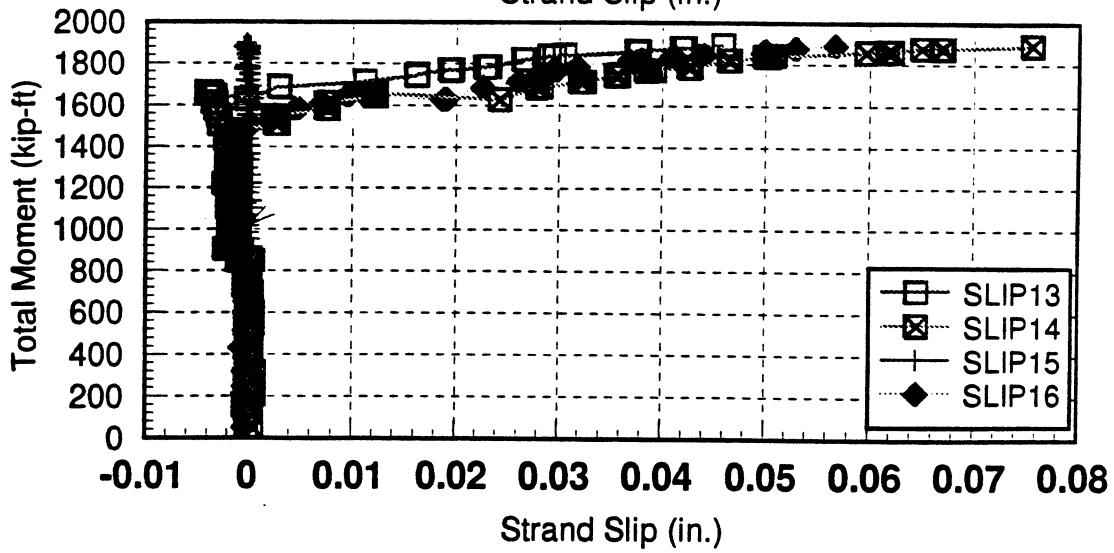

Fig 4.28 to 4.30 Total Moment vs Strand Slip for F12S

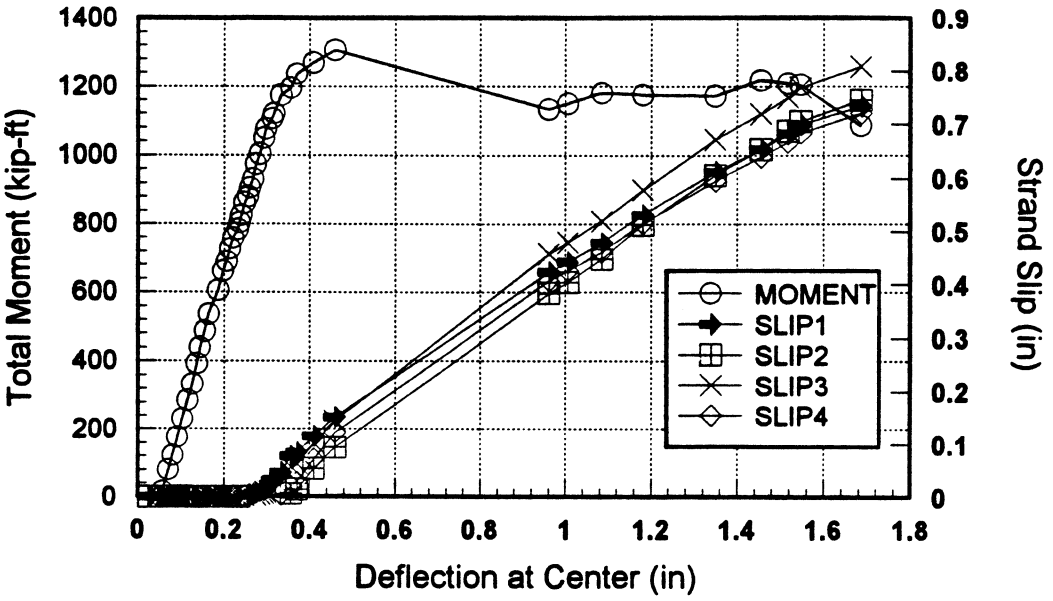

Fig 4.31a Moment and Slip vs. Deflection for F-8-S

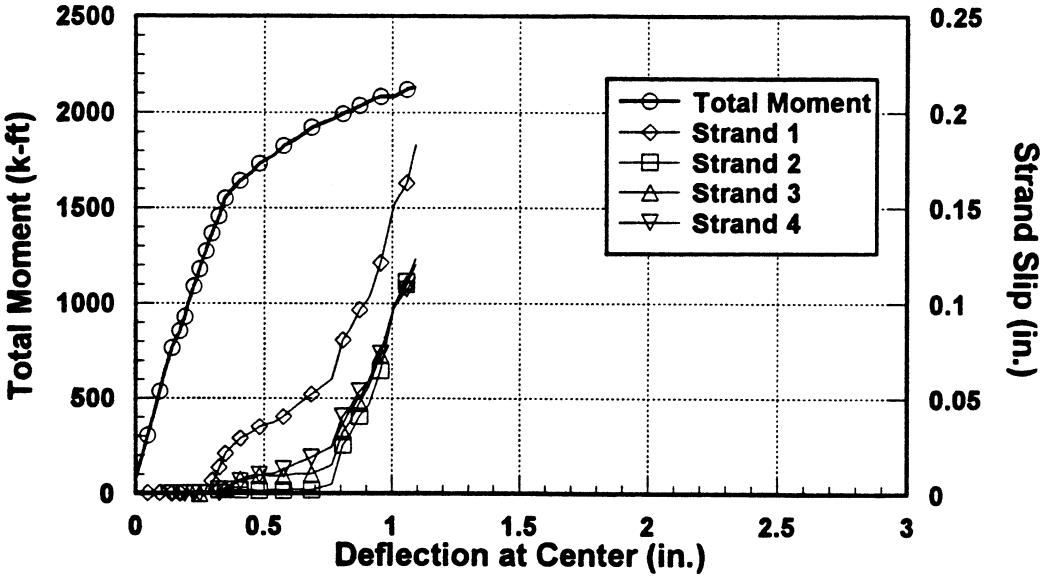

Fig 4.31b Moment and Slip vs. Deflection for R-8-S

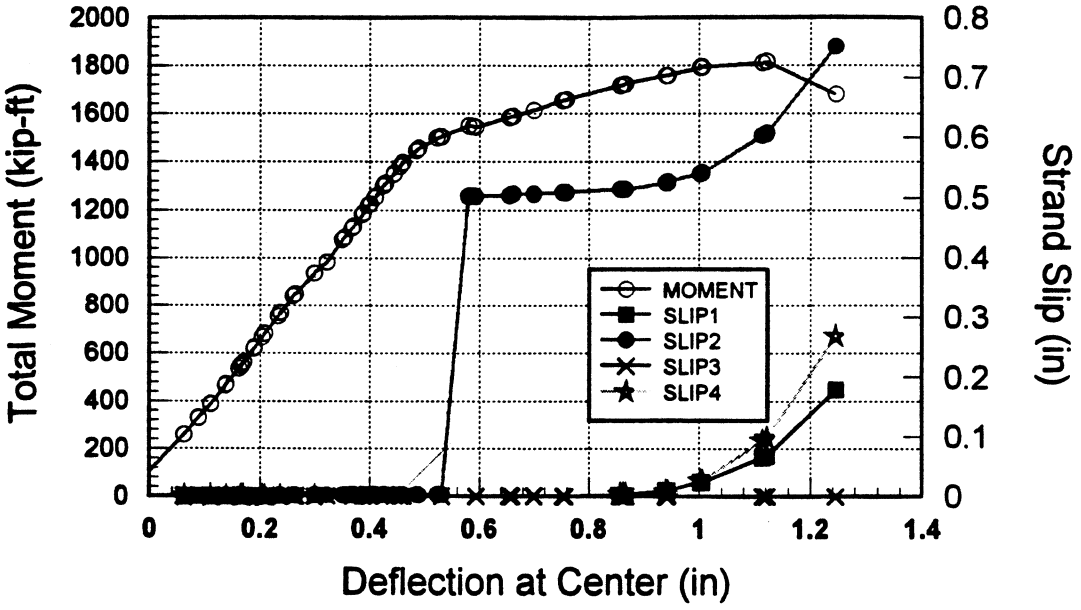

Fig 4.32a Moment and Slip vs. Deflection for F-12-N

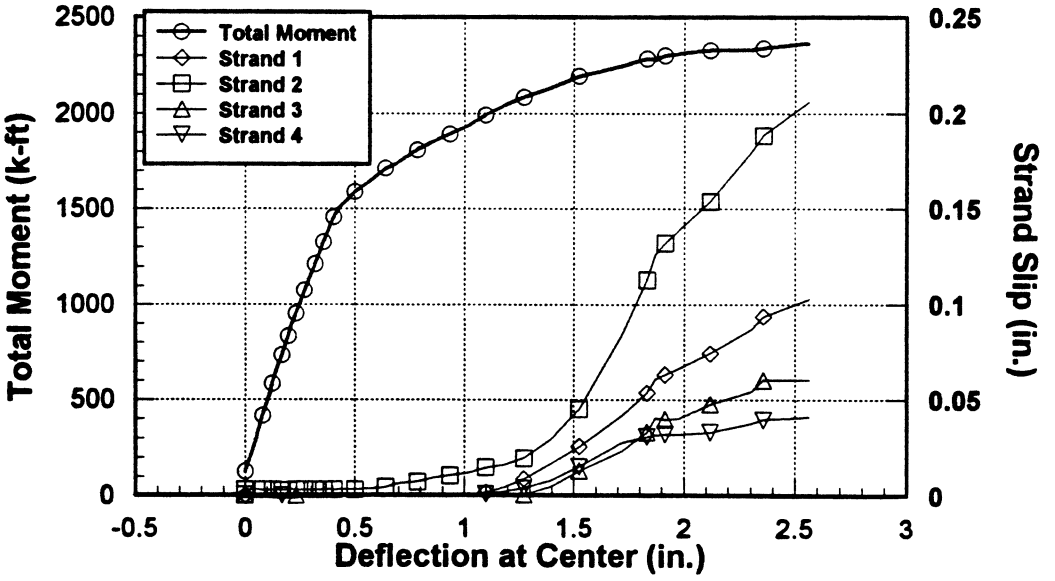

Fig 4.32b Moment and Slip vs. Deflection for R-12-N

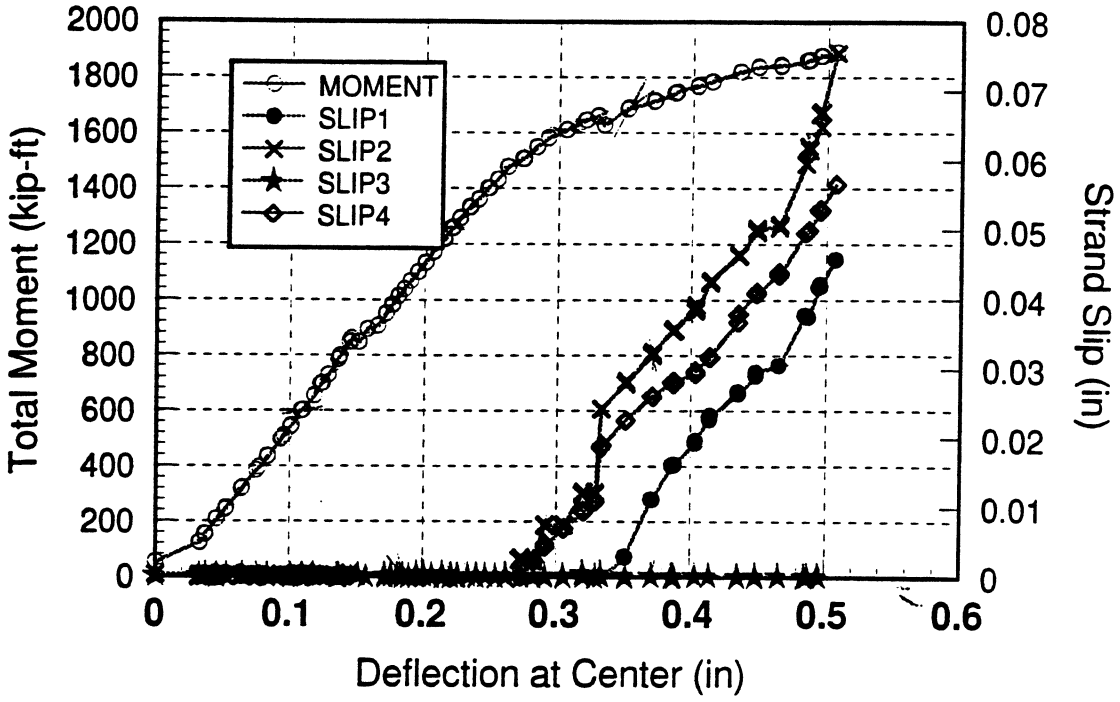

Fig 4.33a Moment and Slip vs. Deflection for F-12-S

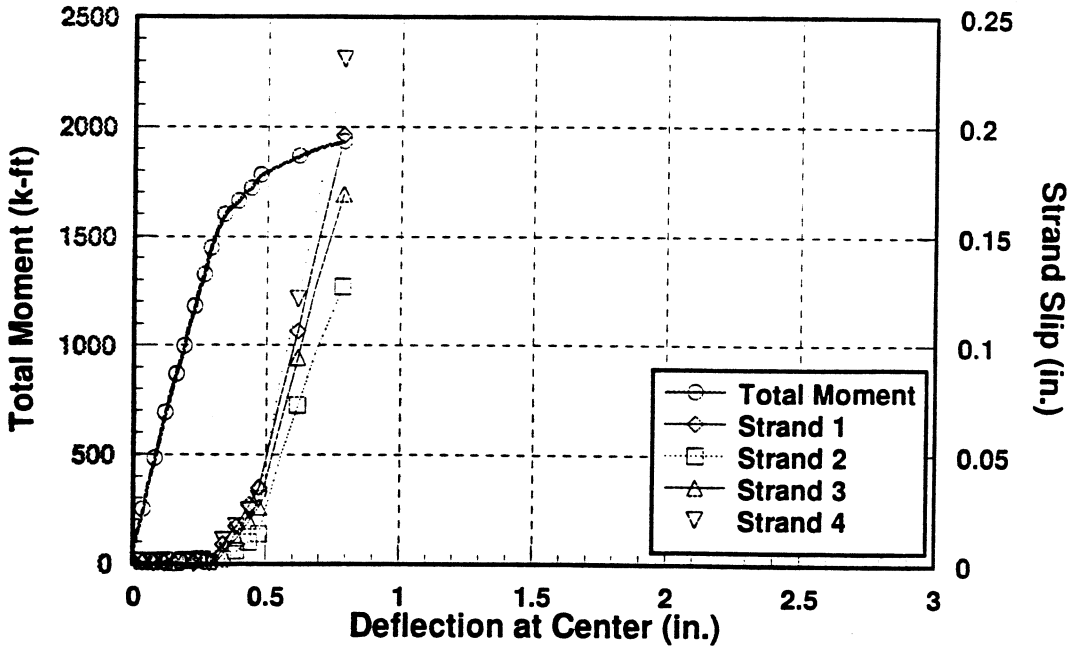

Fig 4.33b Moment and Slip vs. Deflection for R-12-S

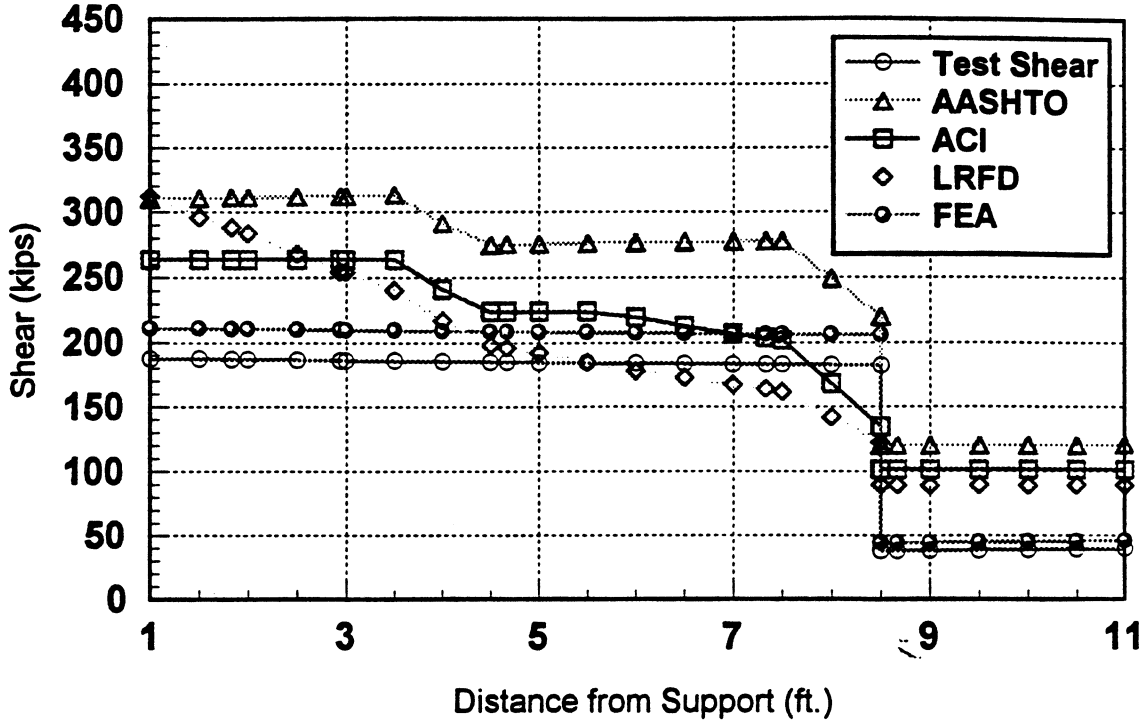

Fig 4.34a Shear Strength vs Distance from Support for F8N

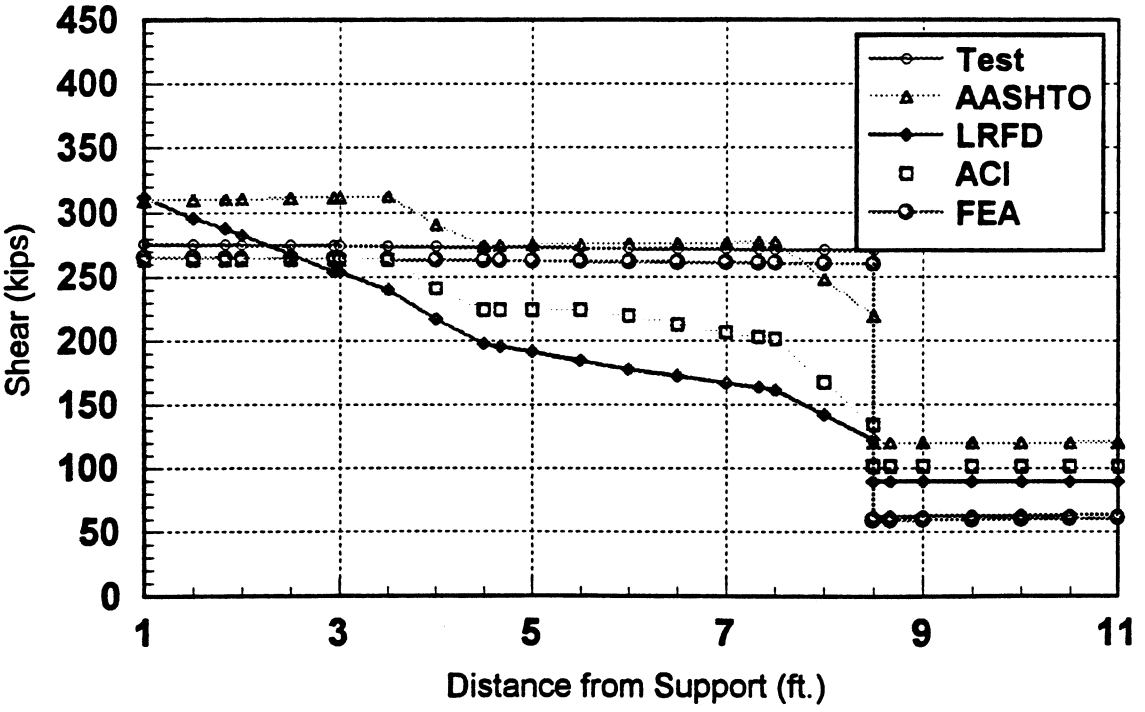

Fig 4.34b Shear Strength vs Distance from Support for R8N

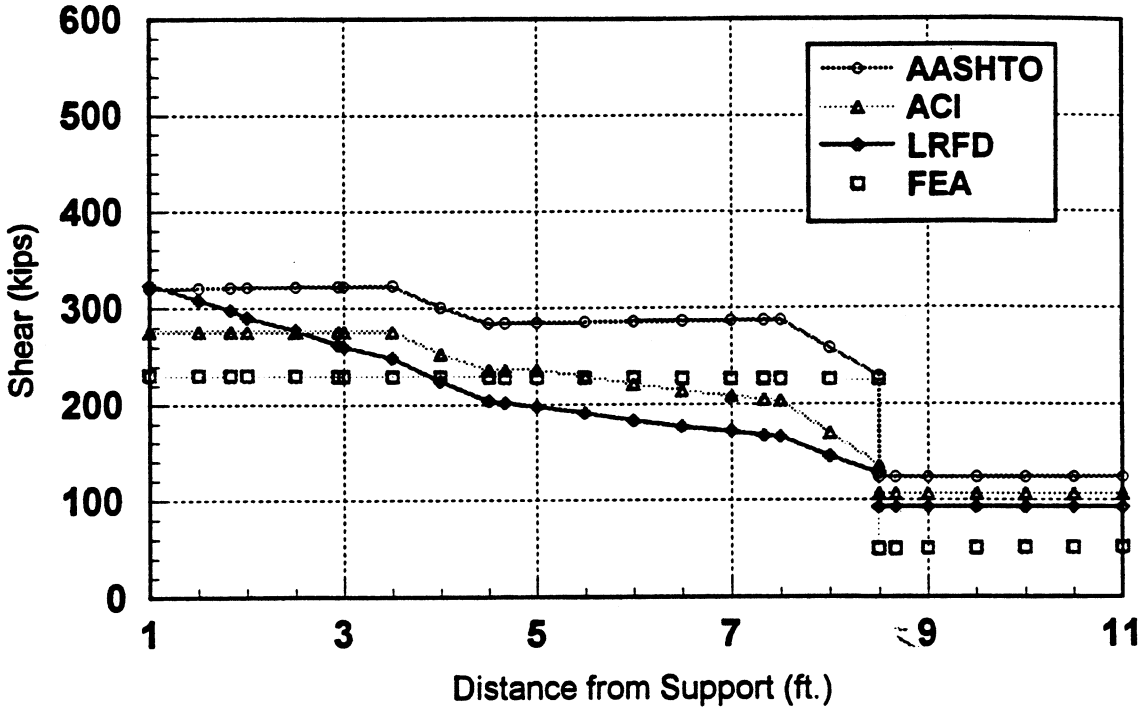

Fig 4.35a Shear Strength vs Distance from Support for F10N

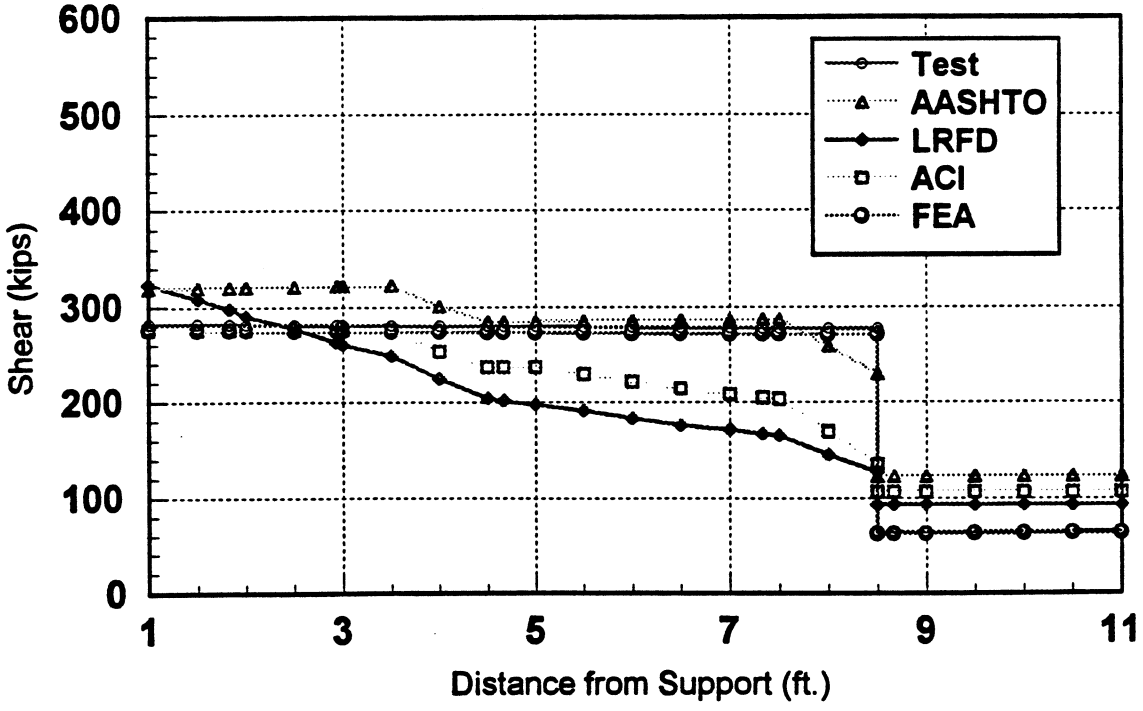

Fig 4.35b Shear Strength vs Distance from Support for R10N

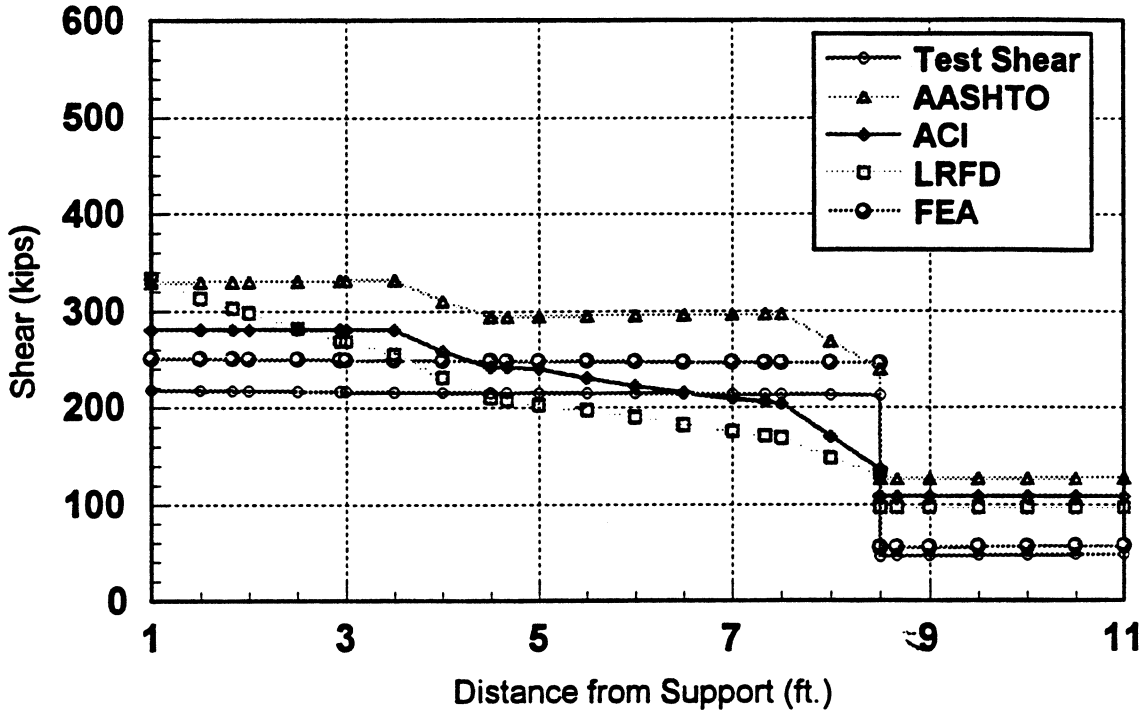

Fig 4.36a Shear Strength vs Distance from Support for F12N

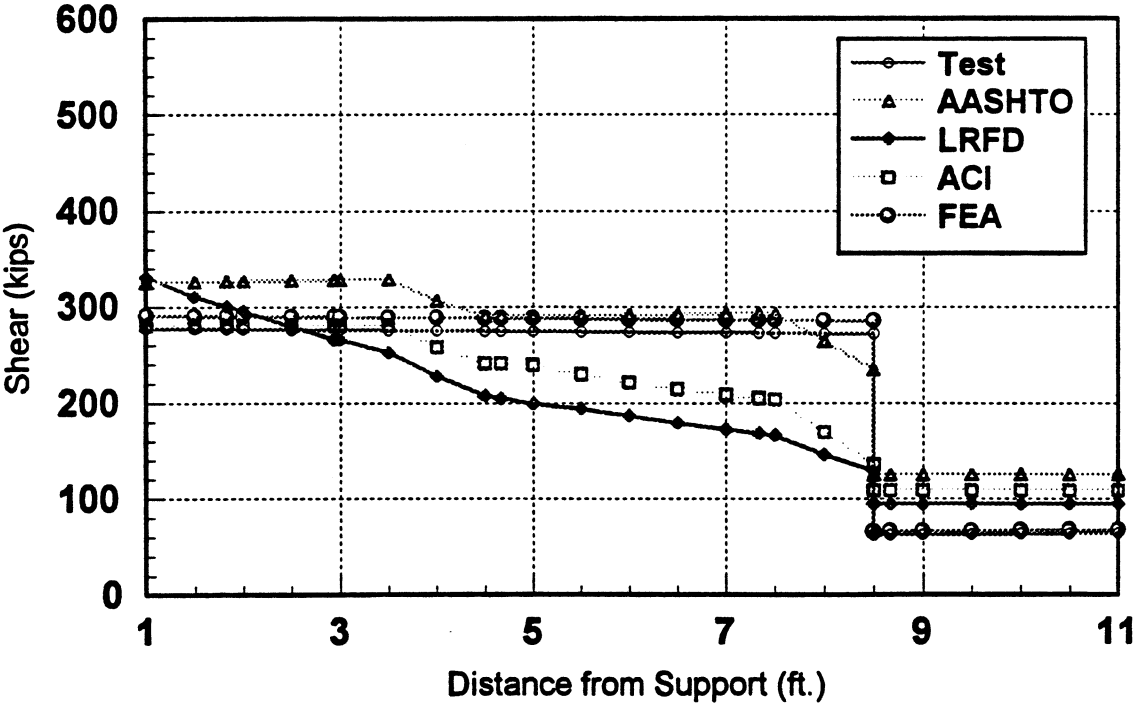

Fig 4.36b Shear Strength vs Distance from Support for R12N

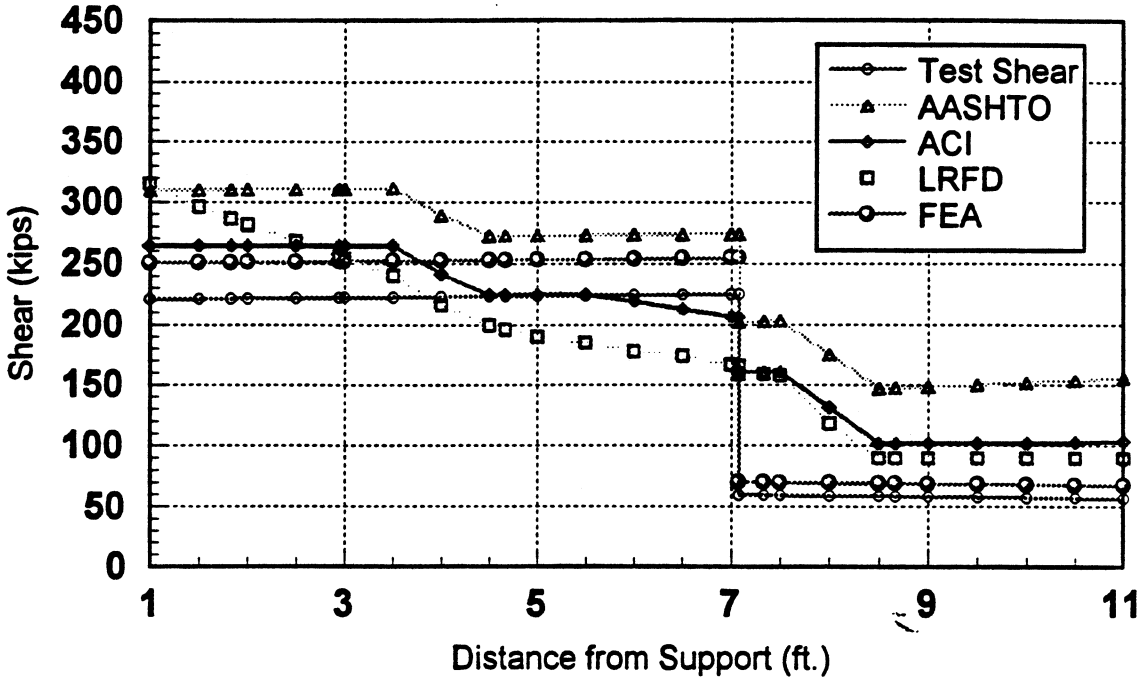

Fig 4.37a Shear Strength vs Distance from Support for F8S

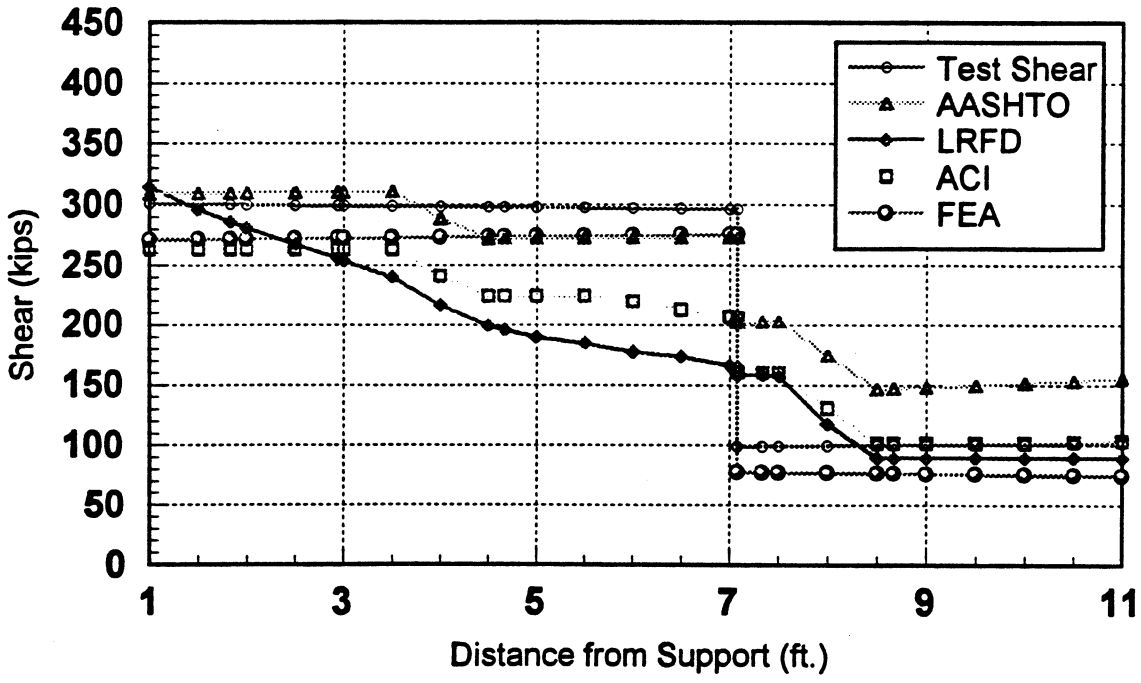

Fig 4.37b Shear Strength vs Distance from Support for R8S

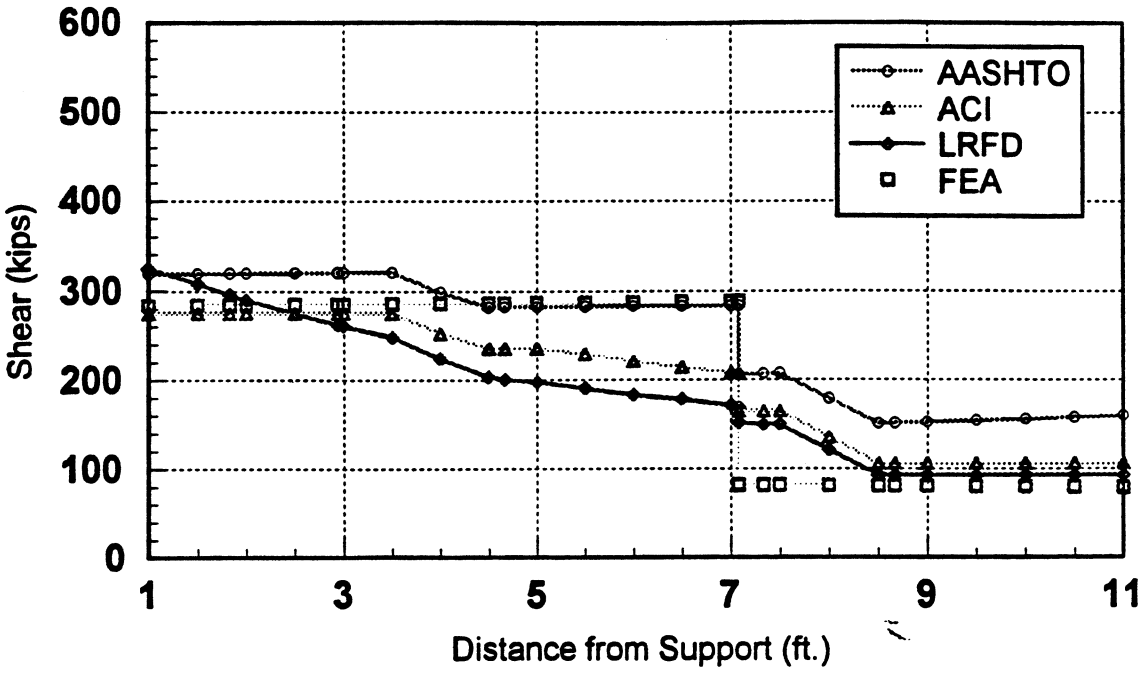

Fig 4.38a Shear Strength vs Distance from Support for F10S

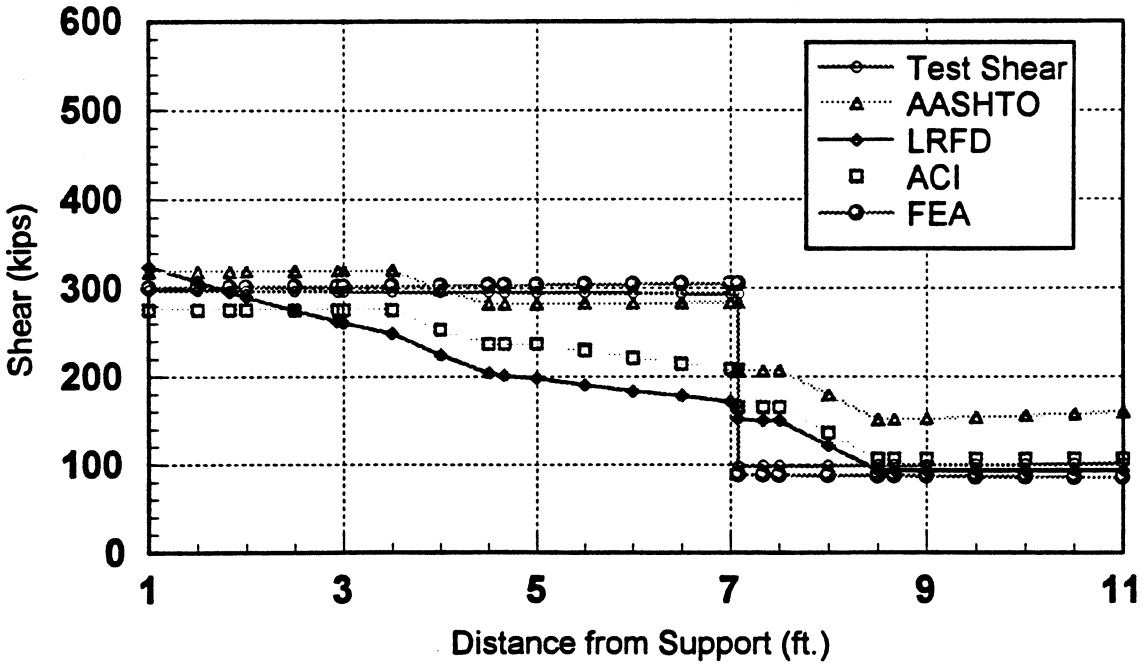

Fig 4.38b Shear Strength vs Distance from Support for R10S

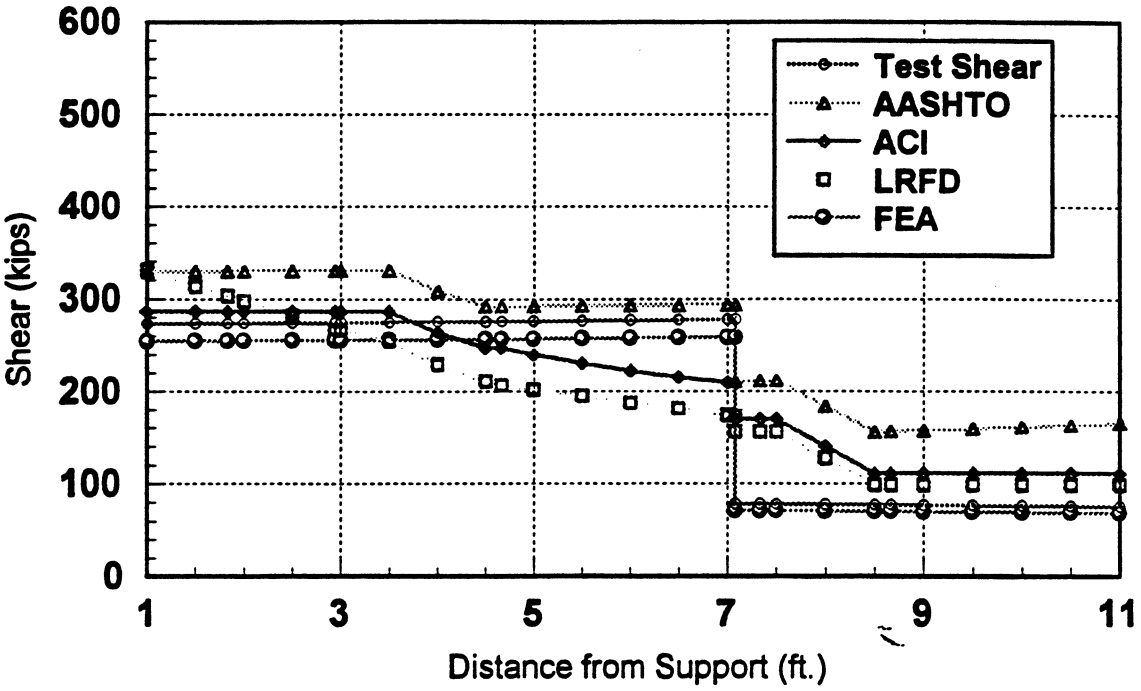

Fig 4.39a Shear Strength vs Distance from Support for F12S

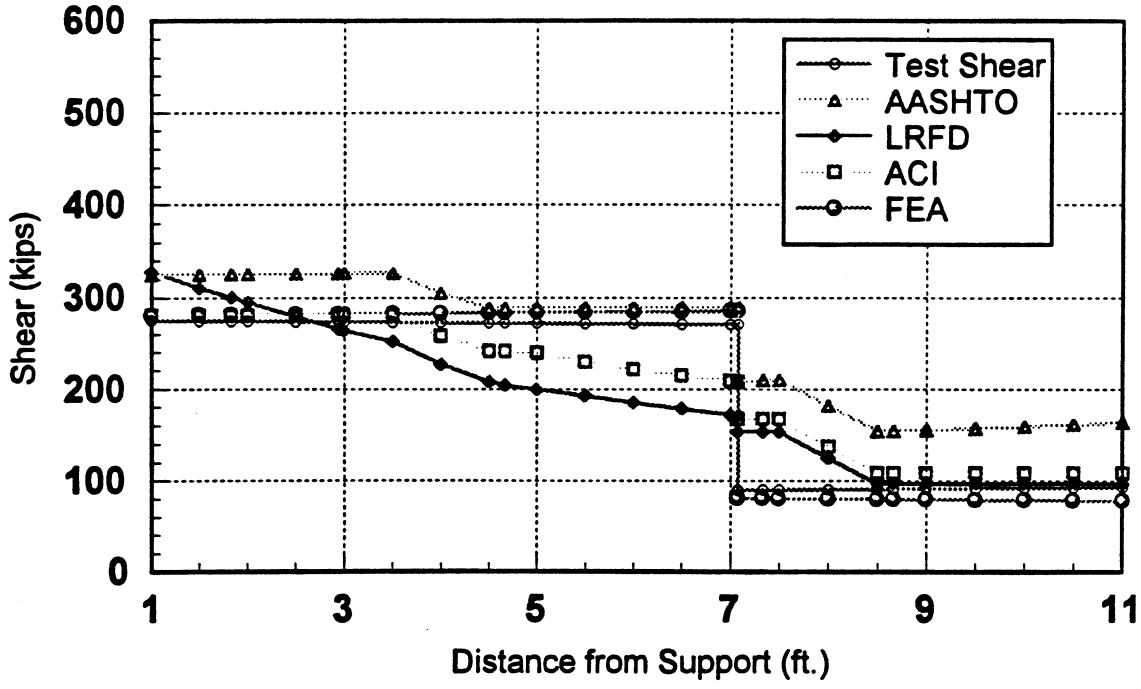

Fig 4.39b Shear Strength vs Distance from Support for R12S

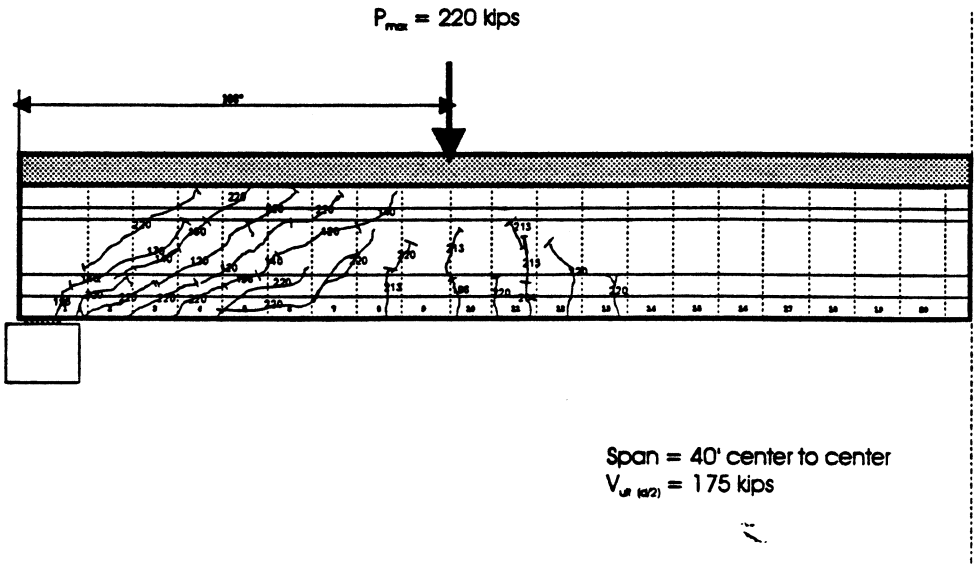

Figure 4.40a Cracking Pattern for Girder F8N

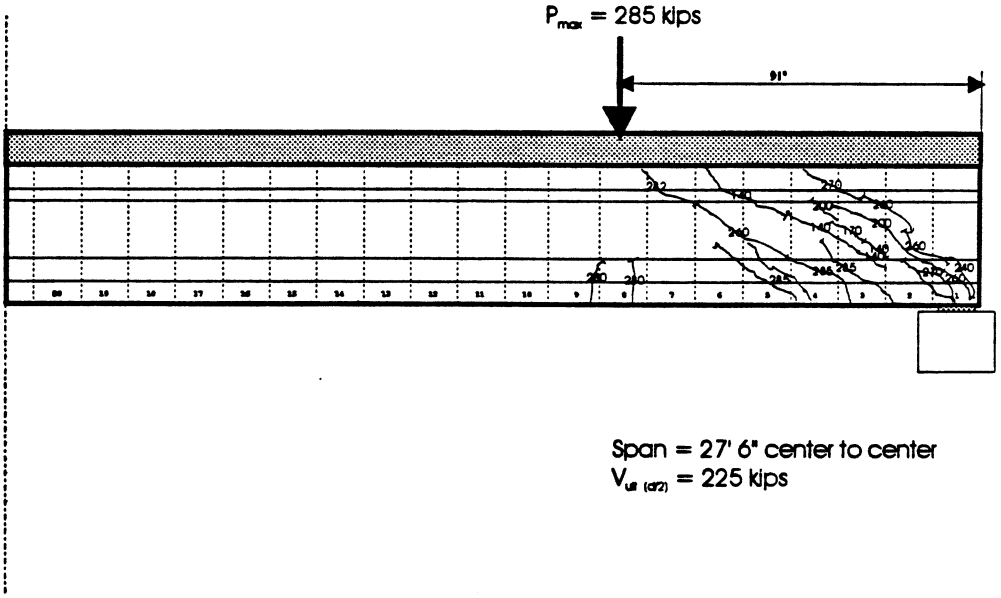

Figure 4.40b Cracking Pattern for Girder F8S

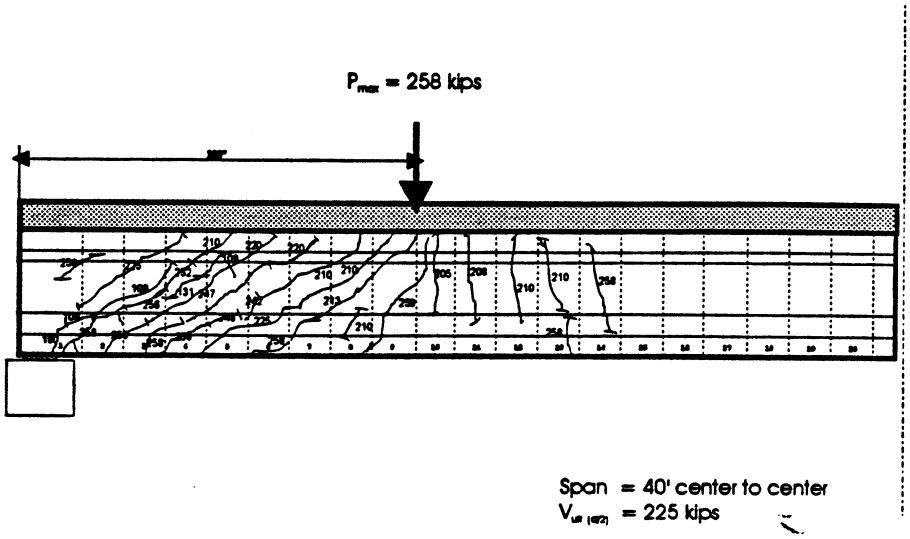

Figure 4.41a Cracking Pattern for Girder F12N

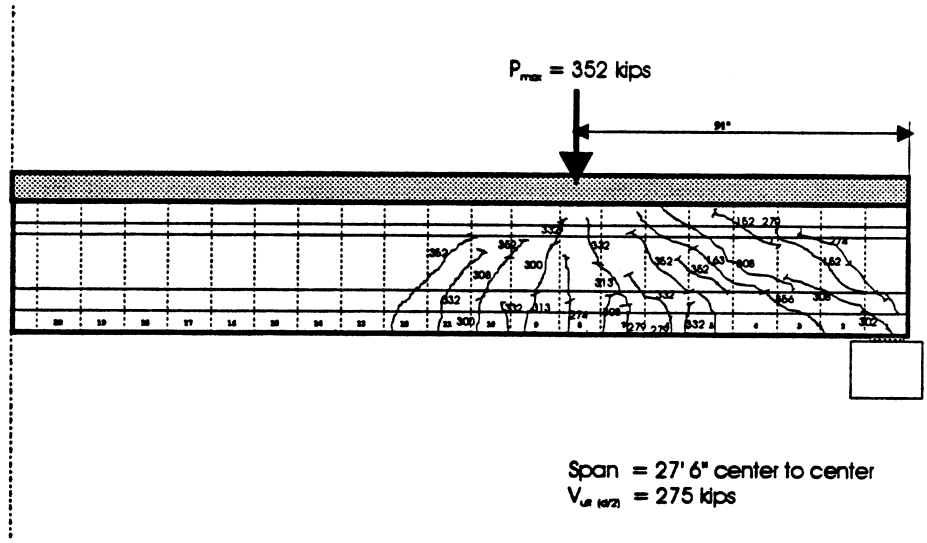

Figure 4.41b Cracking Pattern for Girder F12S

ANSYS 5.1 58
DEC 24 1995
17:42:38
NODAL SOLUTION
STEP=1
SUB =3
TIME=2
UY
RSYS=0
DMX =.3409
SMN =-.005765
SMX =.327107
U

XV =1.22
YV =.158919
ZV =1.22
DIST=203.792
XF =9
YF =33.512
ZF =246.753
A-ZS=-.854E-06
CENTROID HIDDEN

-.005765
.03122
.068206
.105192
.142178
.179164
.21615
.253135
.290121
.327107

Fig 4.42 Finite Element Camber for 8000 psi girder

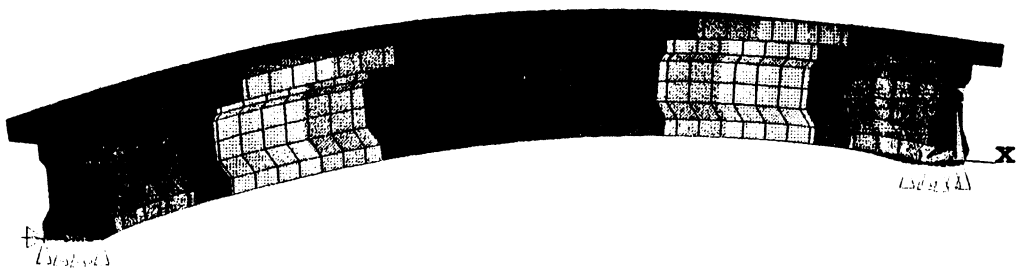

ANSYS 5.1 58
DEC 24 1995
20:27:06
NODAL SOLUTION
STEP=1
SUB =3
TIME=2
UY
RSYS=0
DMX =.309783
SMN =-.004411
SMX =.298106
U

XV =1.22
YV =.158919
ZV =1.22
DIST=203.79
XF =9
YF =33.545
ZF =246.55
A-ZS=-.854E-06
CENTROID HIDDEN

-.004411
.029202
.062815
.096428
.130041
.163654
.197267
.23088
.264493
.298106

Fig 4.43 Finite Element Camber for 10000 psi girder

ANSYS 5.1 58
DEC 24 1995
20:35:42
NODAL SOLUTION
STEP=1
SUB =3
TIME=2
UY
RSYS=0
DMX =.27891
SMN =-.004332
SMX =.268127
U

XV =1.22
YV =.158919
ZV =1.22
DIST=203.798
XF =9
YF =33.534
ZF =246.608
A-ZS=-.854E-06
CENTROID HIDDEN

-.004332
.025941
.056215
.086488
.116761
.147034
.177307
.20758
.237853
.268127

Fig 4.44 Finite Element Camber for 12000 psi girder

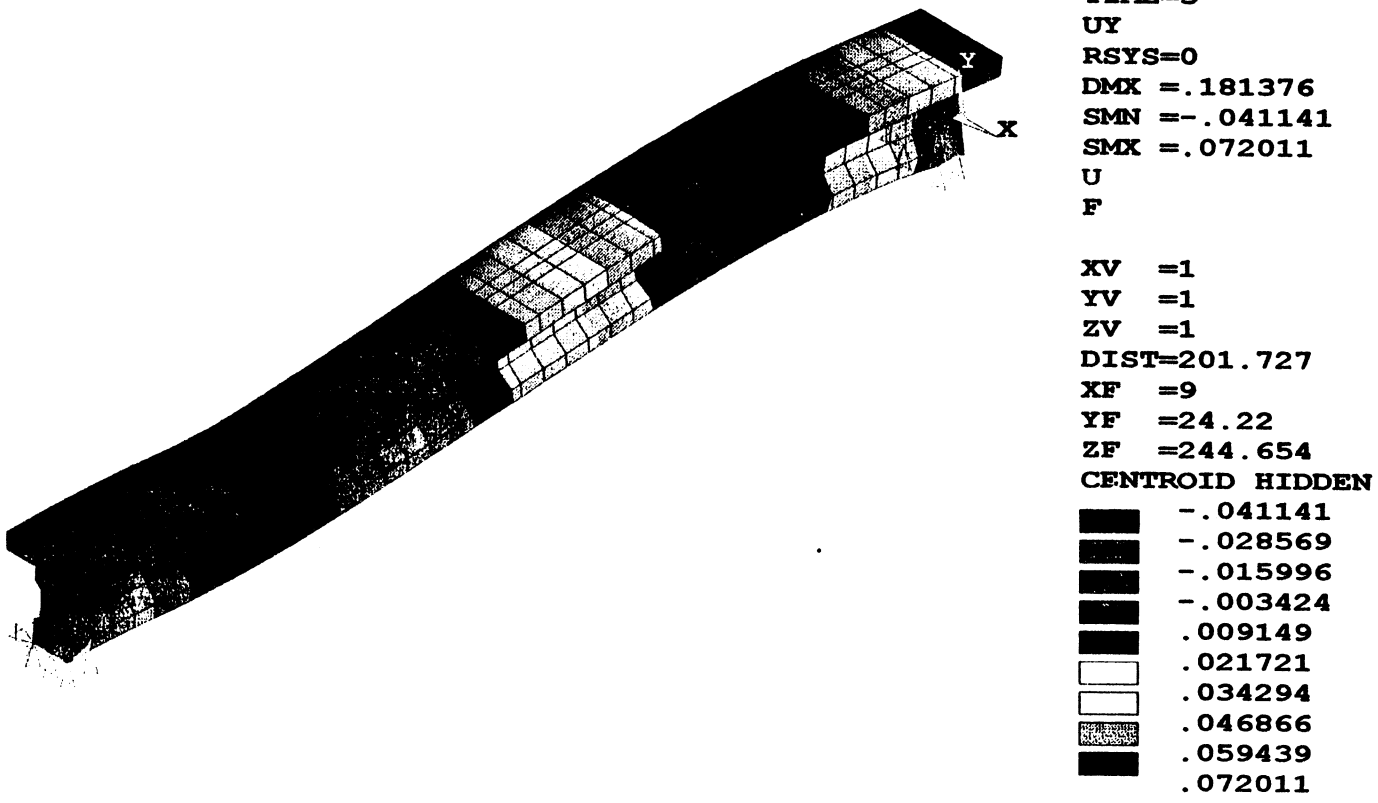

Fig 4.45 Finite Element Deflection for F8N

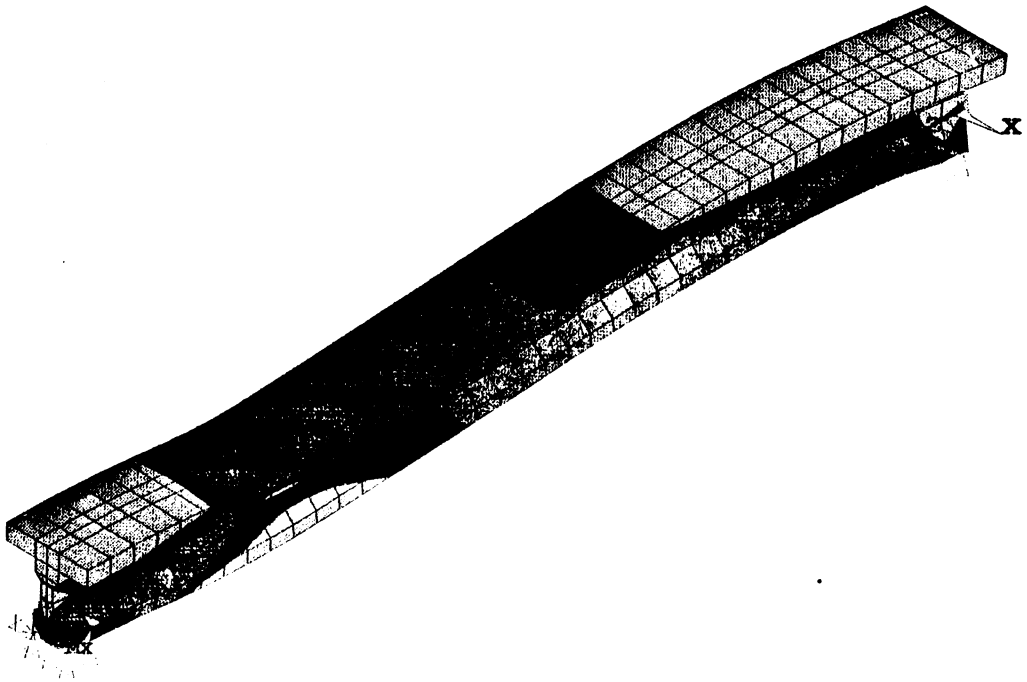

ANSYS 5.1 58
DEC 24 1995
20:04:16
NODAL SOLUTION
STEP=3
SUB =1
TIME=3
SZ (AVG)
RSYS=0
DMX =.181376
SMN =-13540
SMX =7453
U
F

XV =1
YV =1
ZV =1
DIST=201.727
XF =9
YF =24.22
ZF =244.654
CENTROID HIDDEN
-2000
-1800
-1600
-1300
-1100
-800
-600
-400
-100
100
400
600
900

Fig 4.46 Finite Element Stress in Z-dir'n for F8N

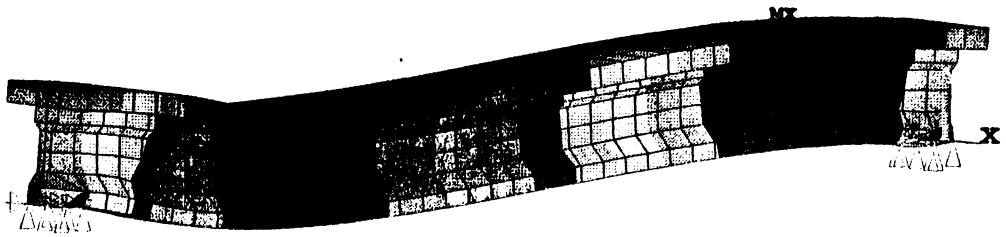

ANSYS 5.1 58
DEC 24 1995
20:12:36
NODAL SOLUTION
STEP=3
SUB =5
TIME=3
UY
RSYS=0
DMX =.165183
SMN =-.096033
SMX =.021205
U
F

XV =1.22
YV =.158919
ZV =1.22
DIST=203.892
XF =9
YF =16.756
ZF =243.17
A-ZS=-.854E-06
CENTROID HIDDEN
-.096033
-.083006
-.06998
-.056953
-.043927
-.030901
-.017874
-.004848
.008179
.021205

Fig 4.47 Finite Element Deflection for R8N

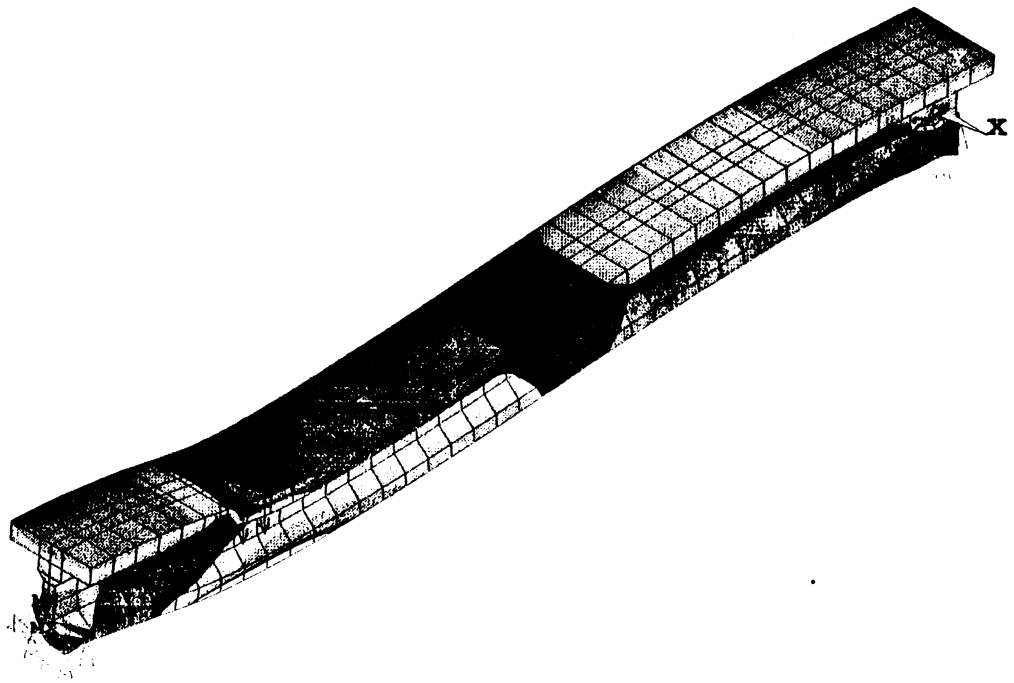

Fig 4.48 Finite Element Stress in Z-dir'n for R8N

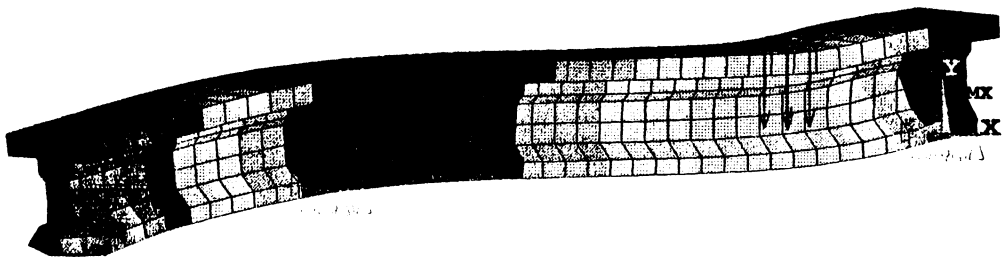

ANSYS 5.1 58
DEC 24 1995
21:05:46
NODAL SOLUTION
TIME=12
UY
RSYS=0
DMX =.241176
SMN =-.168458
SMX =.007013
U
F

XV =1.22
YV =.158919
ZV =1.22
DIST=203.134
XF =9
YF =13.882
ZF =238.159
A-ZS=-.854E-06
CENTROID HIDDEN

-.168458
-.148961
-.129464
-.109967
-.090471
-.070974
-.051477
-.03198
-.012484
.007013

Fig 4.49 Finite Element Deflection for R10S

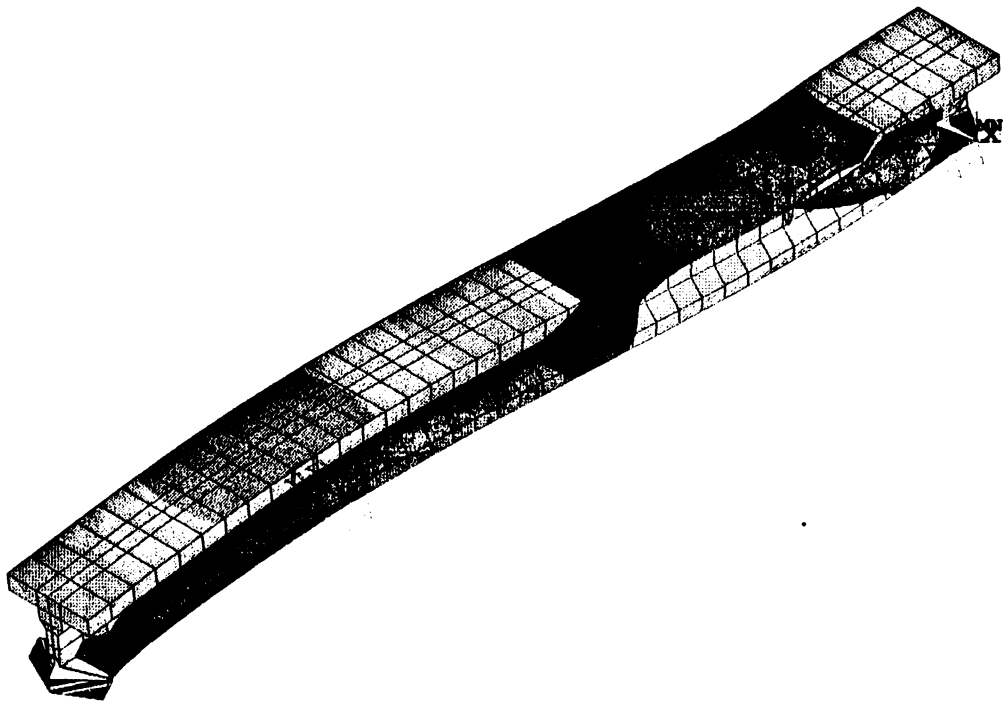

Fig 4.50 Finite Element Stress in Z-dir'n for R10S

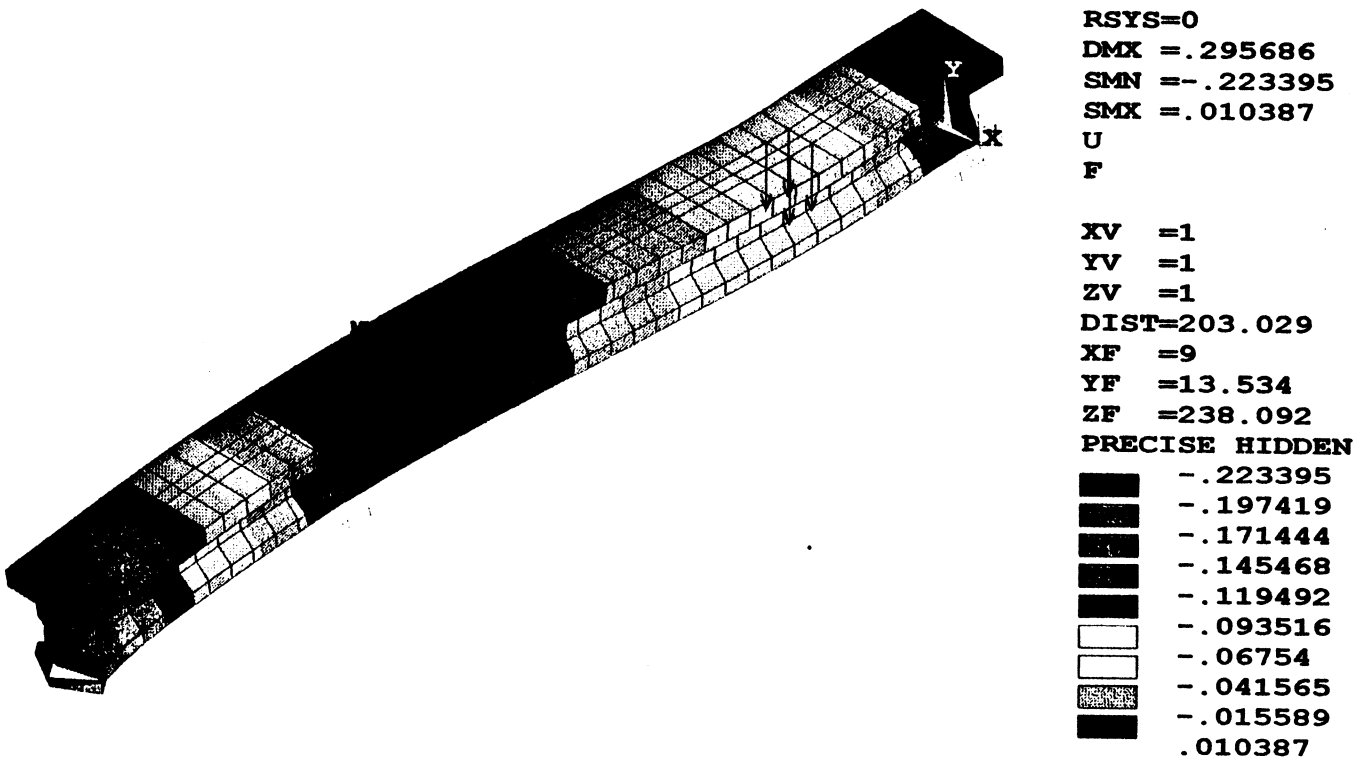

Fig 4.51 Finite Element Deflection for F10S

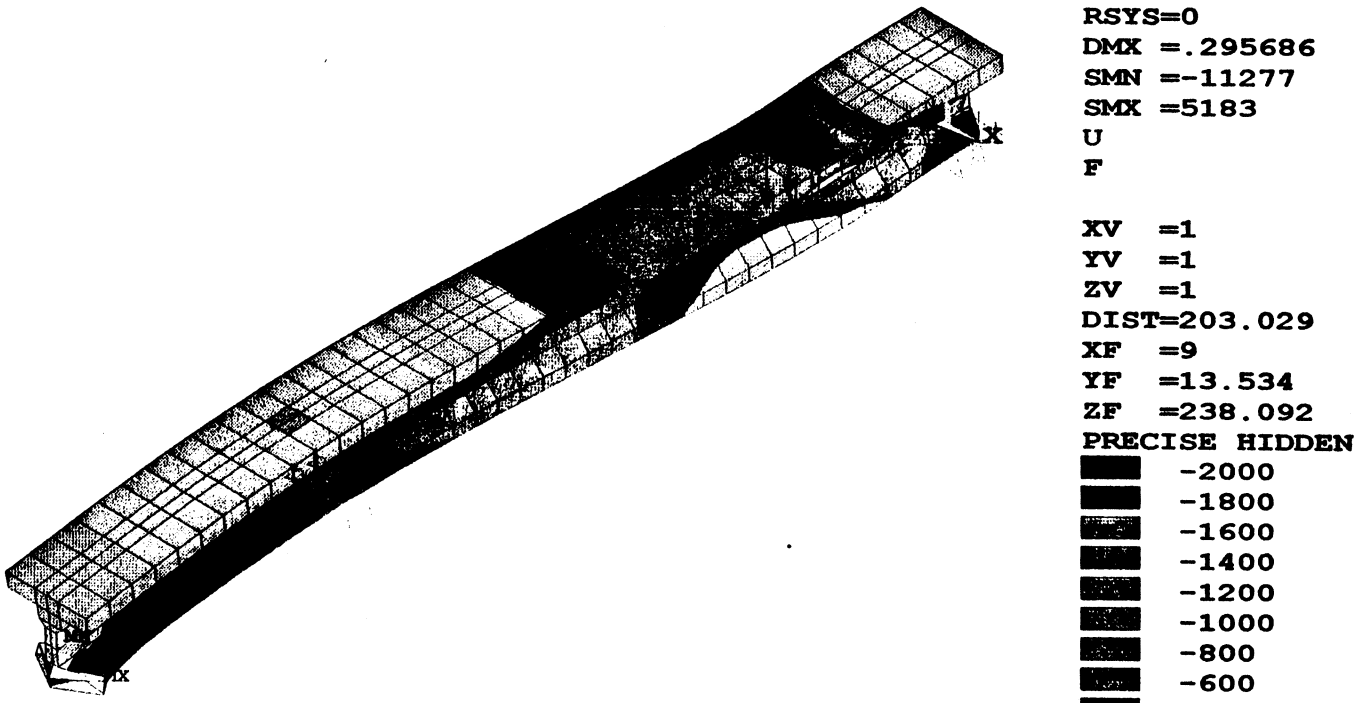

Fig 4.52 Finite Element Stress in Z-dir'n for F10S

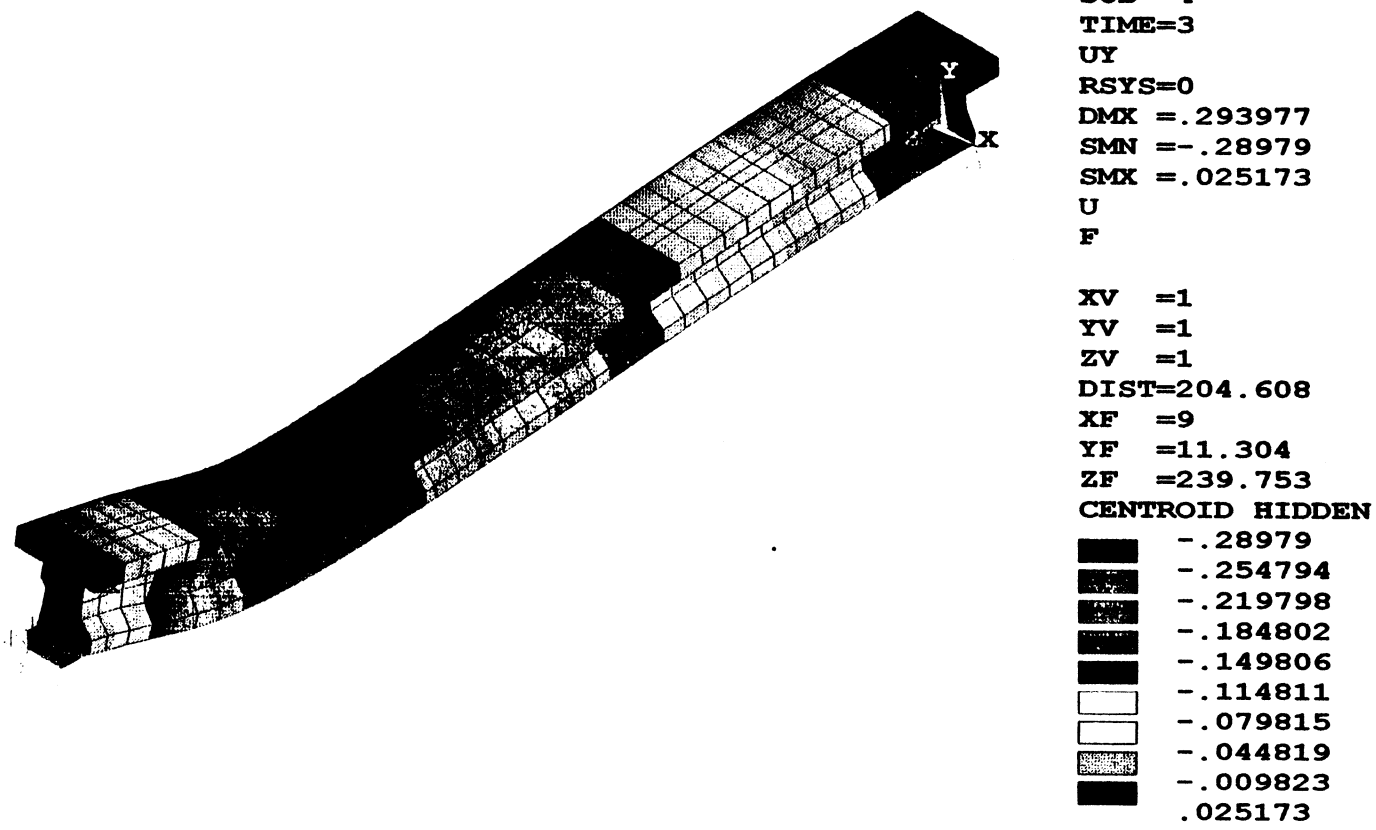

Fig 4.53 Finite Element Deflection for F12N

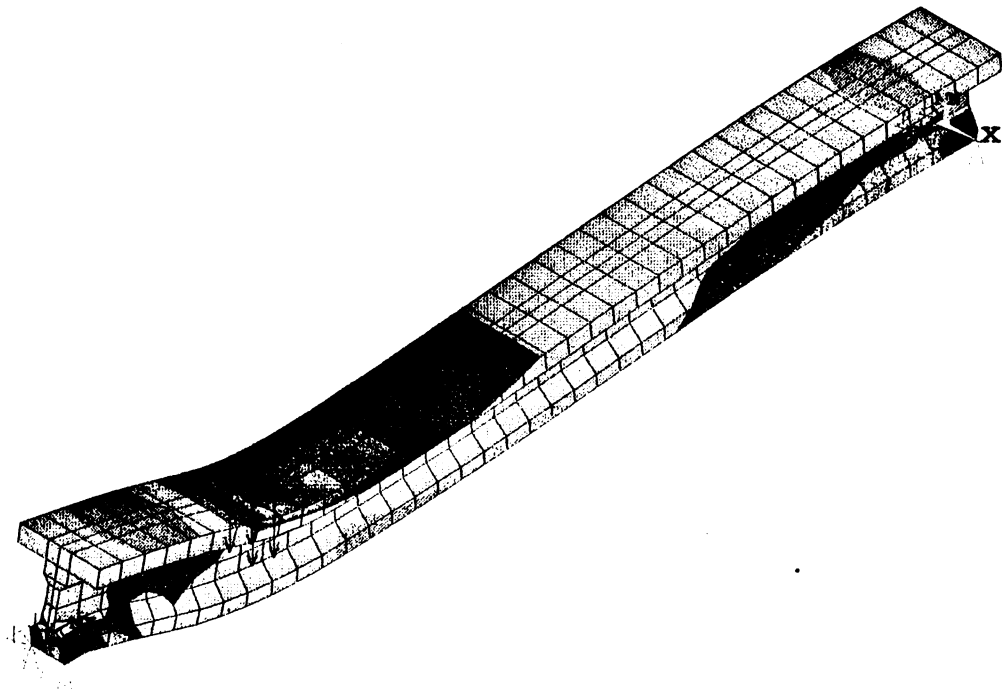

Fig 4.54 Finite Element Stress in Z-dir'n for F12N

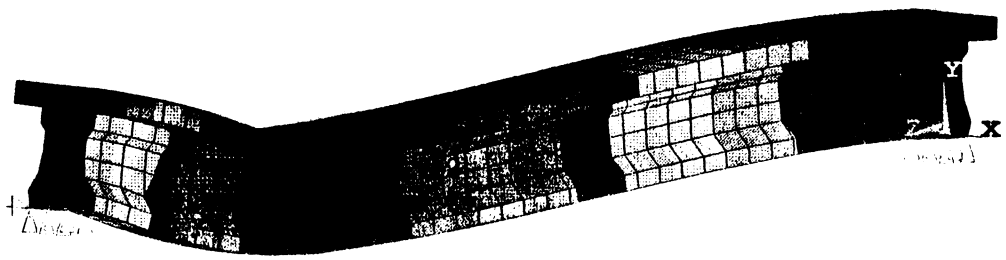

ANSYS 5.1 58
DEC 24 1995
20:40:12
NODAL SOLUTION
STEP=2
SUB =4
TIME=3
UY
RSYS=0
DMX =.161248
SMN =-.1602
SMX =.011615
U
F

XV =1.22
YV =.158919
ZV =1.22
DIST=203.911
XF =9.001
YF =11.072
ZF =241.457
A-ZS=-.854E-06
CENTROID HIDDEN

-.1602
-.14111
-.122019
-.102929
-.083838
-.064748
-.045657
-.026567
-.007476
.011615

Fig 4.55 Finite Element Deflection for R12N

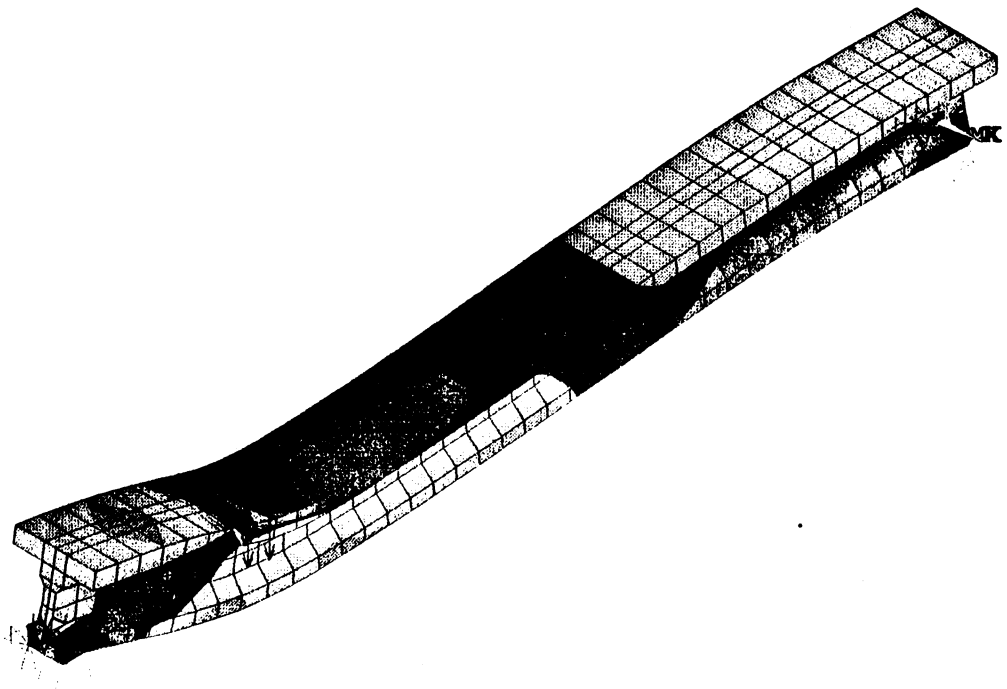

ANSYS 5.1 58
DEC 24 1995
20:47:13
NODAL SOLUTION
STEP=2
SUB =4
TIME=3
SZ (AVG)
RSYS=0
DMX =.161248
SMN =-13213
SMX =4535
U
F

XV =1
YV =1
ZV =1
DIST=203.911
XF =9.001
YF =11.072
ZF =241.457
CENTROID HIDDEN
-3000
-2700
-2400
-2100
-1700
-1400
-1100
-800
-400
-100
200
500
900

Fig 4.56 Finite Element Stress in Z-dir'n for R12N

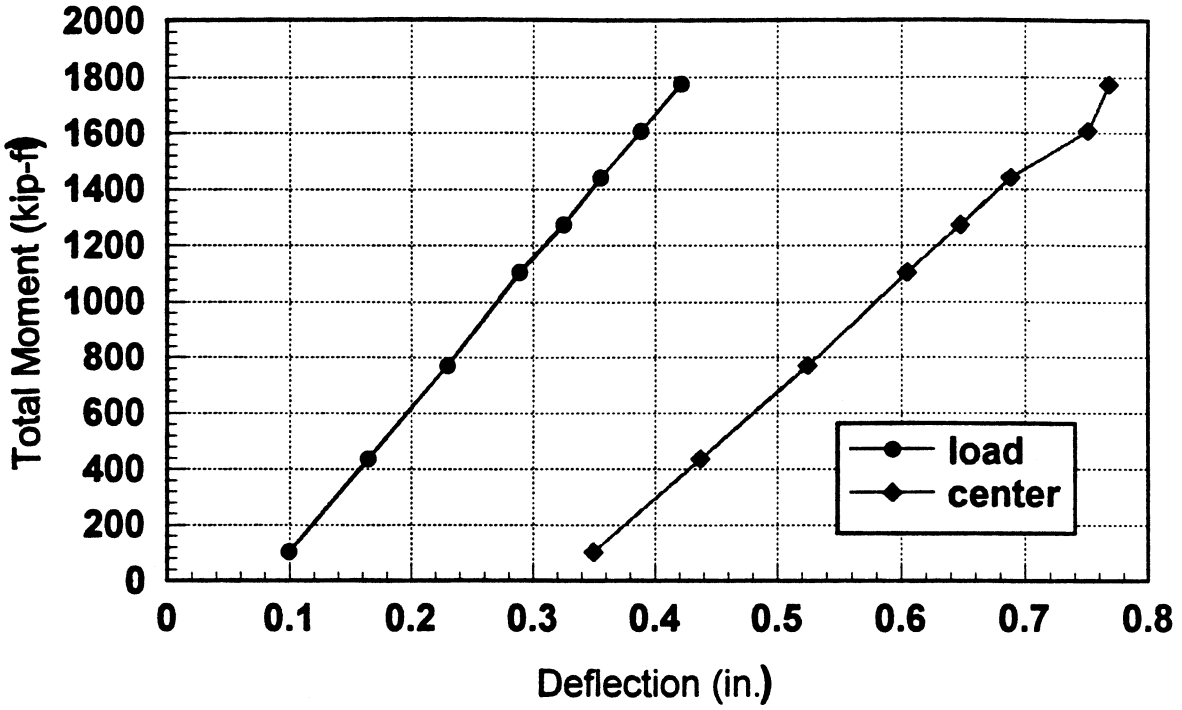

Fig 4.57a Total Moment Vs Deflection for F8N from FEA

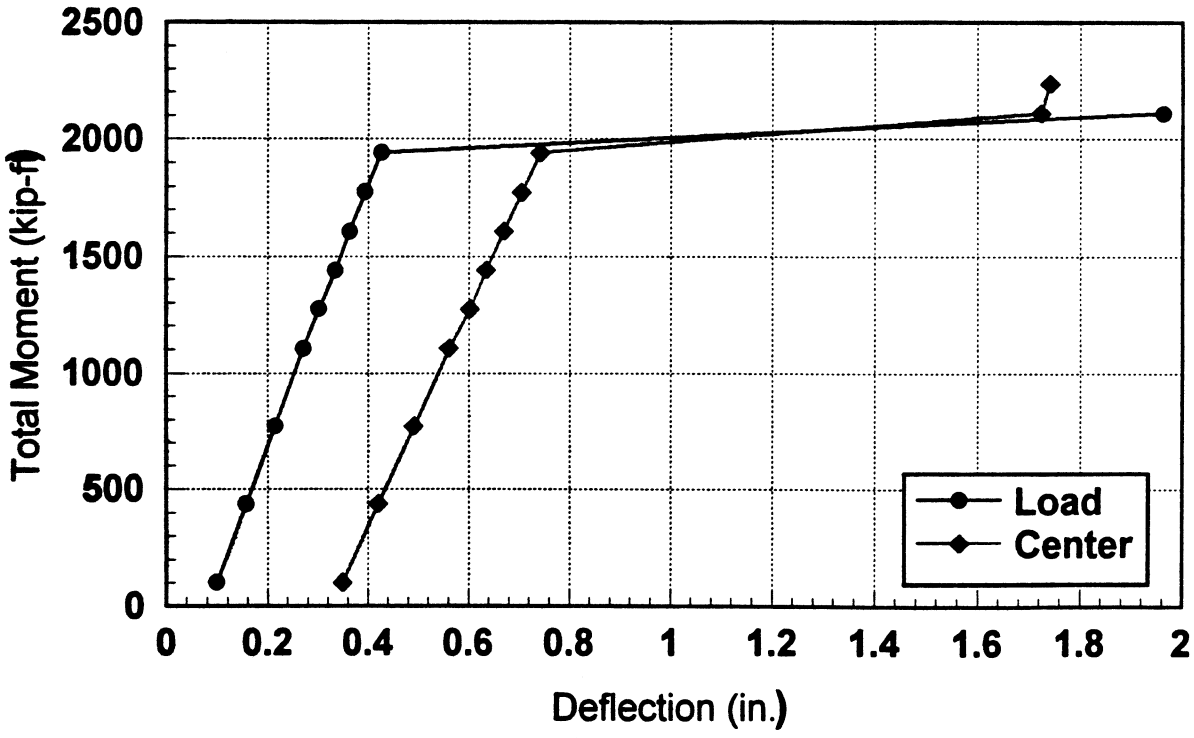

Fig 4.57b Total Moment Vs Deflection for R8N from FEA

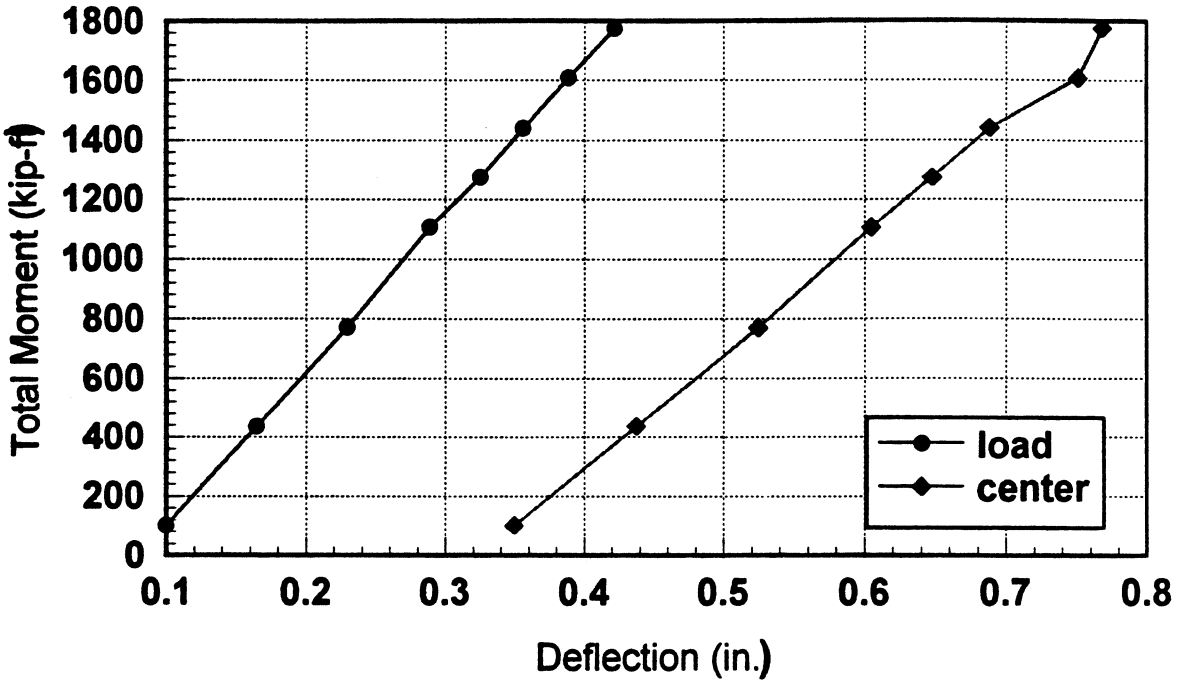

Fig 4.58a Total Moment Vs Deflection for F10N from FEA

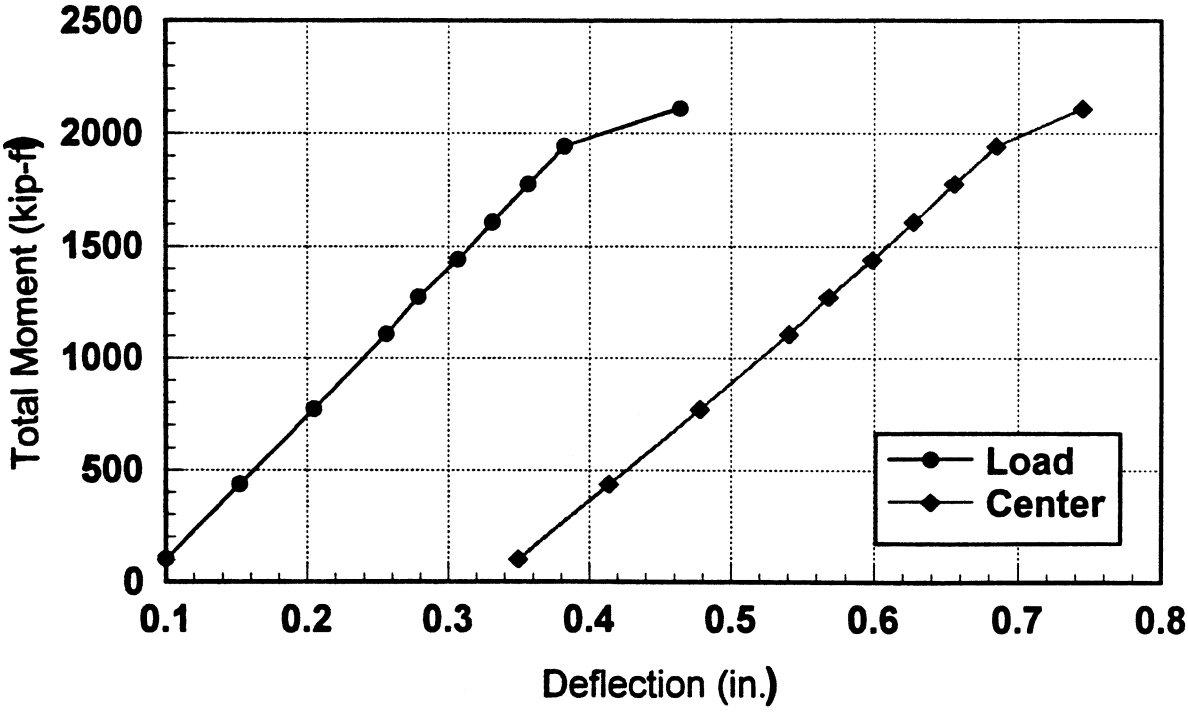

Fig 4.58b Total Moment Vs Deflection for R10N from FEA

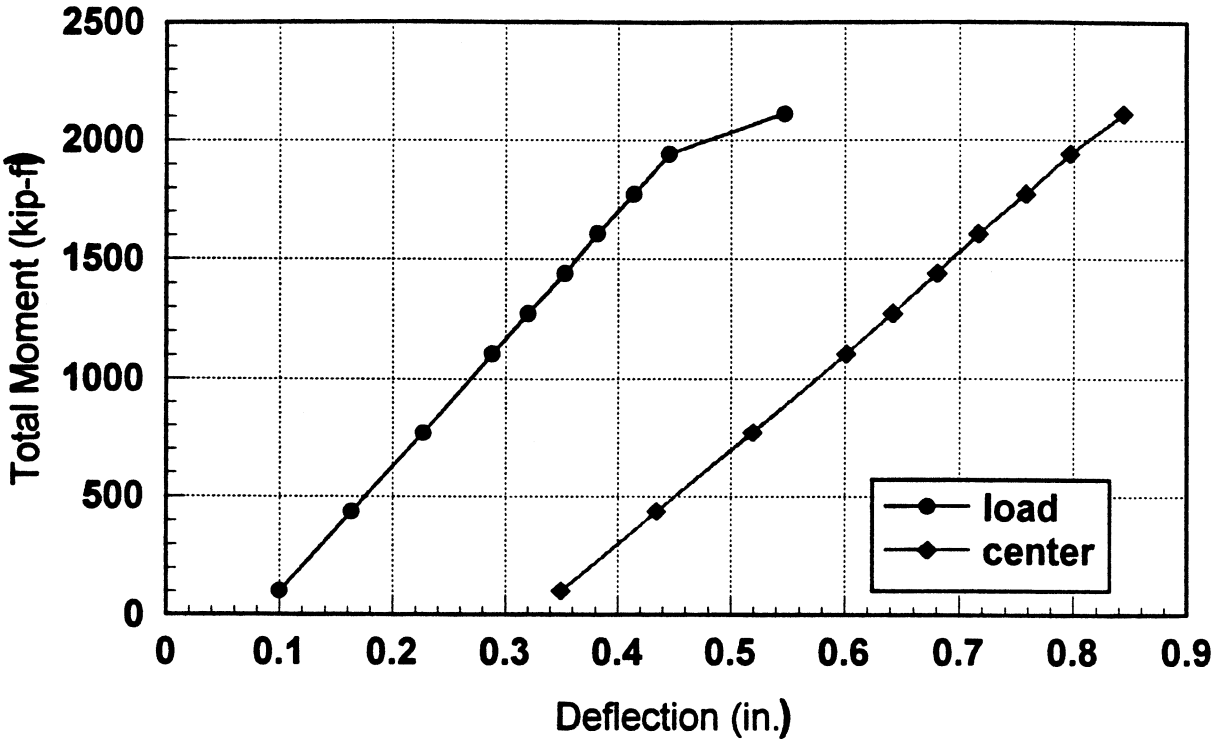

Fig 4.59a Total Moment Vs Deflection for F12N from FEA

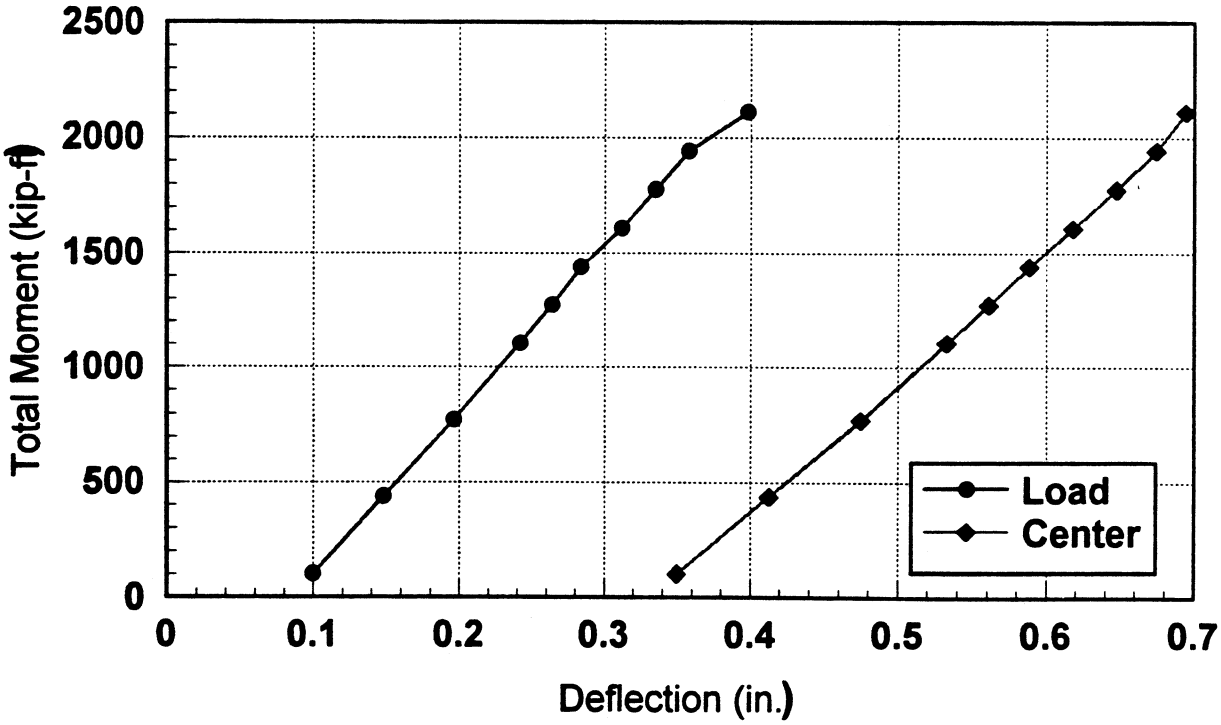

Fig 4.59b Total Moment Vs Deflection for R12N from FEA

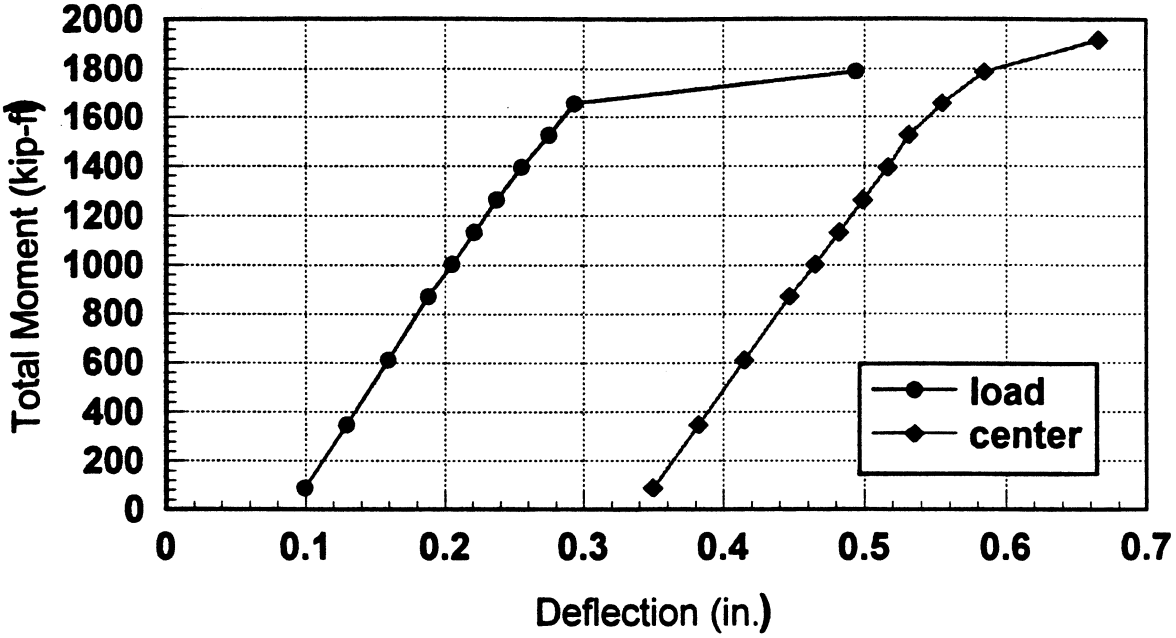

Fig 4.60a Total Moment Vs Deflection for F8S from FEA

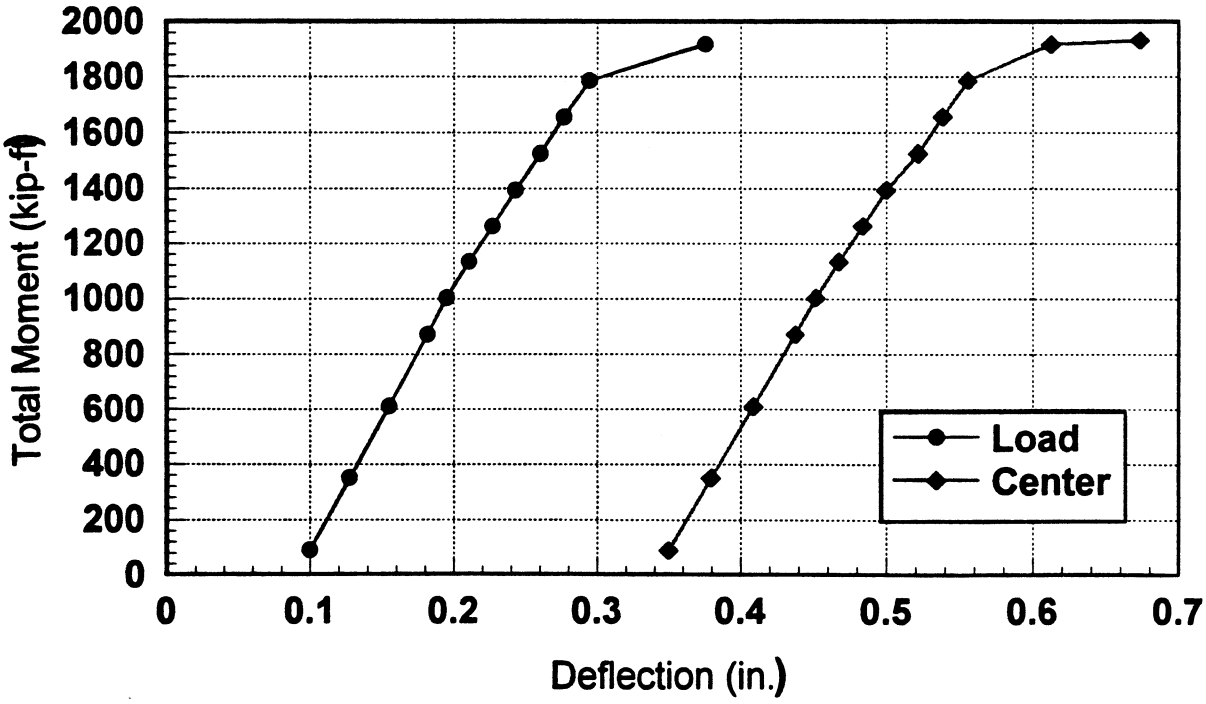

Fig 4.60b Total Moment Vs Deflection for R8S from FEA

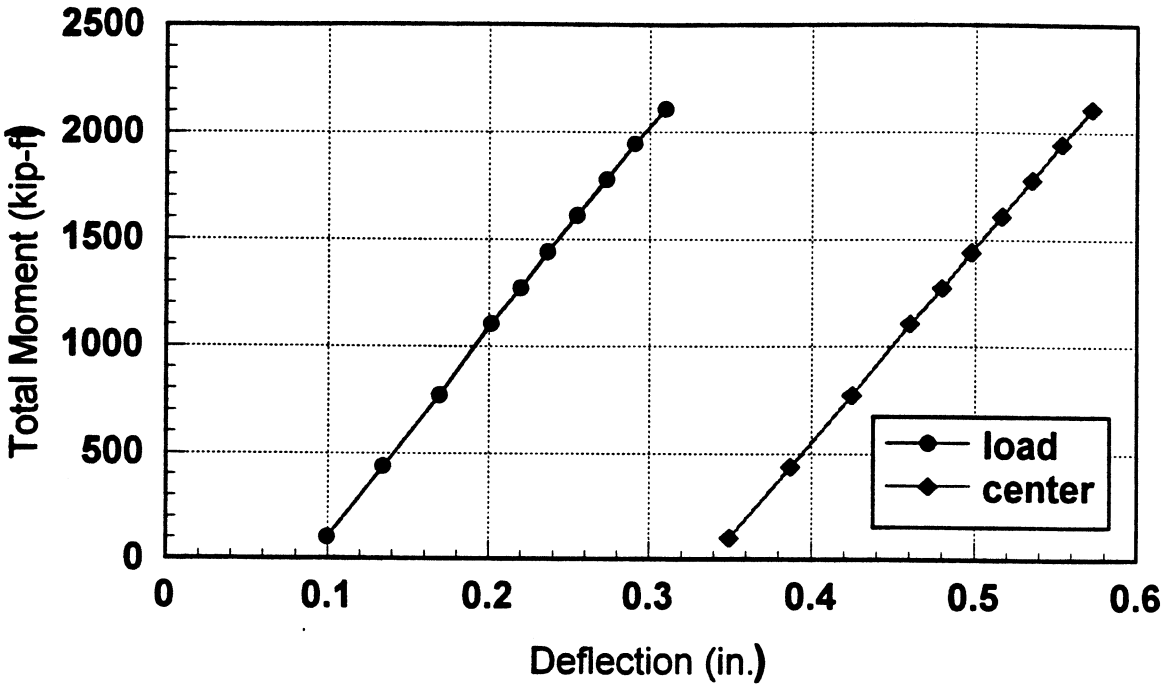

Fig 4.61a Total Moment Vs Deflection for F10S from FEA

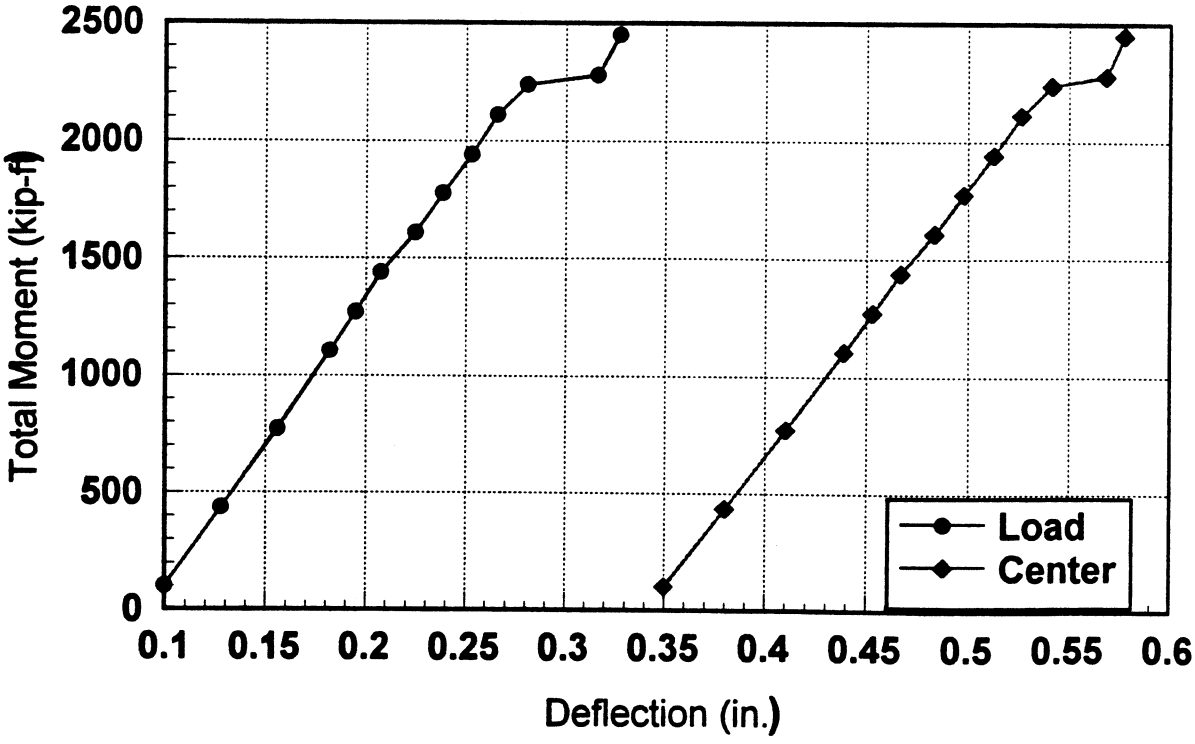

Fig 4.61b Total Moment Vs Deflection for R10S from FEA

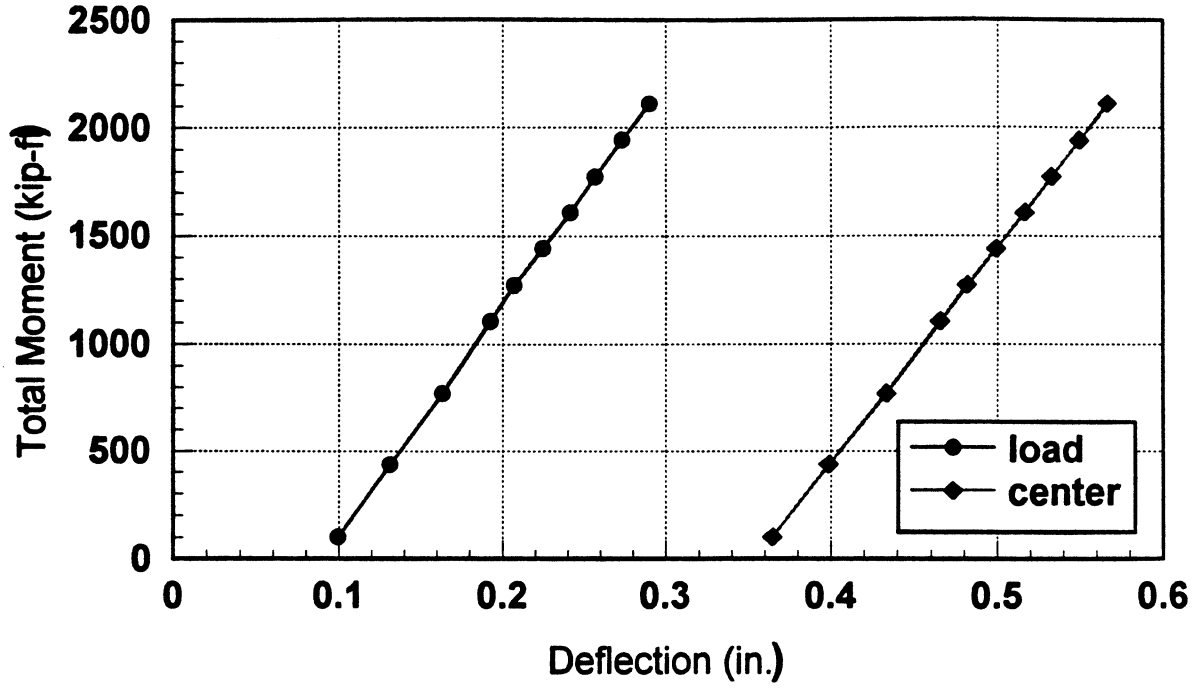

Fig 4.62a Total Moment Vs Deflection for F12S from FEA

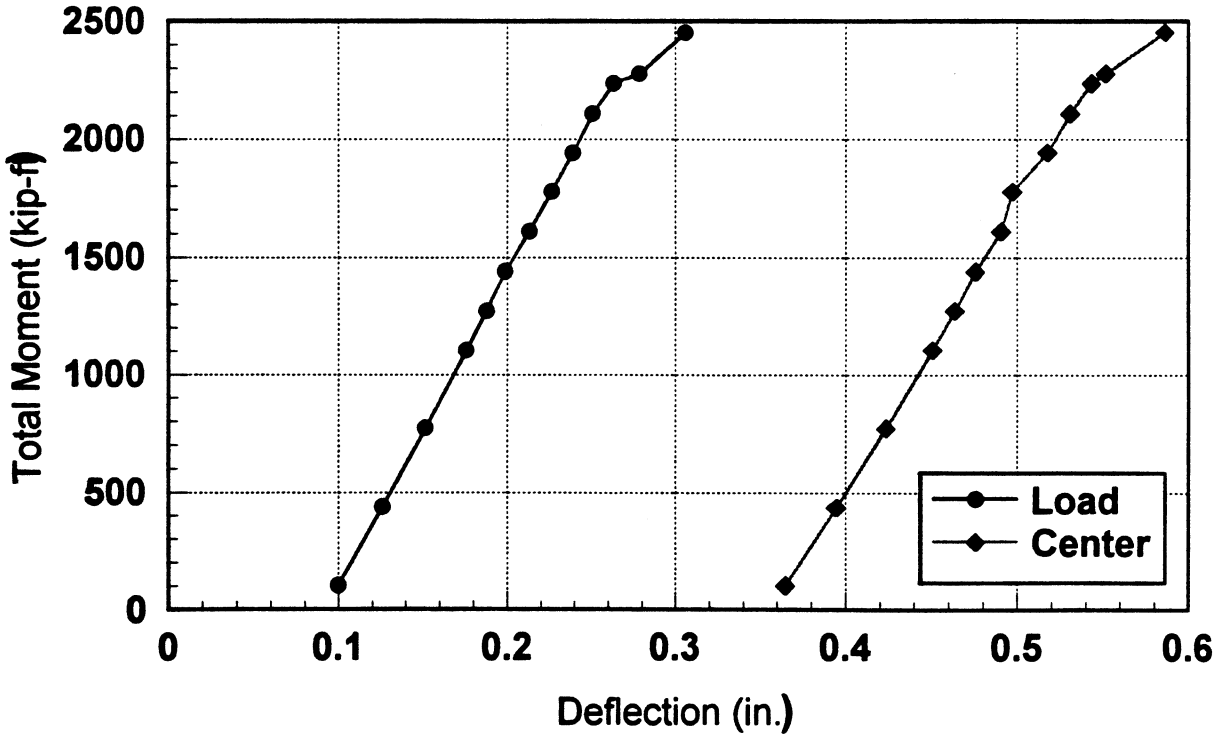

Fig 4.62b Total Moment Vs Deflection for R12S from FEA

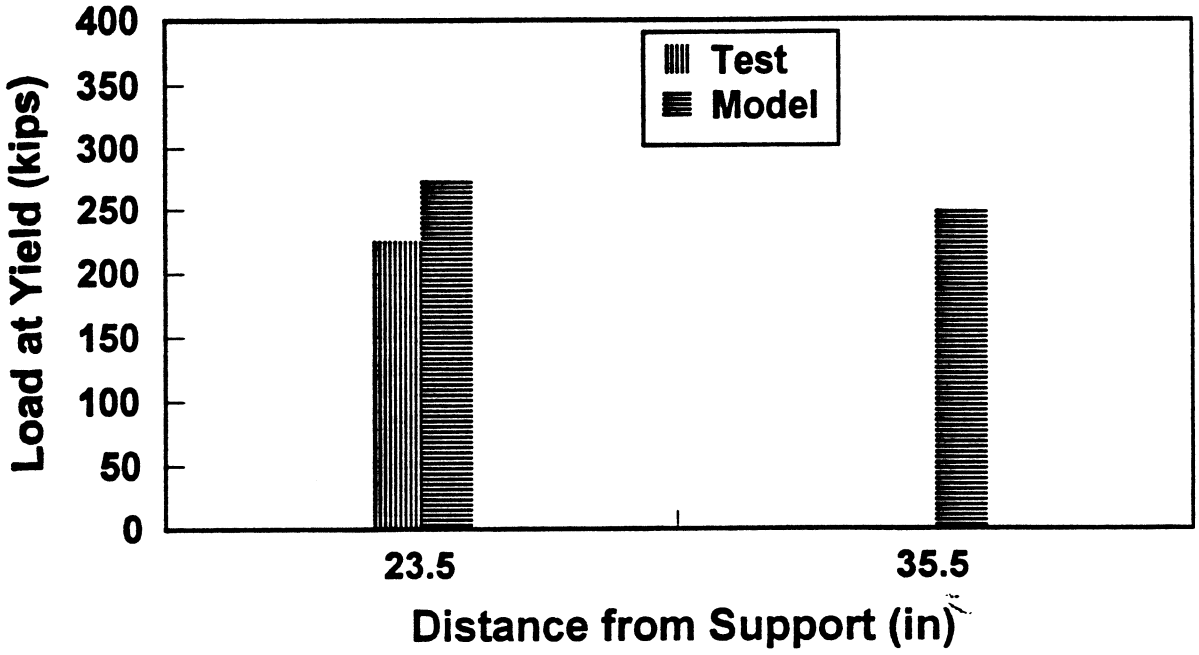

Fig 4.63a Yield Comparision at different confining bars for R8N

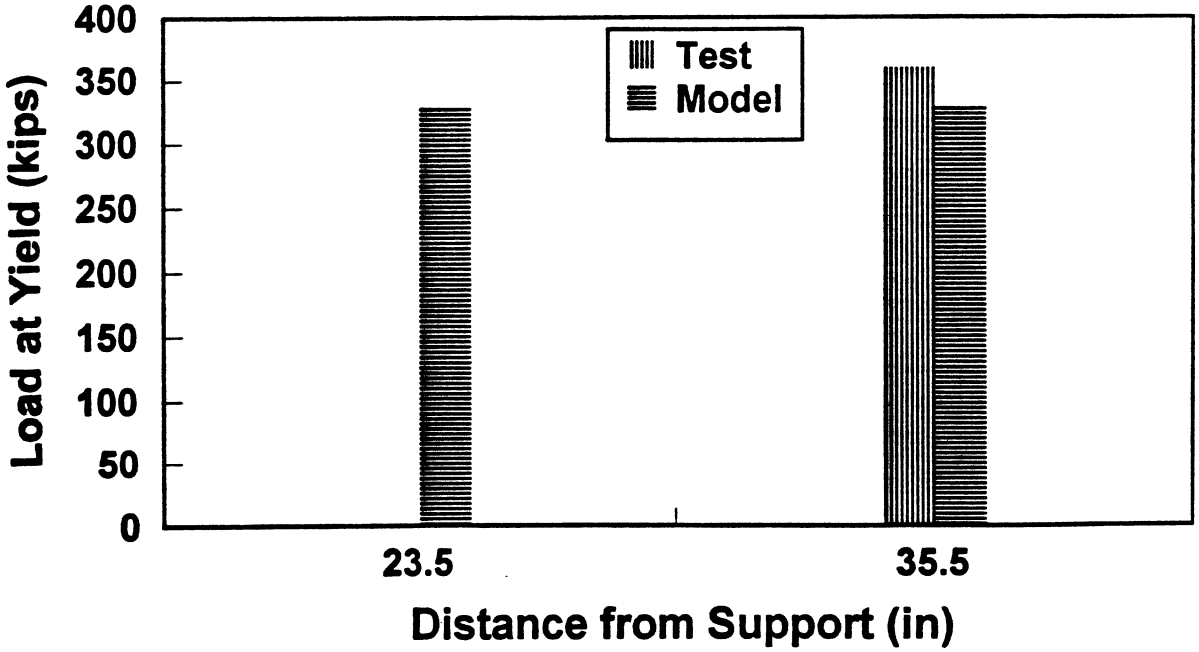

Fig 4.63b Yield Comparision at different confining bars for R8S

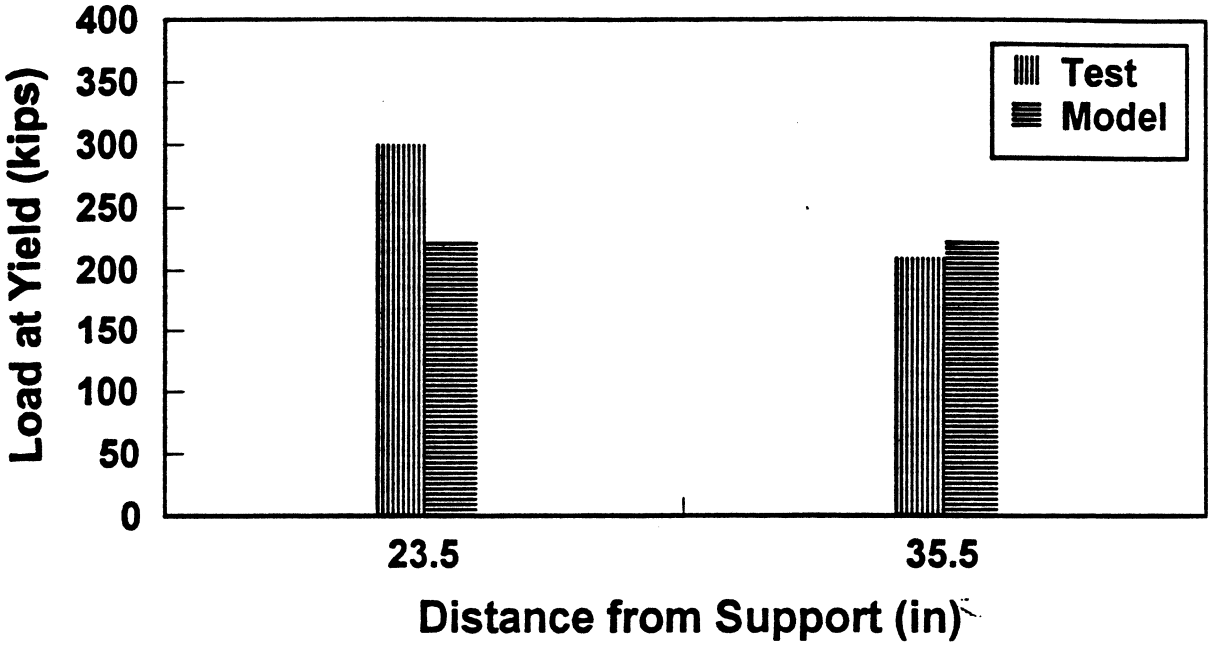

Fig 4.64a Yield Comparision at different confining bars for R10N

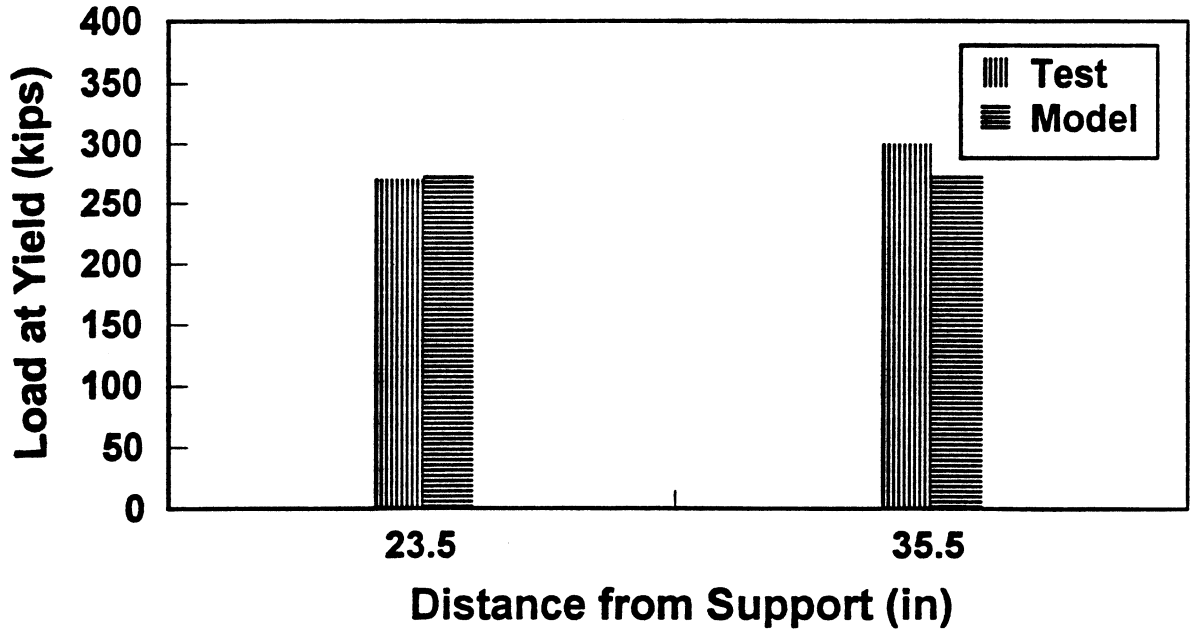

Fig 4.64b Yield Comparision at different confining bars for R10S

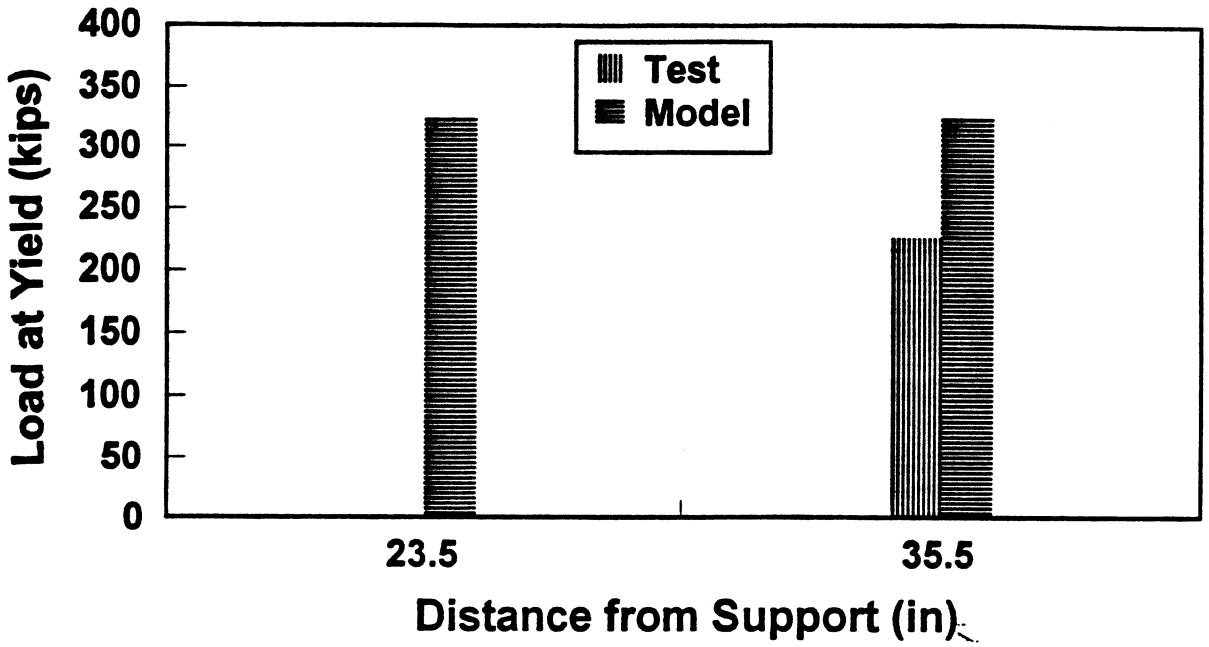

Fig 4.65a Yield Comparision at different confining bars for R12N

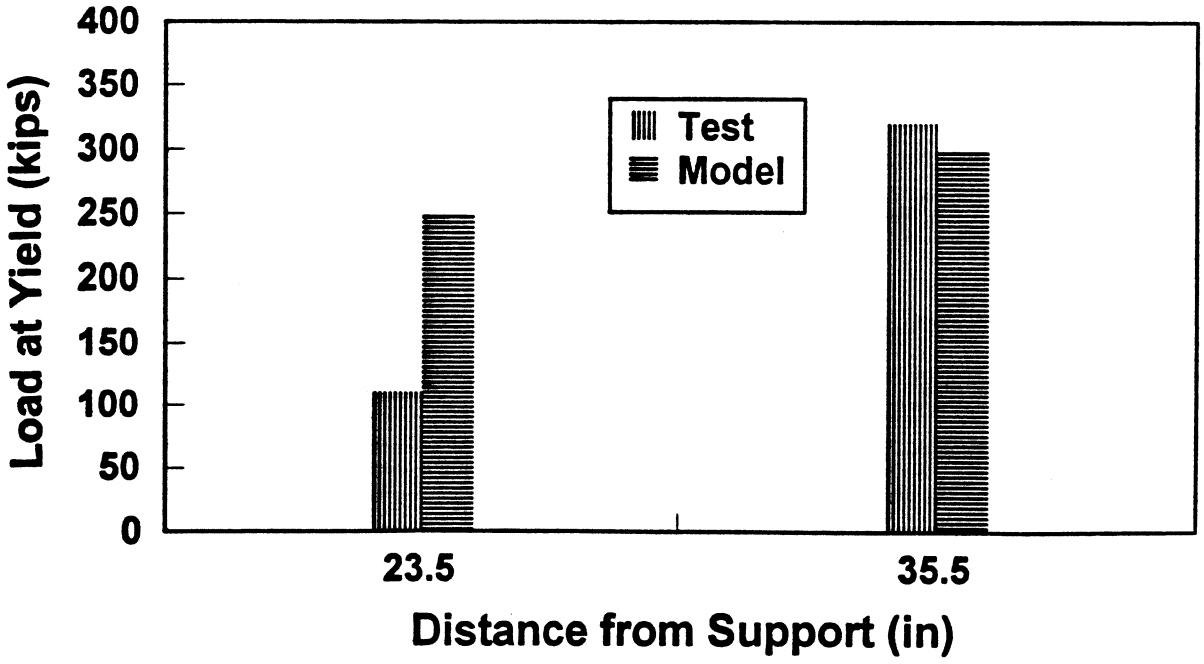

Fig 4.65b Yield Comparision at different confining bars for R12S

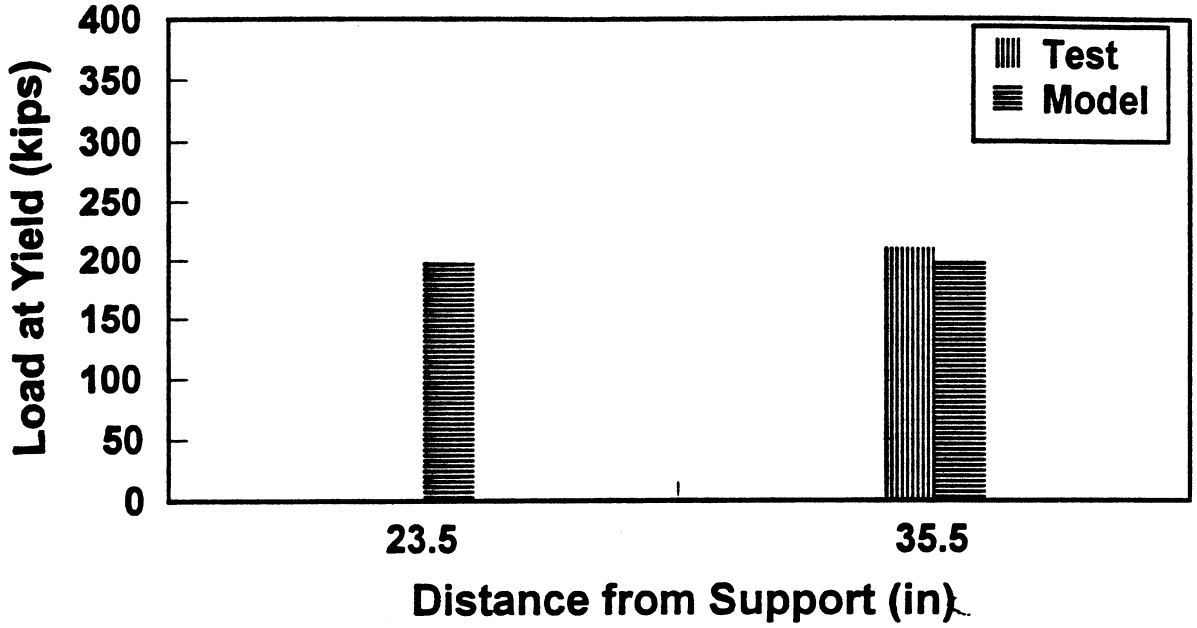

Fig 4.66a Yield Comparision at different confining bars for F8N

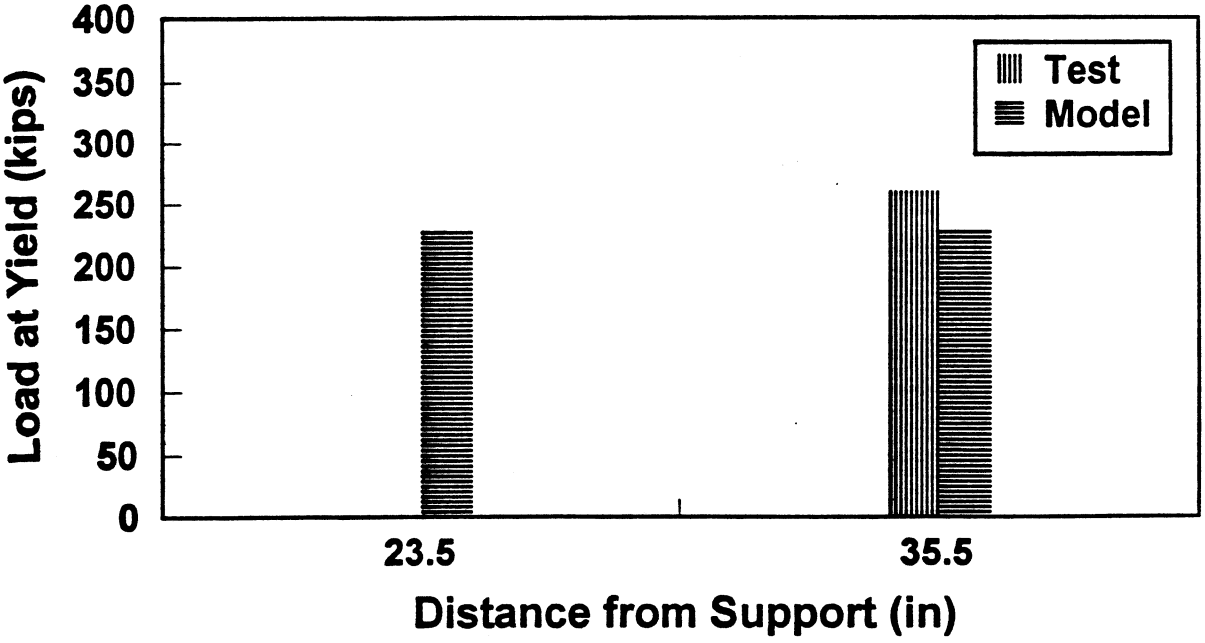

Fig 4.66b Yield Comparision at different confining bars for F8S

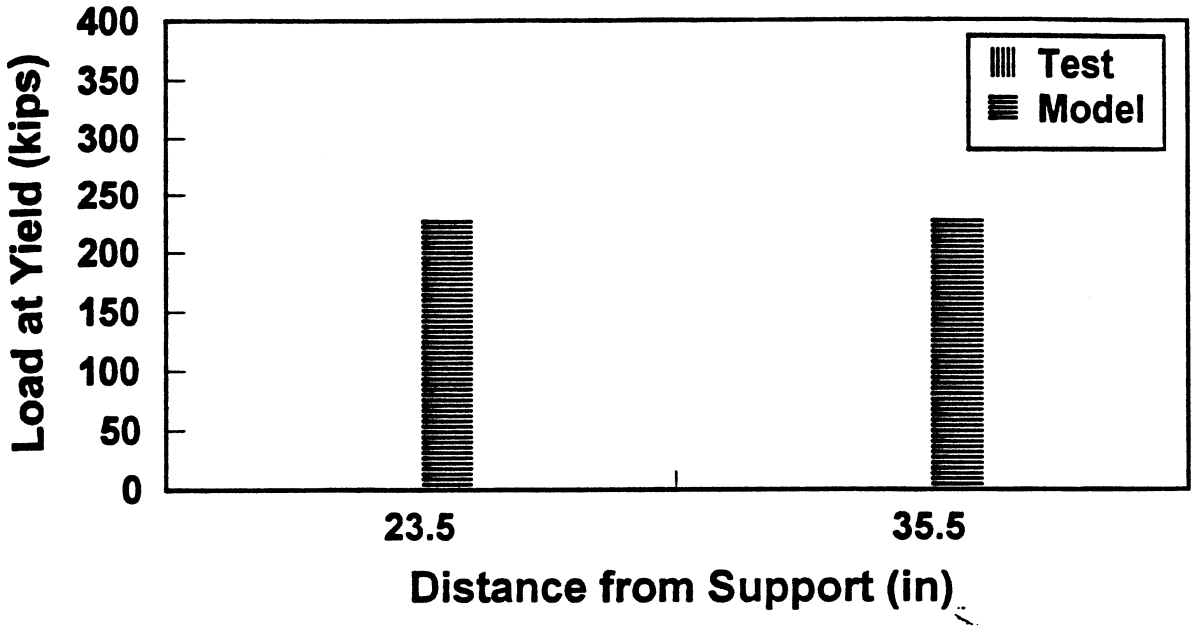

Fig 4.67a Yield Comparision at different confining bars for F10N

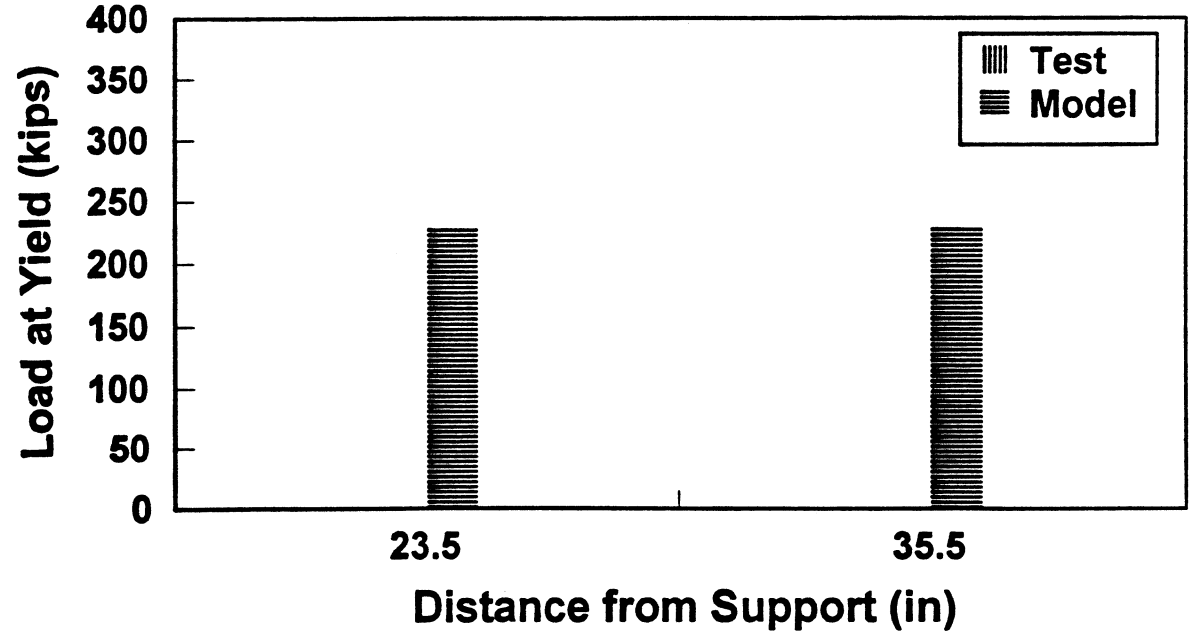

Fig 4.67b Yield Comparision at different confining bars for F10S

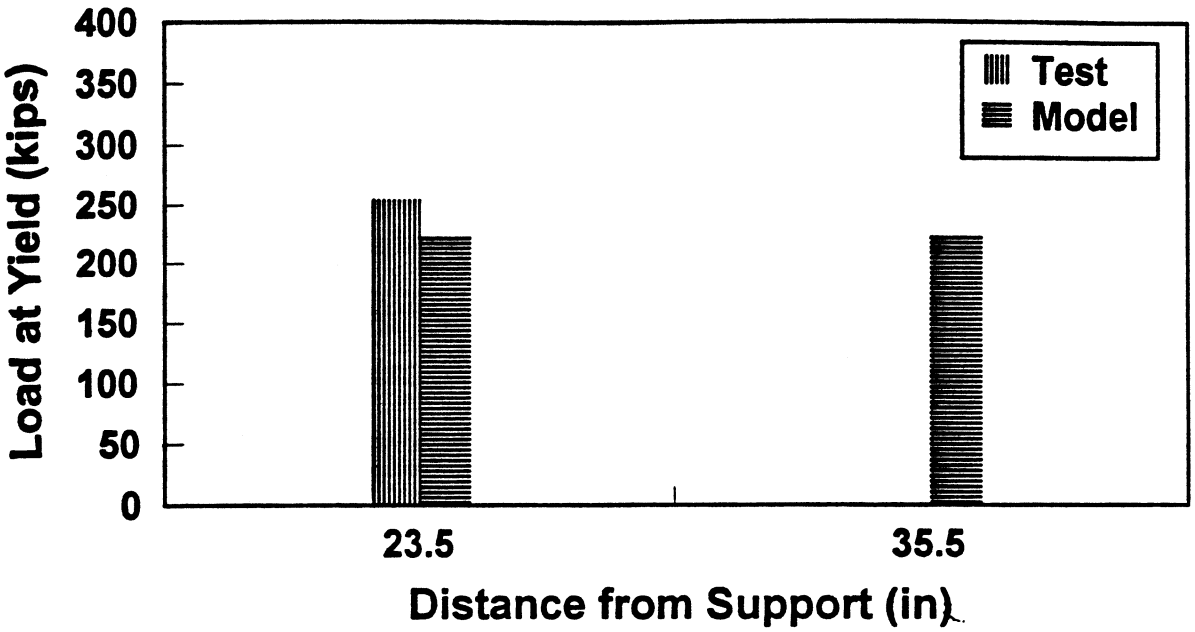

Fig 4.68a Yield Comparision at different confining bars for F12N

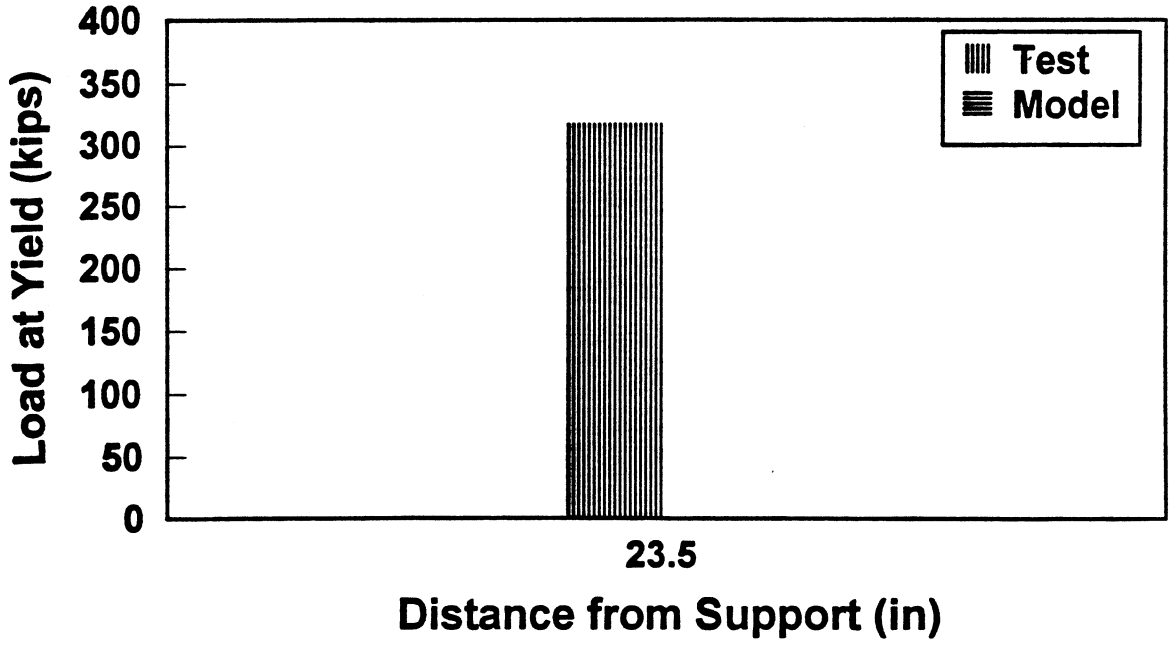

Fig 4.68b Yield Comparision at different confining bars for F12S

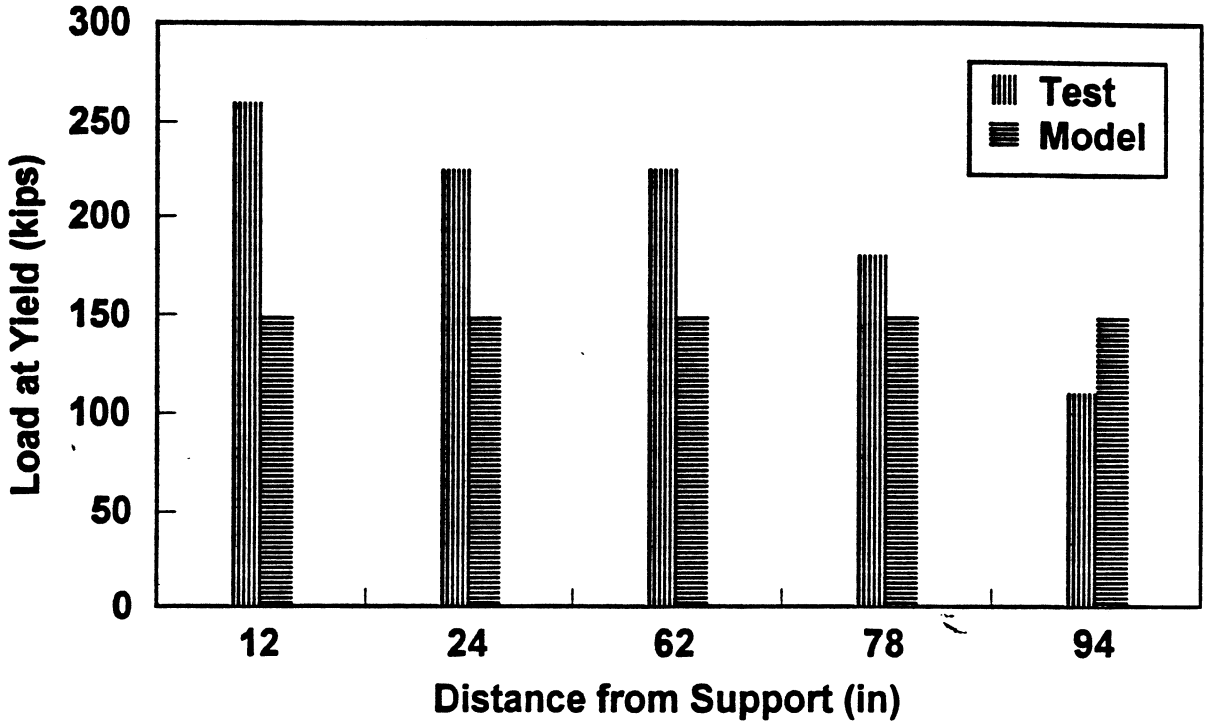

Fig 4.69a Yield Comparision at different C-bars for R8N

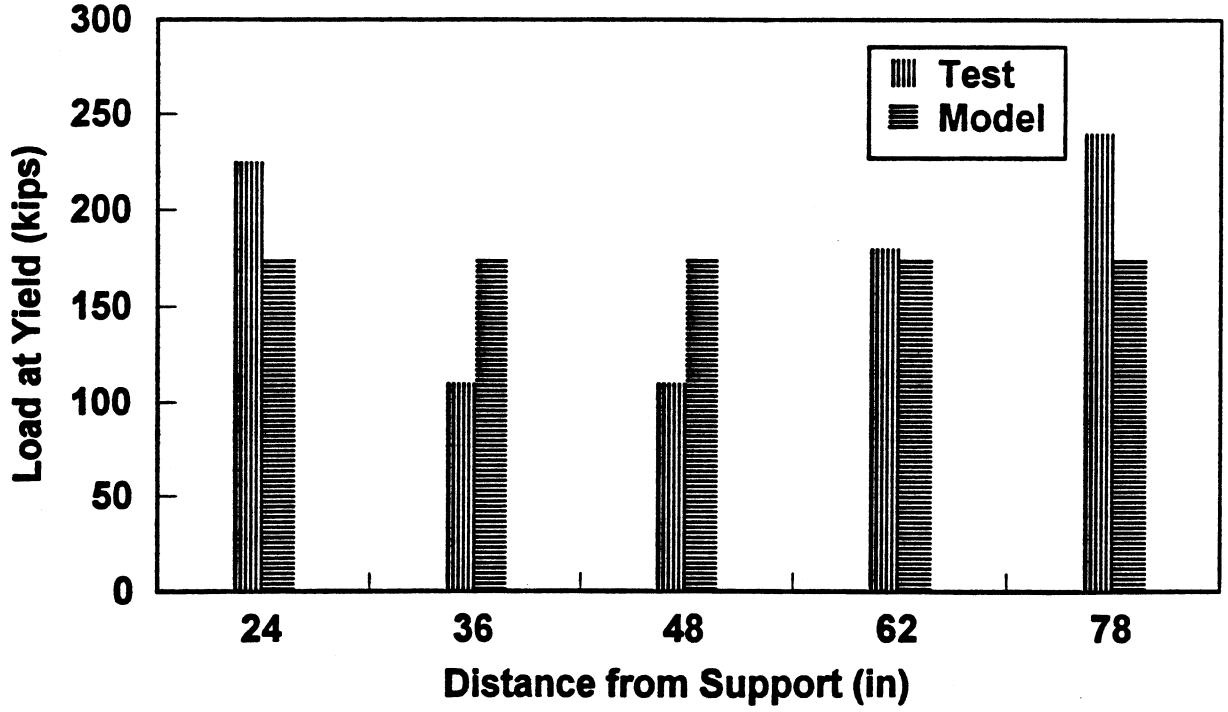

Fig 4.69b Yield Comparision at different C-bars for R8S

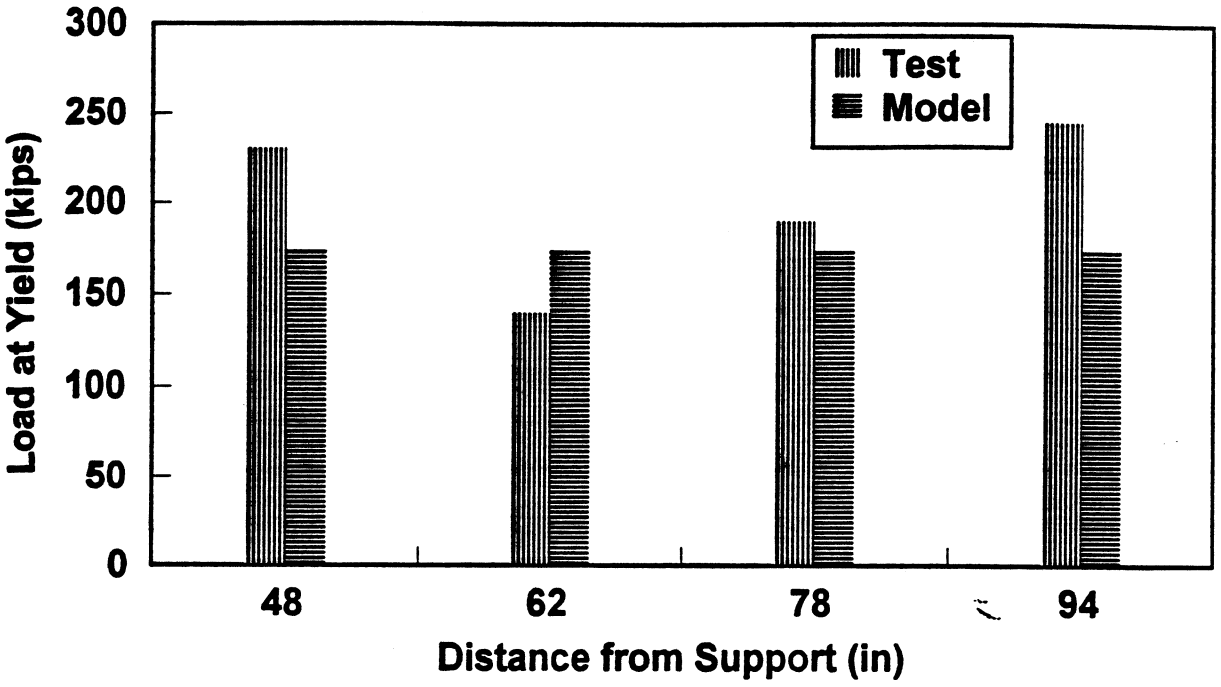

Fig 4.70a Yield Comparision at different C-bars for R10N

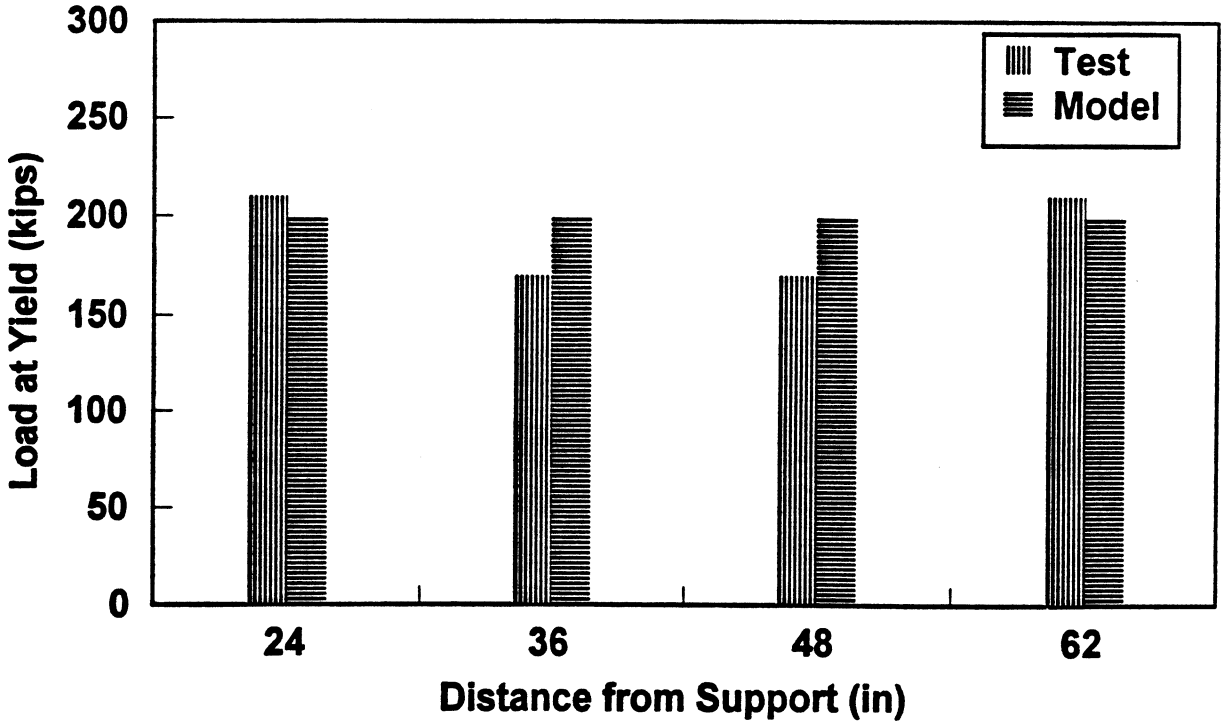

Fig 4.70b Yield Comparision at different C-bars for R10S

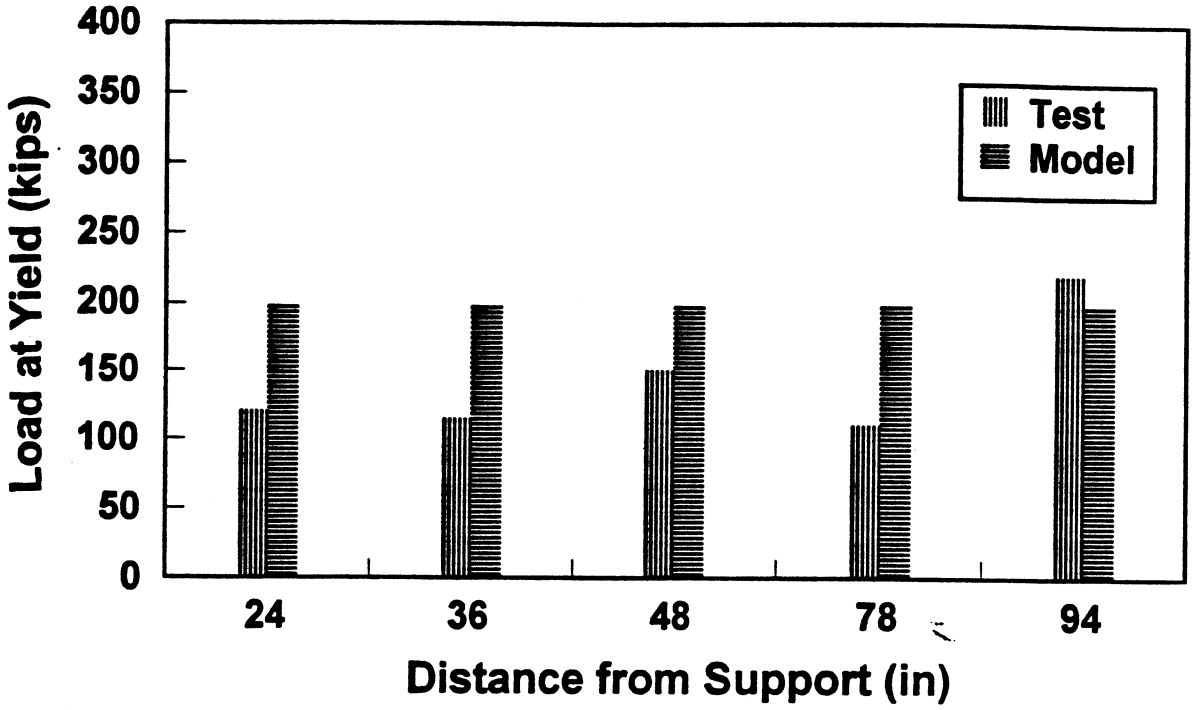

Fig 4.71a Yield Comparision at different C-bars for R12N

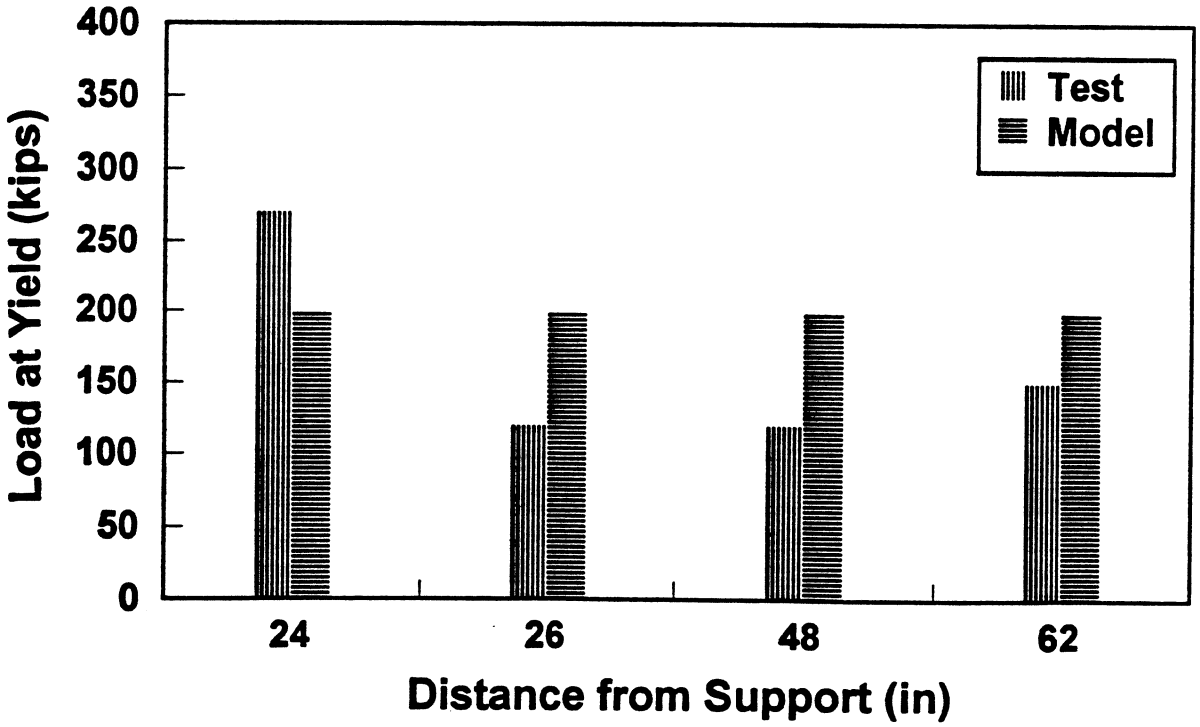

Fig 4.71b Yield Comparision at different C-bars for R12S

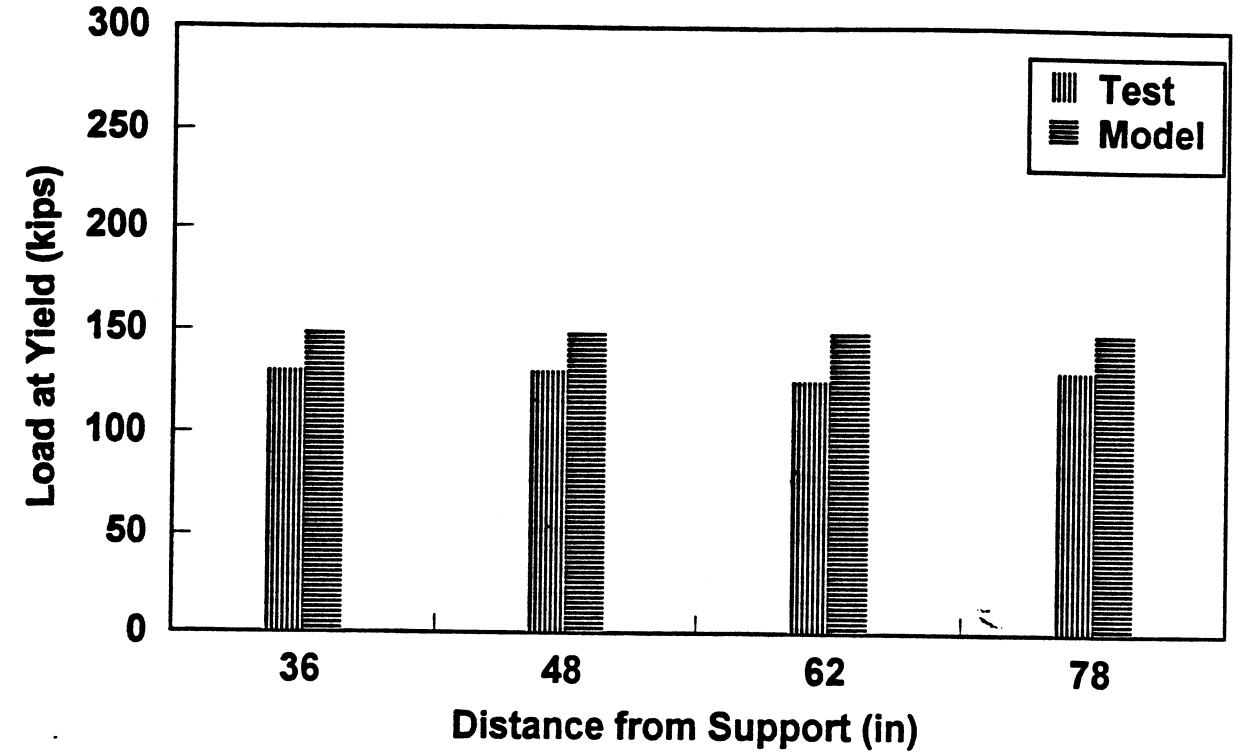

Fig 4. 72a Yield Comparision at different C-bars for F8N

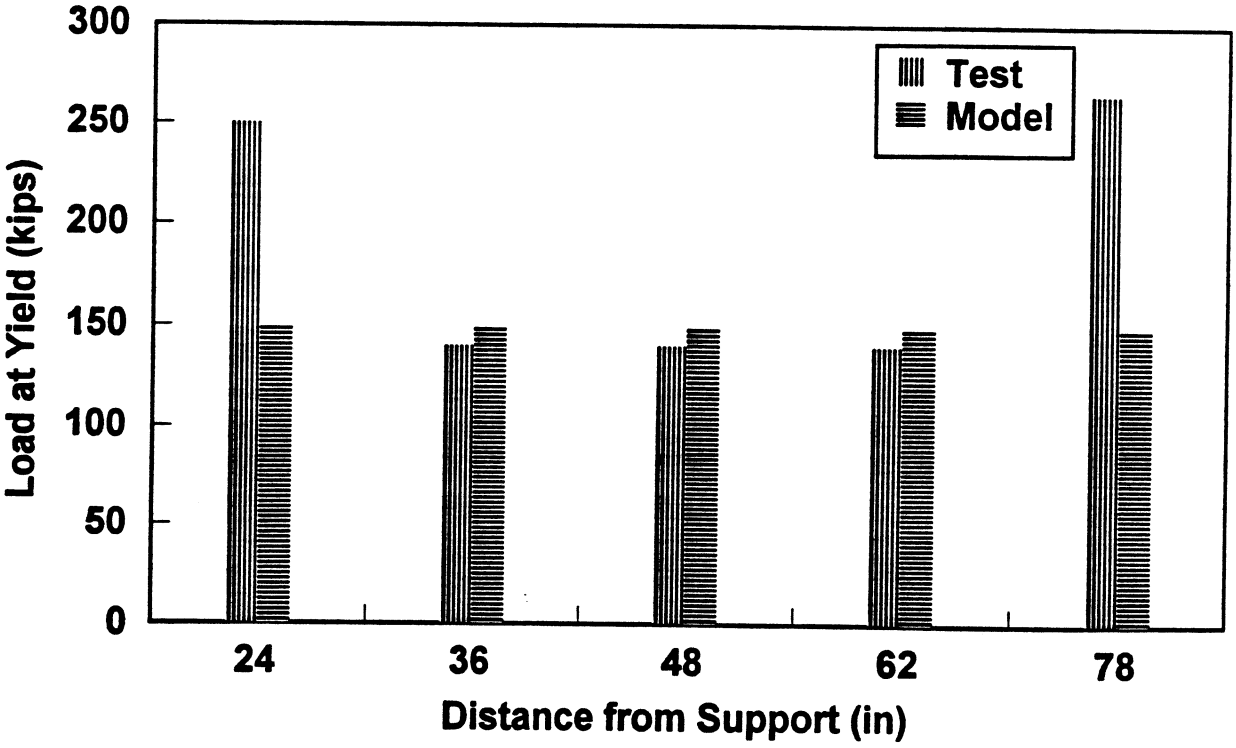

Fig 4. 72b Yield Comparision at different C-bars for F8S

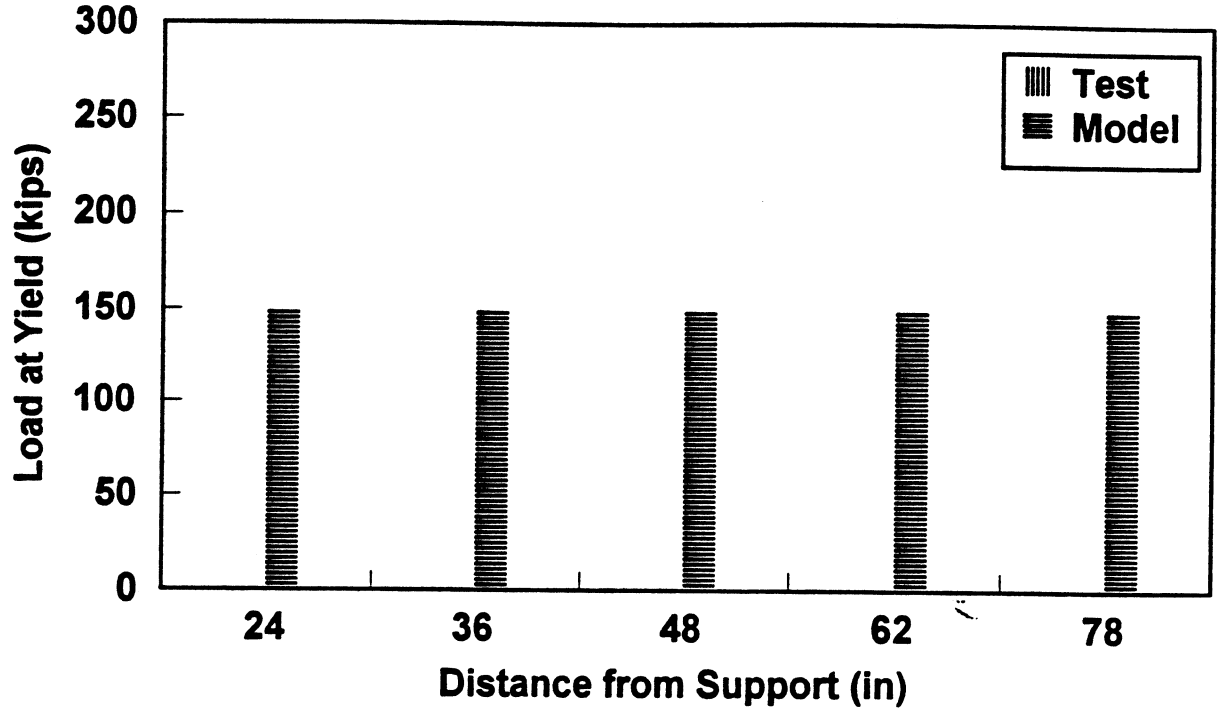

Fig 4.73a Yield Comparision at different C-bars for F10N

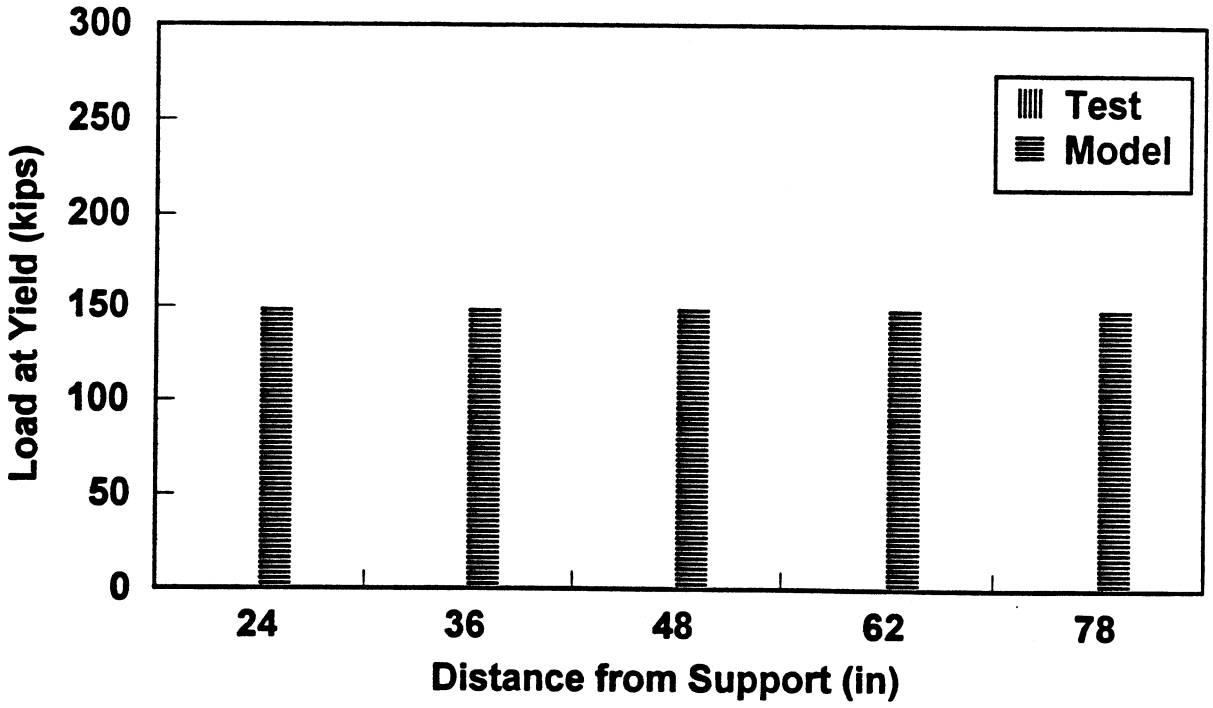

Fig 4.73b Yield Comparision at different C-bars for F10S

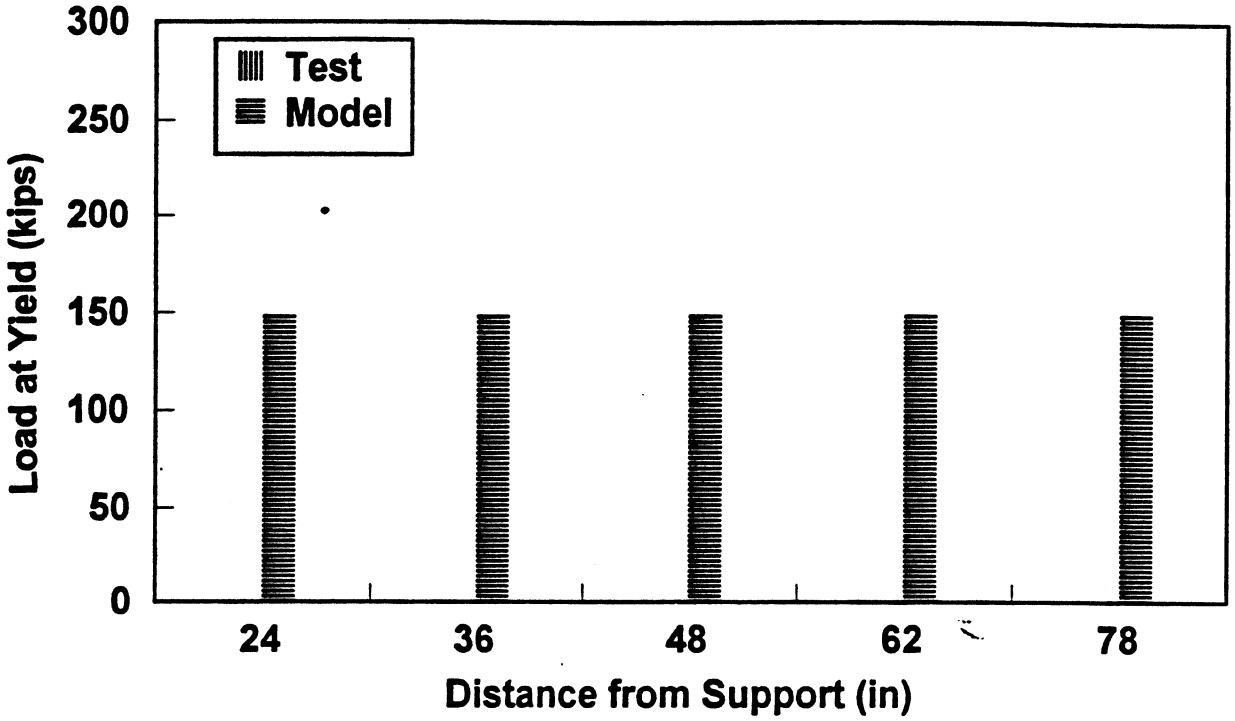

Fig 4.74a Yield Comparision at different C-bars for F12N

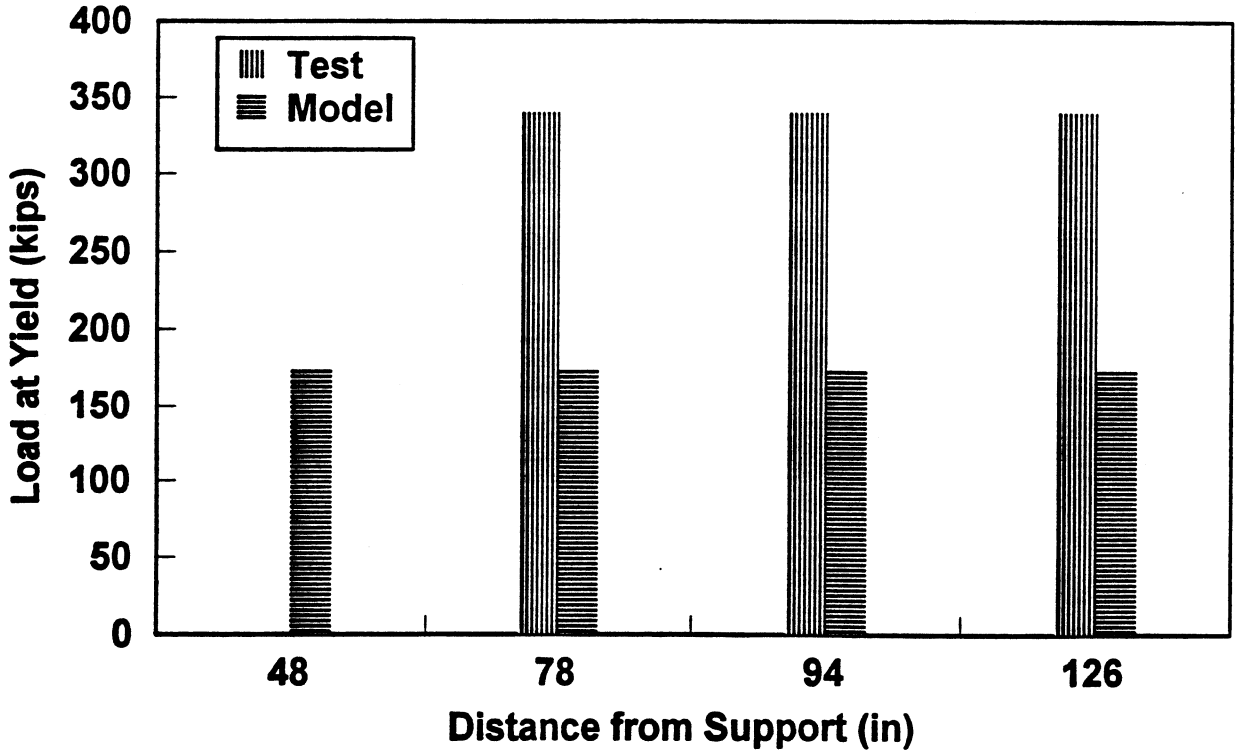

Fig 4.74b Yield Comparision at different C-bars for F12S

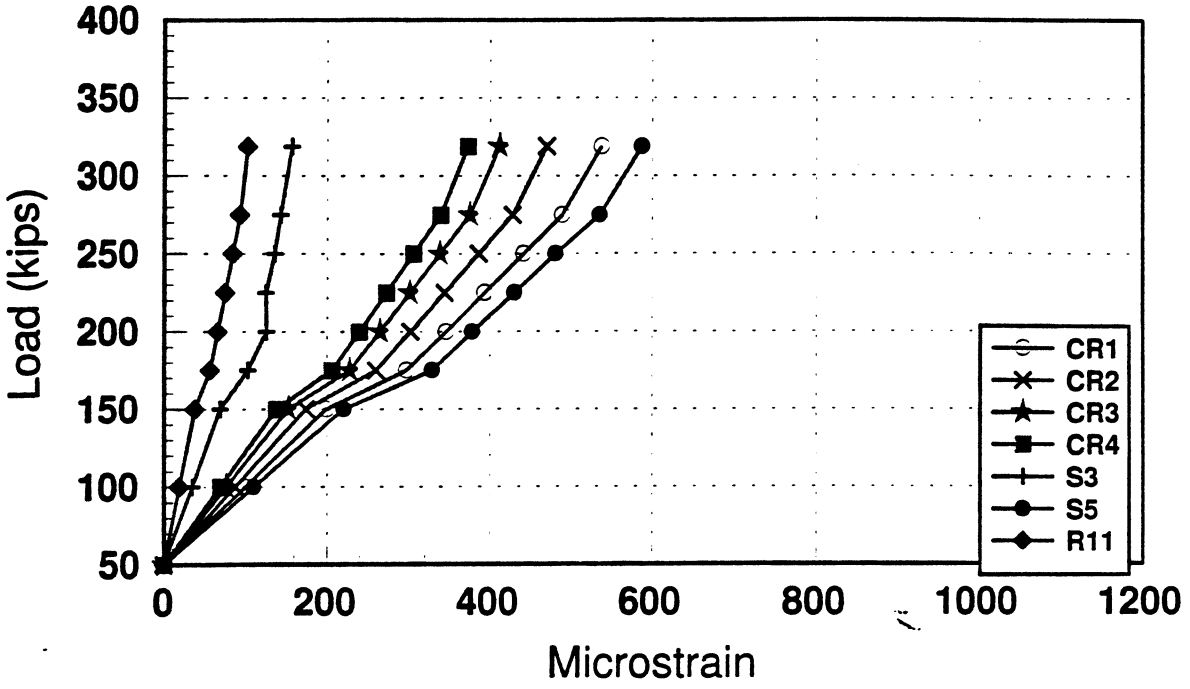

Fig 4.75a Strain in concrete for R8N from FEA

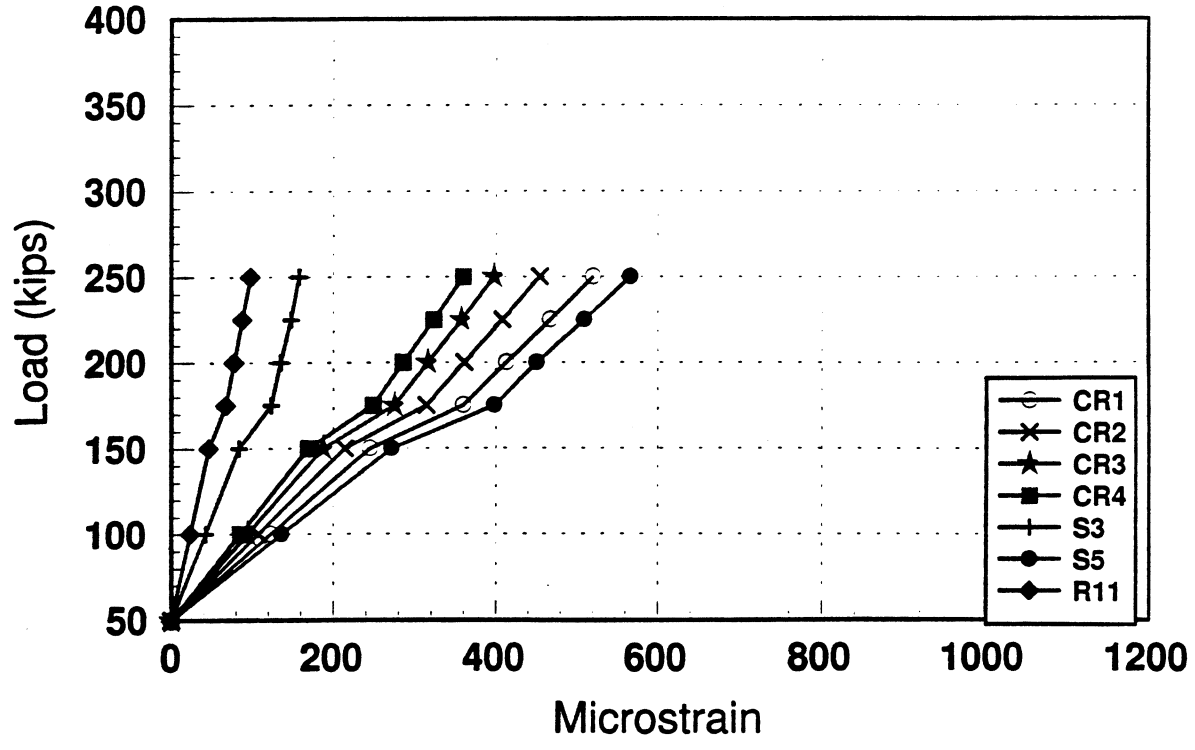

Fig 4.75b Strain in concrete for F8N from FEA

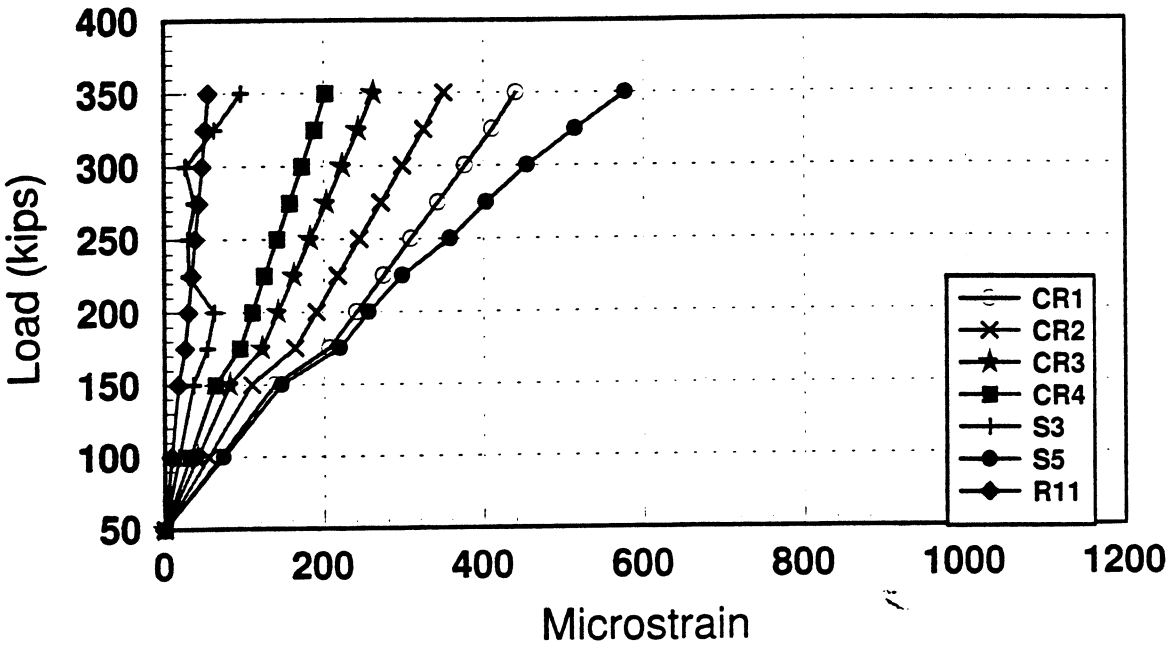

Fig 4.76a Strain in concrete for R8S from FEA

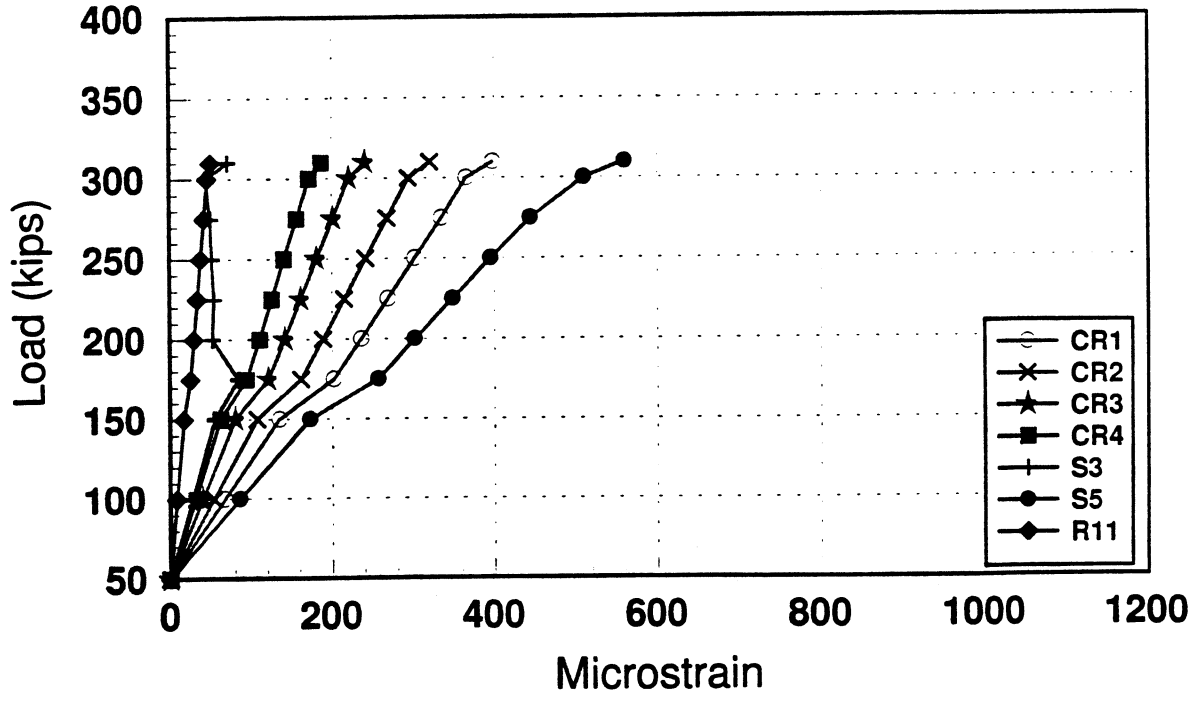

Fig 4.76b Strain in concrete for F8S from FEA

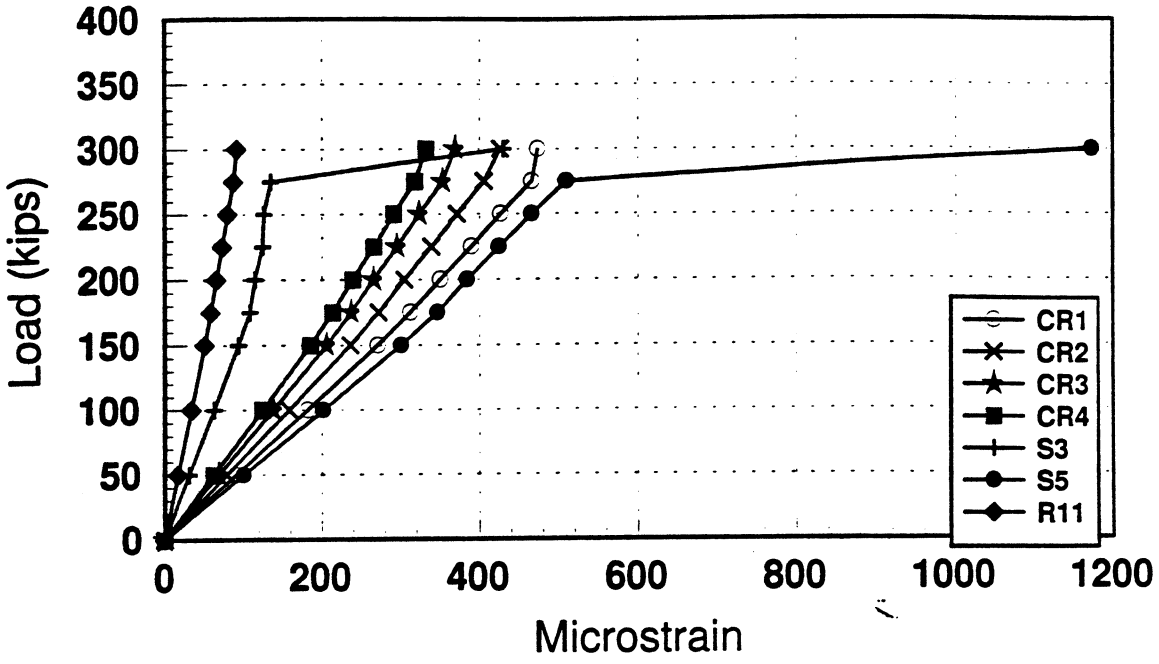

Fig 4.77a Strain in concrete for R10N from FEA

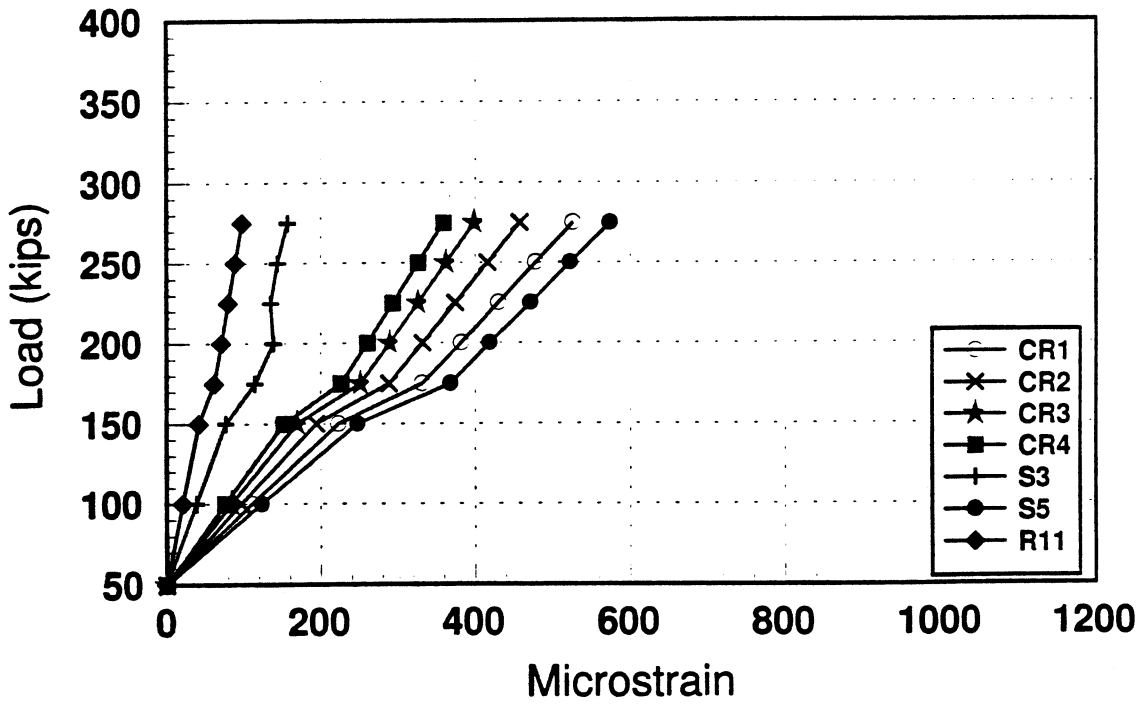

Fig 4.77b Strain in concrete for F10N from FEA

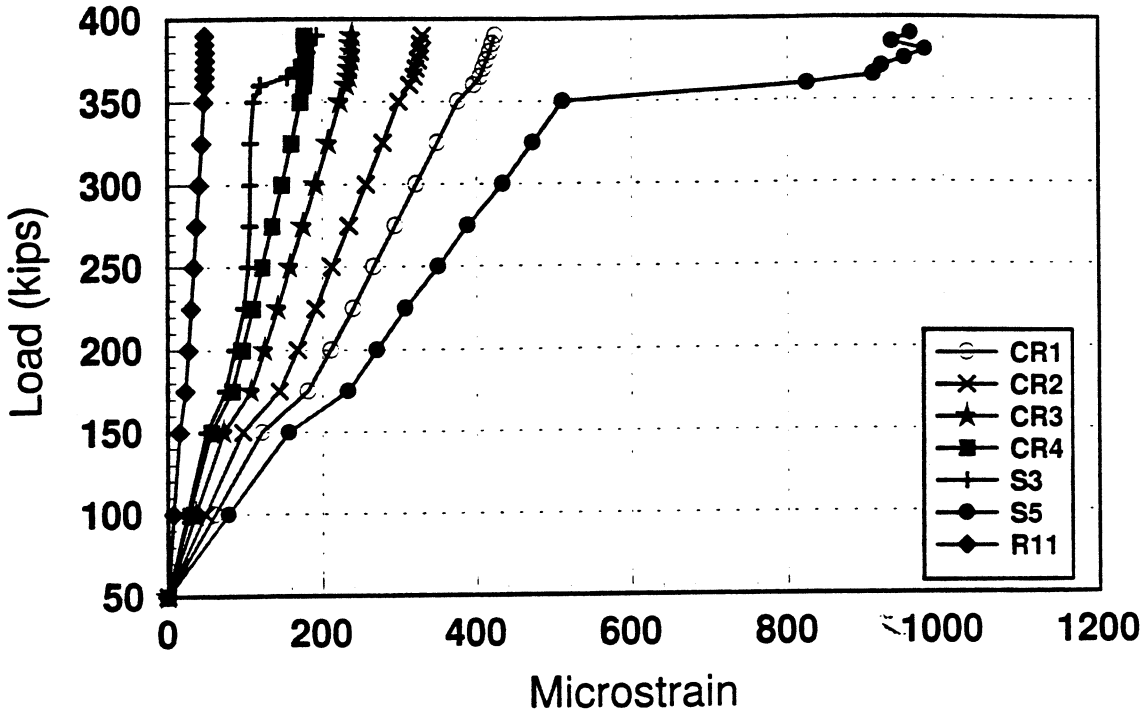

Fig 4.78a Strain in concrete for R10S from FEA

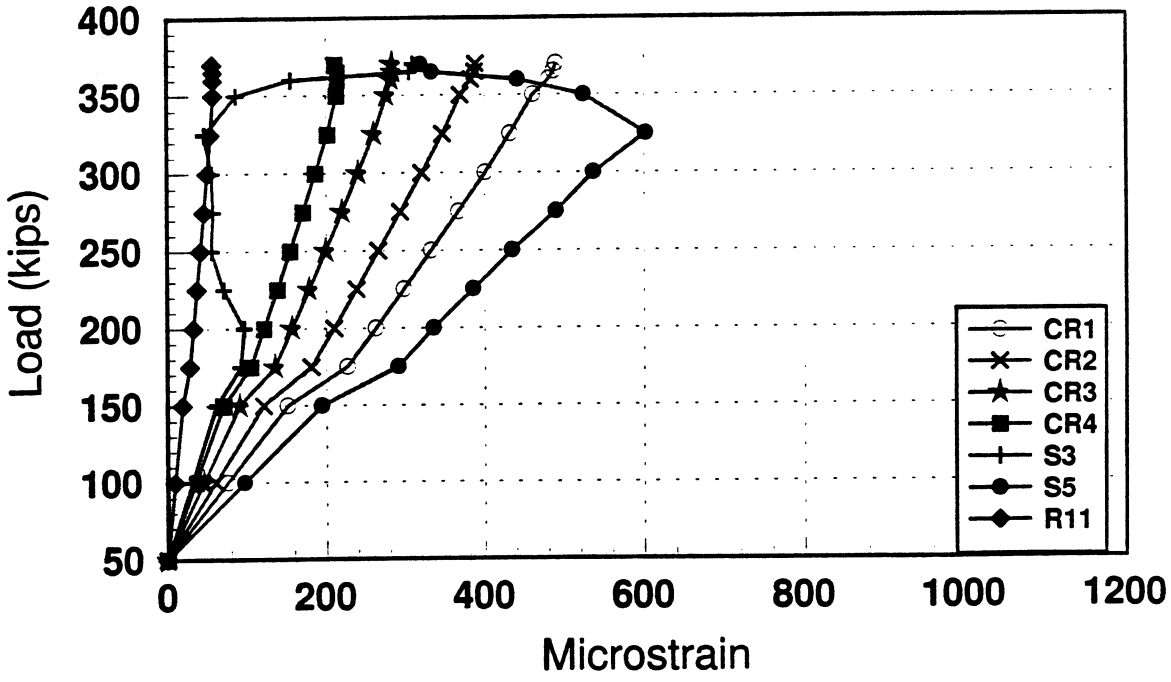

Fig 4.78b Strain in concrete for F10S from FEA

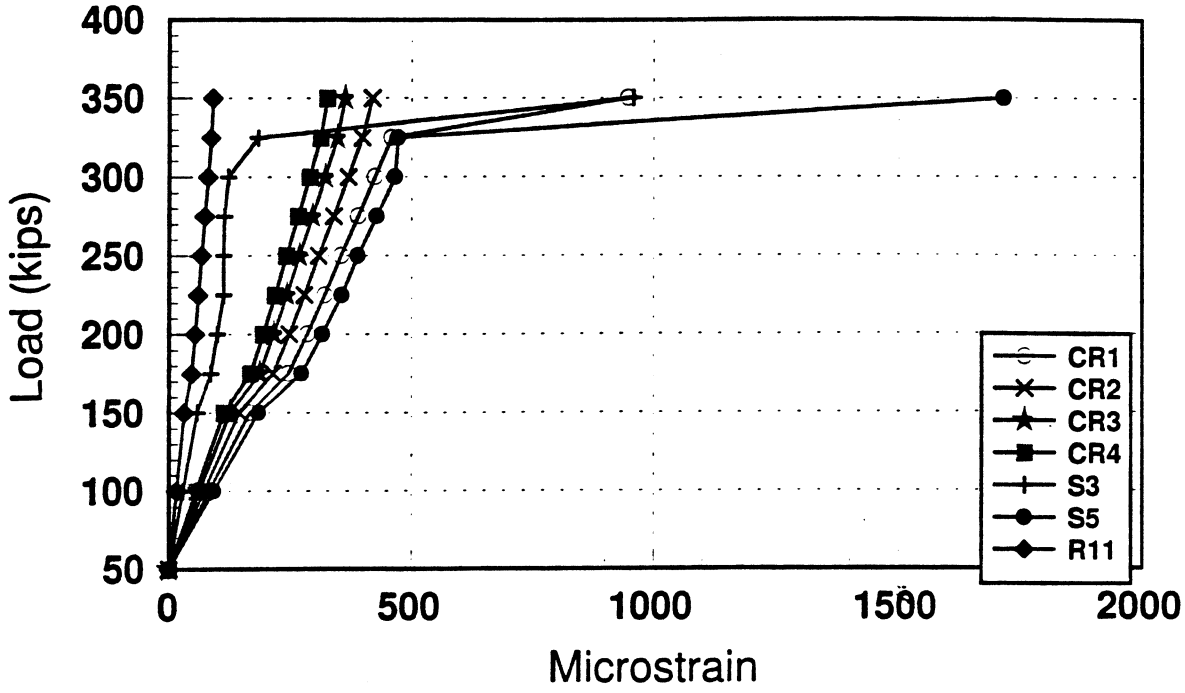

Fig 4.79a Strain in concrete for R12N from FEA

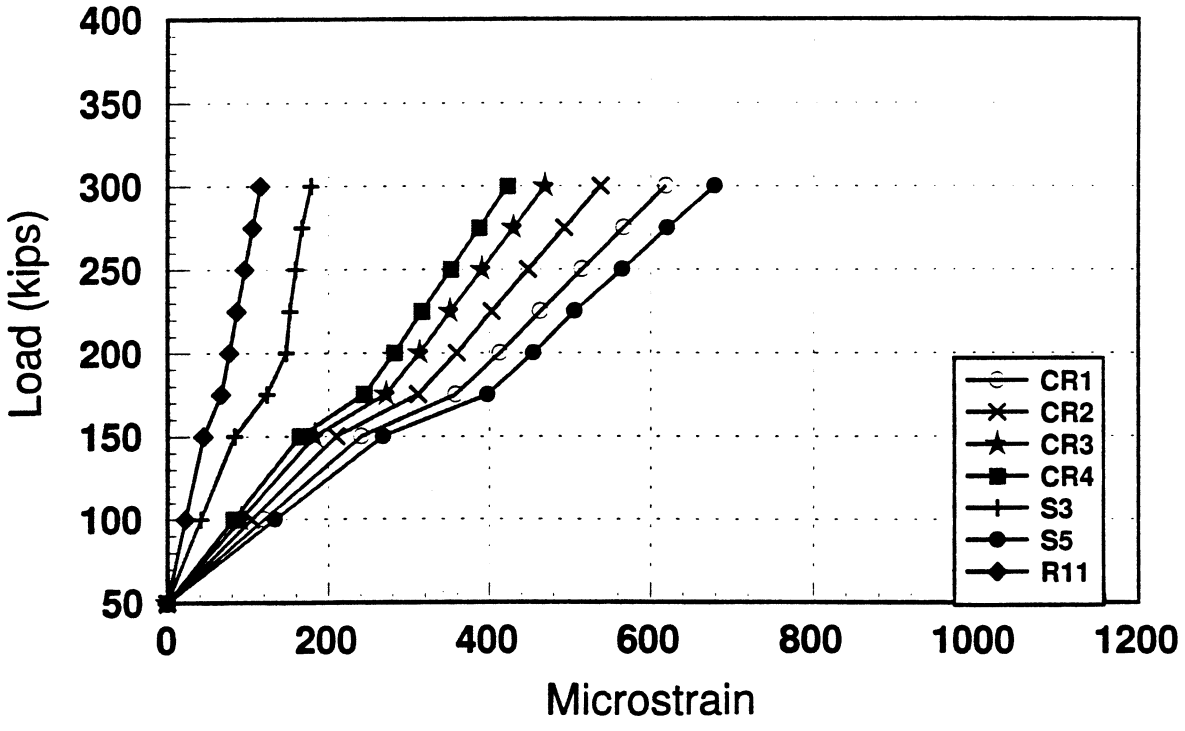

Fig 4.79b Strain in concrete for F12N from FEA

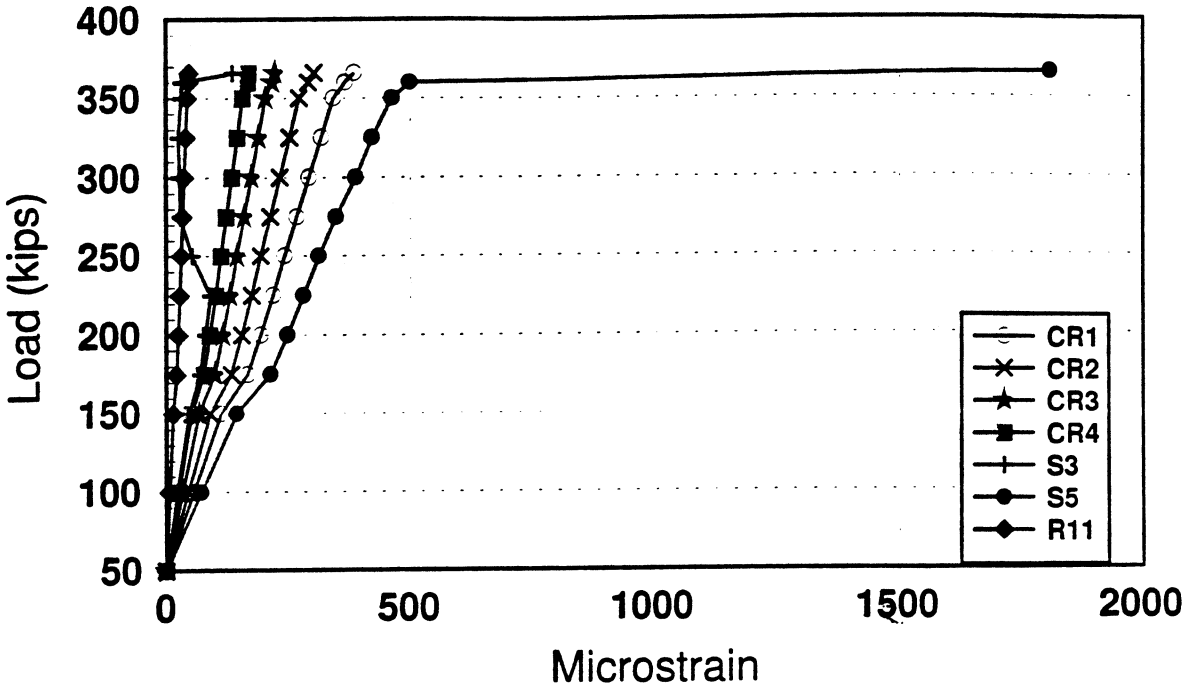

Fig 4.80a Strain in concrete for R12S from FEA

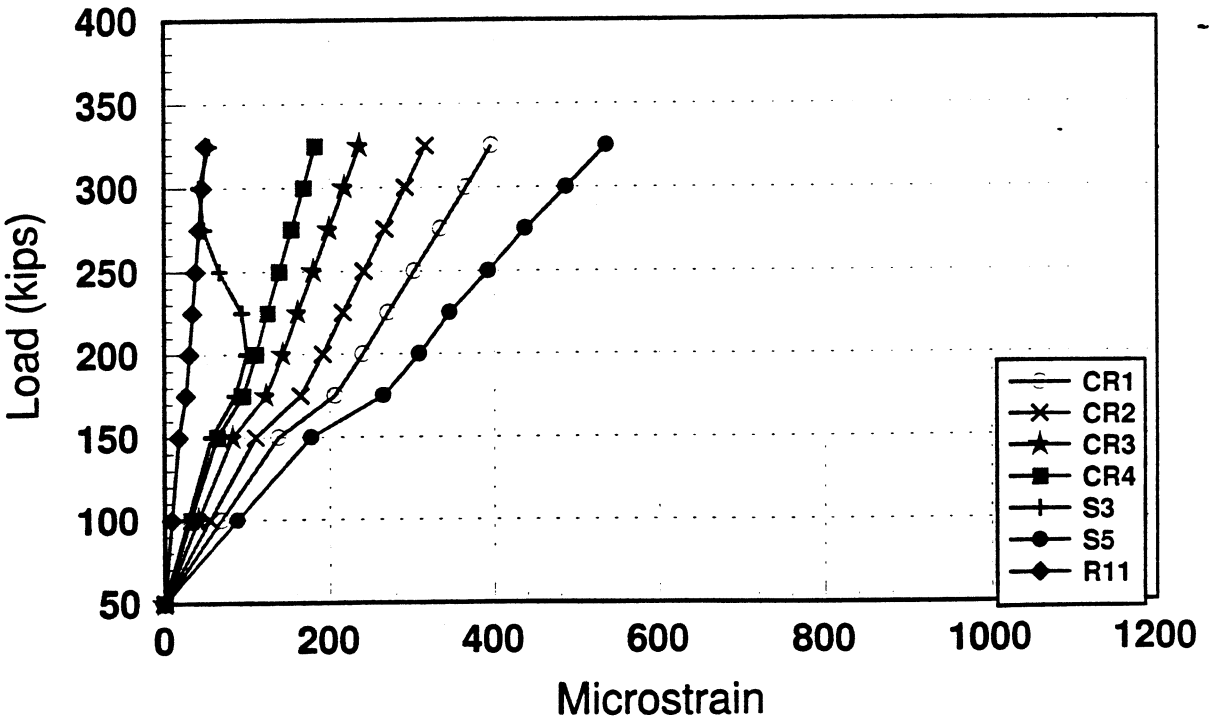

Fig 4.80b Strain in concrete for F12S from FEA

CHAPTER 5
CONCLUSIONS AND RECOMMENDATIONS

5.1 CONCLUSIONS

The objective of this study was to evaluate the effect of fatigue loading shear capacity of high performance prestressed concrete girders. For that purpose, two large scale AASHTO type II girders were tested under cyclic loading conditions. The amplitude of cyclic loading was the same for the both girders. About $2x10^6$ cycles were applied on the 8,000 psi girder and $3x10^6$ cycles on girder of 10,000 psi strength. After cyclic loading both girders were tested statically at both ends to study the effect of fatigue loading on the static shear capacity. Based on the these two tests, the following conclusions were deduced:

1. Both AASHTO-LRFD and ACI codes have overpredicted the shear capacity for the girders.

2. Fatigue loading has reduces flexural moment capacity of both girders.

3. Fatigue loading reduced the bond strength and allows for abrupt-total slip of the prestressing strands upon static testing.

4. The effect of fatigue is less on higher strength concrete then on a lower strength concrete for the same stress ratio. Therefore, it can be postulated that at the same stress ratio, higher strength concrete provide better resistance to fatigue loading.

5. The number of loading cycles applied in this investigation did not affect the shear capacity of the beams as compared with the flexural capacity.

6. The stiffness values of both girders (Cord Stiffness) were reduced by fatigue loading for the first 500,000 cycles. Beyond this number of cycles, fatigue loading did not appreciably affect the stiffness values.

7. The reduction in the stiffness was the main reason why the static capacity was reduced.

8. The first 500,000 cycles can be considered as the stage of crack initiation. The endurance level, however, was achieved after the 500,000 cycles.

9. One should recognized that this endurance level is very much related to several loading factors including stress ratio, and constant vs. variable loading amplitudes. Because of the limited capacity of the loading frame used in this study, the loading amplitude was kept constant on both girders. This, however, caused a reduction in the applied stress ratio for the 10,000 psi girder, which eventuated in higher fatigue and static capacity.

10. The non-linear finite element model predicted the static strength and shear capacity close to the results from both experiments.

11. The strains in the rebars from FEA matched closely with those obtained from the experiment.

12. The shear cracks were also modeled very closely by the FEA program.

13. Providing that the applied stress ratio during fatigue testing would not induce bond failure in the strands during fatigue loading, the nonlinear finite element represents a very good tool to simulate actual field conditions.

14. The damaged fatigue factor that being obtained from FEA considers mutual bonding between the strands and the surrounding concrete. Fortunately, slippage did not occur during the present study. Therefore, the obtained damaged fatigue factors can be used to estimate the reduction of the overall stiffness of the girders.

15. Further studies should be done for larger stress ratios, especially for high strength concrete girders, which may induce bond failure during fatigue loading. Additionally, variable amplitude of loading has proved to influence the dynamic behavior of reinforced concrete. This scheme of loading, which proximate the actual service load, has never been investigated on full scale prestressed beams. It may be beneficial to explore such a loading condition and its effect on the service life of AASHTO Type II girders

5.2 RECOMMENDATIONS

1. An investigation needs to be conducted to study the effect of shear reinforcement on the fatigue strength of high performance prestressed concrete girders.

2. The effect of the confining bars on the shear resistance needs to be studied.

3. The effect of fatigue under different stress ratios and loading cycles should be investigated

4. The codes overpredict the shear strength of statically-tested girders and needs to be either modified or the testing practice of applying consequent loads on both ends of the same beam be reviewed.

5. The effect of the slab on the performance of the girder also needs to be studied.

6. Finite element modeling is a relatively inexpensive and faster technique to study various parameters and should be used more often. It provides more versatility to study all theoretical and practical considerations. One should be aware, however, that FEA should not be overused to draw categorical conclusions about any structural system. The FEA model is as good as the model itself. Yet, many variables govern the suitability of the FEA model, including the hardware and the software being used in the analysis. Thus, FEA modeling should be considered as a supplemental procedure to assist engineers in their analysis.

REFERENCES

1. Erwin L. Espiritu, "Fatigue Strength of Plain Florida Concrete under Constant Amplitude Loading", Florida State University, Spring 1993.

2. Muhamed Husein Harajli, "Deformation and Cracking of partially Prestressed Concrete beams under Static and Fatigue Loading", dissertation, The University of Michigan, 1985.

3. Susan N. Lane and Walter Podolny, Jr., "The Federal Outlook for High Strength Concrete Bridges", PCI JOURNAL, V. 38, No. 3, May-June 1993, pp. 20-31.

4. Hilsdorf, H. K. And Kesler, C. E., " Fatigue Strength of Concrete Under varying Flexural Stresses", ACI Journal, Vol. 63, No. 10, Oct. 1966, pp. 1059-1075.

5. Shah, S. P. and Chandra, S., "Fracture of Concrete Subjected to cyclic and Sustained Loading", ACI Journal, Vol. 67, No. 2, Feb. 1970, pp. 195-211.

6. Nordby, G. M., "Fatigue of Concrete- A Review of Research", ACI Journal, Vol. 55, No. 2, Aug. 1958, pp. 191-219.

7. Lovegrove J. M. and Salah El Din, "Deflection and Cracking of Reinforced Concrete under Repeated Loading and Fatigue", ACI, SP 75-6, 1982, pp. 133-152.

8. Charles W. Dolan, and Robert W. LaFraugh, "High Strength Concrete in the Precast Concrete Industry", PCI JOURNAL, Vol. 38, No. 3, May-June 1993.

9. Charles W. Dolan, Craig A. Ballinger, and Robert W. LaFraugh, "High Strength Prestressed Concrete Bridge Girder Performance", PCI JOURNAL, Vol. 38, No. 3, May-June 1993.

10. John J. Roller, Barney T. Martin, Henry G. Russell and Robert N. Bruce, Jr., "Performance of Prestressed High Strength Concrete Bridge Girders", PCI JOURNAL, Vol. 38, No. 3, May-June 1993.

11. Michael E. Kreger, Patrick M. Bachman and John E. Breen, " An Exploratory Study of Shear Fatigue Behavior of Prestressed Concrete Girders", PCI JOURNAL, Vol. 34, No. 4, July-August 1989.

12. Douglas W. Riedel, " Fatigue Strength of Prestressed Concrete T-Beams With Welded Wire Fabric as Shear Reinforcement", MS Thesis, Rice University, April 1986.

13. Rabbat, B. G., Kaar, P. H. , Russell, H. G. and Bruce, R. N., Jr., "Fatigue Tests of Pretensioned girders with Blanketed and Draped Strands", PCI JOURNAL, Vol. 24, No. 4, July-August 1979, pp. 88-114.

14. Bruce W. Russell and Ned H. Burns, "Static and Fatigue Behavior of Pretensioned Composite Bridge Girders Made with High Strength Concrete", PCI JOURNAL, Vol. 38, No. 3, May-June 1993, pp. 116-128.

15. Price K. M., and Edwards, A. C., "Fatigue Strength of Prestressed Concrete Flexural members", ACI Journal, Vol. 71, No. 4, pp. 282-292.

16. John Poulson, "Cracking and Shear Capacity of High-Strength Prestressed Concrete Girders", MS Thesis, Florida State University, Spring 1994.

17. ANSYS User's Manuals, Version 5.0/5.0 A, 1994.

18. "AASHTO LRFD Bridge Design Specifications," American Association of State Highway and Transportation Officials, 1994.

19. Julie A. Bannantine, Jess J. Comer and James L. Handrock, *Fundamentals of Metal Fatigue Analysis*, Copyright 1990 by Prentice Hall, Inc., Englewood Cliffs, NJ.